Multi-band reflectarray antennas in Ku and THz frequency bands

PAR

Hamed HASANI

ÉCOLE POLYTECHNIQUE
FÉDÉRALE DE LAUSANNE

Suisse
2015

To my parents **Sima** and **Esmaeil**. . .

Acknowledgements

Acknowledgements

gratitude to my wonderful and lovely friends Rafal Glogowski and his life companion Joanna for their memorable hospitality and invaluable company both in Portugal and Switzerland. During my three years stay in the laboratory of LEMA, EPFL I must say that I have enjoyed a lot the friendly environment and wonderful company of its current and past members. My warmest thanks goes to Anton, Baptist, David, Eden, Apostolos, Joana, Jovanche, Mina, Michele, Maria, Tomislav, Nuno, Santiago, Nevena and Marc in addition to my dear fellow countrymen Hussein Esfahlani, Mohsen Yousefbeiki and Mohsen Bahramipanah all with whom I spent delightful and unforgettable moments.

I would also like to acknowledge the wonderful and lovely members of the theatre troupe of EPFL *Les Polyssons*: Elise, Clarina, Karin, Sophie, Virgile, Thomas and Antoine along with our two admirable *metteurs en scène* Christine Laville and Anthony Gerber, thanks to whom I had one of the most amazing experiences in my life by performing with them in the play *Le repas des fauves* that went on stage in April and May 2015. *Un grand merci à vous tous!*

Finally I am most grateful to the everlasting support and love of my parents Sima and Esmaeil to whom I owe every achievement in my life, to my sister Shahla for having always been there for me in difficult times and to my dear brothers Khalil and Hossein that in spite of the long distances have always been with me.

Julien

From February 2013 till June 2014 my thesis was supervised at EPFL by Prof. Julien Perruisseau-Carrier who unfortunately passed away on 6th June 2014 at the age of 35.

For me it was a great privilege having known Julien and having worked under his invaluable supervision. And I must say that it was his inspiring perseverance and perspicacity as well as his good sense of humour that made his death a tragedy for the people who have known him and have worked with him.

It goes without saying that with his enormous contributions to different areas of Electromagnetism and with his dedication and commitment to the scientific research, Julien will always remain unforgettable.

Lausanne, 07 October 2015   Hamed Hasani

ii

Abstract

Printed reflectarrays are low-cost, low-profile high gain antennas demonstrating distinctive advantages over conventional parabolic reflectors and phased-arrays. The flat, low weight reflecting surface of a reflectarray makes it an attractive alternative with respect to bulky parabolic reflectors especially for space and satellite systems. As compared to high-cost phased-array antennas, with incorporation of solid state devices, reflectarrays are able to demonstrate electronic beam scanning in a very low-cost way.

A distinctive advantage of a reflectarray antenna lies in its potential to be readily designed as a multi-band antenna which demonstrates independent performance at several frequencies. A characteristic that is difficult to achieve using conventional parabolic reflectors.

The aim of this thesis is to present low-cost, simple, multi-band printed reflectarray antennas in Ku and THz frequency bands. In Ku band we present a dual-band reflectarray performing at 12 and 14 GHz and a quad-band reflectarray antenna performing at 12, 13, 14 and 15.5 GHz. The presented prototypes benefit from the advantage of having a single-layer structure which reduces the design complexity as well as the fabrication cost. In addition, multi-band reflectarrays are able to perform at any polarization due to the dual-linear polarized design of their unit-cells. Furthermore, the design of the unit-cell is such that, at each frequency, the phase response depends on only one parameter of the cell. This advantage eliminates the need for time consuming optimizations. Based on proposed unit-cells dual-band and quad-band reflectarrays with arbitrary beam direction versus frequency have been simulated, fabricated and measured. Simulation and measurement results as well demonstrate the satisfactory independent performance of the prototypes at each intended frequency.

In THz region, for the first time we present a tri-band unit-cell based on which reflectarray prototypes performing at the three frequencies 0.7, 1.0 and 1.5 THz, are designed. The presented reflectarrays possess all the advantages of those designed for Ku band with the additional advantage of having high resistivity silicon as the substrate thanks to a sophisticated fabrication process. The use of silicon as substrate is a big advantage since it facilitates the integration of solid state devices for reconfigurability. Based on the proposed unit-cell reflectarray samples with arbitrary independent performance at each frequency are designed, simulated, fabricated and measured. Measurement results obtained using a THz-TDS (Terahertz Time-Domain Spectroscopy) measurement system, demonstrate the satisfactory independent performance of the reflectarray samples at each frequency.

This thesis also presents a dual-band, dual-polarized *reconfigurable* unit-cell for beam-scanning reflectarray operating at 12 and 14 GHz. The cell however suffers from high-cross-polarization

level. A *chessboard* cell arrangement is proposed to mitigate the high cross-polarization level at the reflectarray far-field region. Simulation results show the effectiveness of the chessboard arrangement in eliminating the cross-polarization allowing the design of a low-cross polarization reconfigurable reflectarray antenna out of a unit-cell with high cross-polarization level.

Finally, the thesis presents the concept of a *versatile flat prism* which is a reflectarray with a pre-designed frequency-scanning behaviour. The limitations and challenges as well as solutions for implementation of such a device are presented and discussed.

Keywords: Ku band, THz, Dual polarization, Reflectarray, Periodic structures, Metasurfaces, Mutli-band, High gain antennas, Satellite communications, Reconfigurable antennas.

Résumé

Les réseaux réfléchissants imprimés, communément appelés reflectarrays, sont des antennes à faible coût, de profil réduit et de gain élevé qui possèdent des avantages distincts par rapport aux réflecteurs paraboliques classiques ou aux antennes réseau. La surface plane et la légèreté d'un reflectarray en font une alternative intéressante aux réflecteurs paraboliques encombrants, particulièrement dans le cas de systèmes spatiaux ou de satellites. Comparé aux réseaux phasés, un reflectarray est capable de fournir un balayage électronique du faisceau à un bien moindre coût.

Les reflectarrays ont l'avantage de pouvoir facilement être conçus pour fonctionner dans de multiples bandes de fréquences indépendantes entre elles. Cette caractéristique est difficile à réaliser avec des réflecteurs paraboliques classiques.

L'objectif de cette thèse est de présenter des reflectarrays imprimés simples et multi-bandes en bande Ku ainsi que dans la bande des THz. En bande Ku, nous présentons un reflectarray double-bande fonctionnant à 12 et 14 GHz et un reflectarray quadri-bande fonctionnant à 12, 13, 14 et 15.5 GHz. Les prototypes présentés sont tous monocouche, ce qui réduit la complexité de la conception ainsi que le coût de fabrication. En outre, les reflectarrays multi-bandes sont capables de fonctionner suivant toutes les directions de polarisation, grâce à une conception en polarisation linéaire double de leurs cellules. De plus, la cellule est conçue de manière à ce que les réponses en phase de leur coefficient ne dépendent que d'un seul paramètre, différent dans chaque bande de fréquence, ce qui présente l'avantage considérable de rendre les optimisations inutiles. Fondés sur les cellules proposées, des reflectarrays double-bande et quadri-bande sont proposés, réalisés et caractérisés. Ils présentent une direction de réflexion du faisceau prédéfinie de manière arbitraire. Les diagrammes de rayonnement simulés et mesurés démontrent le fonctionnement satisfaisant de prototypes réalisés.

Une cellule tri-bande est présentée pour la première fois dans la bande de THz. Fondés sur cette dernière, deux reflectarrays fonctionnants à 0.7, 1.0, et 1.5 THz sont conçus. Ces réseaux ont les mêmes avantages que ceux proposés en bande Ku. De plus, l'utilisation d'un substrat en Silicium à haute résistivité a été rendue possible par un processus de fabrication sophistiqué, permettant ainsi la réduction des pertes. L'utilisation de silicium comme substrat présente l'avantage de faciliter l'intégration des éléments semi-conducteurs utilisés pour une éventuelle reconfigurabilité du réseau.

Des reflectarrays avec des performances indépendantes à chaque fréquence et choisies de manière arbitraire ont été conçus, simulés, fabriqués et mesurés. Les résultats de mesure obtenus en utilisant un système de mesure de THz-TDS (Terahertz Time-Domain Spec-

troscopy), démontrent la performance satisfaisante des reflectarrays à chaque fréquence.
Cette thèse présente de plus une cellule double-bande, double-polarisation reconfigurable
pour un balayage de faisceau électronique fonctionnant à 12 et 14 GHz. La cellule souffre
cependant d'un niveau de polarisation croisée élevé. Pour atténuer cet inconvénient et
abaisser la polarisation croisée en champ lointain, un arrangement des éléments nommé en
damier (chessboard) est proposé. Les résultats de simulation montrent l'efficacité de cette
méthode.
A la fin de la thèse, on présente le concept de prisme planaire versatile (flat versatile prism)
qui est en fait un reflectarray présentant une variation fréquence-balayage préconçue. Les
limites et les défis ainsi que des solutions pour la réalisation d'un tel dispositif sont présentés
et discutés.

Mots clefs: Bande Ku, THz, double polarisation, reflectarray, structures périodiques, metasurfaces, Mutli-bande, antennes à gain élevé, communications par satellite, antennes reconfigurables

Resumo

Os agregados de antenas reflectoras impressos, amplamente conhecidos pelo correspondente termo inglês, printed reflectarrays, são antenas de baixo custo, de baixo perfil e de ganho elevado e que aprensentam ainda várias vantagens quando comparadas com as antenas reflectoras parabólicas e os agregados de fase. A superfície plana e leve de um reflectarray é uma alternativa bastante atractiva quando comparada com as volumosas antenas parabólicas, especialmente para aplicações no espaço ou para satélites. Por outro lado, quando comparados com os agregados de fase, os reflectarrays tem a vantagem de alcançar um varrimento electrónico do feixe com um custo mais baixo. Mas a principal vantagem de um reflectarray reside no seu potencial de ser facilmente concebido como uma antena multi-banda demonstrando desempenhos independentes em diversas frequências. Esta é uma das características mais difíceis de alcançar quando se utiliza as antenas parabólicas convencionais.

O objectivo desta dissertação é desenvolver reflectarrays impressos simples, de baixo custo e multi-banda para as bandas de frequência Ku e THz. Na banda Ku são propostas duas antenas, um reflectarray de banda dupla que opera a 12 e a 14 GHz e um outro reflectarray de banda quádrupla que opera a 12, 13, 14 e 15.5 GHz. Estas antenas têm a vantagem de terem apenas uma camada o que reduz a complexidade na fase de concepção e também de fabrico. Além disso, os reflectarrays multi-banda têm a capacidade de operar com qualquer polarização devido às suas células apresentarem dupla polarização linear. É ainda importante referir que a célula foi desenhada para que, a cada frequência, a fase dependesse apenas de um parâmetro. Esta vantagem suprime a necessidade de demoradas optimizações. Com base na célula individual proposta, os reflectarrays de banda dupla e de banda quádrupla com direcção arbitrária do feixe versus frequência foram simulados, fabricados e medidos. Os resultados das simulações e das medidas demonstram que as antenas têm um comportamento satisfatório para cada uma das frequências pretendidas.

Na banda dos THz, é proposta pela primeira vez uma célula de banda tripla na qual se baseiam os reflectarrays que operam a 0.7, 1.0 e 1.5 GHz. Estes reflectarrays não só possuem todas as vantagens das antenas na banda Ku acima referidas, como também apresentam uma vantagem adicional, a de terem silicone altamente resistivo como substrato graças a um sofisticado método de fabrico. O uso de silicone como substrato é uma grande vantagem uma vez que facilita a integração de semi-condutores para reconfiguração. Reflectarrays baseados na referida célula e com desempenhos independentes a cada frequência foram concebidos, simulados, fabricados e medidos. Os resultados das medidas obtidos usando um equipamento de medida em THz (em inglês, Terahertz Time-Domain Spectroscopy [THz-TDS]) comprovam

que a antena tem um desempenho satisfatório e de acordo com o esperado.

Esta dissertação também propõe uma célula reconfigurável de banda dupla e com dupla polarização para um reflectarray cujo objectivo é fazer um varrimento do feixe a 12 e 14 GHz. No entanto, esta célula apresenta níveis altos de polarização cruzada. Uma combinação de células que se assemelha a um tabuleiro de xadrez foi adoptada (e denominada chessboard cell arrangement) a fim de combater este mesmo problema na região de campo distante. Os resultados das simulações mostram que a referida combinação de células é eficaz na resolução do problema a que se propôs.

Por fim, esta dissertação apresenta o conceito de um prisma plano versátil que no fundo é um reflectarray com um comportamento pré-concebido de varrimento em frequência. As limitações e os desafios desta estrutura bem como várias soluções para a sua implementação são abordadas e discutidas.

Palavras-chave: banda Ku, THz, dupla polarização, agregado de antenas reflectoras (reflectarray), estruturas periódicas, metasurfaces, banda múltipla, antenas de ganho elevado, comunicações por satélite, antenas reconfiguráveis.

Contents

Contents

List of Figures

List of Tables

1 Introduction

1.1 Motivation and context of the work

High-gain antennas [3] are an indispensable component of any long-distance wireless system such as satellite communications [4, 5] or Radar [6]. The traditional antenna candidates for such applications have been parabolic reflectors [7] and arrays [8]. A parabolic antenna (or a dish) is a reflective metallic surface that converges an incoming plane wave toward its focus. Conversely, the spherical out-going wave of a point source, placed at the focal point, is transformed into a plane wave, propagating as a collimated beam. Parabolic reflectors provide a relatively low-cost and straightforward way to achieve high gain. An antenna array, on the other hand, consists of a set of individual antennas (or elements) each excited with a specific amplitude and phase. This enables the array to perform as a single antenna with improved directional properties and thus higher gain. In case of a steerable array, where the phase and amplitude of each individual radiating element is electronically controlled, the array directional features can be electronically manipulated without requiring physical motion of the whole antenna. Combined with microstrip technology at high frequency bands (C, X, Ku, Ka) allocated for satellite systems, steerable array antennas (or phased-array antennas) are frequently used as high gain antennas due to their compact size.

The deployment of parabolic and phased-array antennas is, however, subject to several challenges. Due to its specific curvature, a parabolic reflector grows into a bulky structure, difficult to manufacture and handle, specially for space satellite communication systems. In addition, the beam steering with a parabolic reflector is only possible through the use of mechanical scanning. On the other hand, microstrip phased-array antennas which are capable of electronic beam steering suffer from very high implementation cost since each element of the array must be connected to a sophisticated module containing a phase-shifter and an amplifier. In addition, the efficiency of a phased-array degrades at higher frequencies due to the use of transmission lines. Methods have been introduced in order to reduce the number of radiating elements and hence the modules in phased-array antennas. The resultant arrays are commonly known as sparse or thinned arrays [9, 10]. The implementation of these arrays
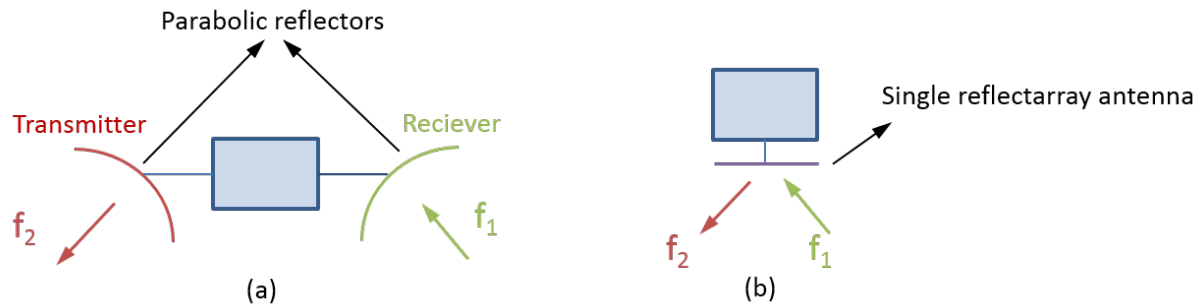
Figure 1.1: The advantage of a high-functional reflectarray antenna. A reflectarry antenna can replace two separate parabolic reflectors, each with a specific beam direction at two specific frequencies of f_1 and f_2.

however is less straightforward since their design relies on an extensive optimization process which needs to be repeated for different design requirements (working frequency, side-lobe level, gain, etc).

As a compromise between a parabolic reflector and an antenna array, a third high-gain antenna type known as Printed Reflectarray Antenna has emerged [1]. It is composed of a reflecting flat plate illuminated by a feed. On the plate there is an array of passive printed elements each with its own specific size and shape in order to compensated the phase difference caused by the feed to element path and thus producing a co-phased plane and hence, a directive pattern in the antenna far-field region. Printed reflectarray antennas have been proposed as an alternative to the conventional parabolic reflector antennas by demonstrating distinguished advantages over the former such as light weight, low manufacturing cost, low profile, good efficiency and simplicity of design making it an attractive antenna in wireless communication domains especially in satellite communication systems. In addition, by electronically tuning the radiating elements using varactor diodes, PIN diode switches, ferro-electric devices, and MEMS switches, a printed reflectarray antenna is capable of electronic beam scanning in a very simple low-cost way as compared to the high-cost phased-array antennas [11–18]. The extensive research on reflectarray antennas has revealed their potential functionality in frequency and polarization. As an example, figure 1.1 demonstrates how the high functionality of a reflectarray antenna leads to a notable cost reduction. As shown, thanks to its multi-frequency performance, a reflectarry antenna can replace two separate parabolic reflectors, each with a specific beam direction at a specific frequency. Furthermore, figure 1.2 shows the distinct advantage of a printed reflectarray over a parabolic reflector for a ground station transceiver. As shown, a parabolic reflector beam direction always remains the same at the uplink and downlink frequencies whereas a reflectarray antenna can be easily designed to have arbitrary and independent beam direction at each frequency. As a results, with a multi-band reflectarray antenna the ground terminal can maintain its connection with two (or several) differently positioned geostationary (GEO) satellites. Combined with tunable elements, the multi-frequency capability can turn into reconfigurable, multi-frequency performance and
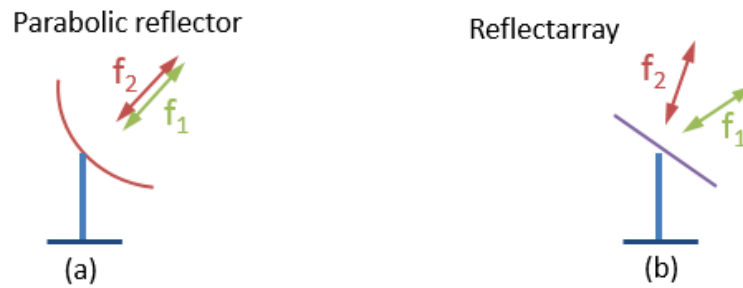
Figure 1.2: The advantage of a high-functional reflectarray antenna in a satellite communications' ground station. While the beam direction at different frequencies remains unchanged in a parabolic reflector, the multi-band performance of a reflectarray antenna allows wireless connection with several (here two) geostationary satellites in different positions at different frequencies (here f_1 and f_2).

Figure 1.3: The Terahetz radiation. The frequency scale is in Hertz [37].

hence a highly functional yet low-cost high-gain antenna can be developed.

The reflectrarray antenna concept is not limited only to microwave frequencies. In recent years, many developments of reflectarray antennas in Terahertz (THz), infra-red and visible frequencies have also been reported [2, 19–36]. The resulting devices are also presented as a family of meta-surfaces capable of deflecting an incident plane wave into an arbitrary direction.

In physics, Terahertz (THz) radiation consists of electromagnetic waves with frequencies varying from 0.3 to 3 THz corresponding to wavelengths of 1 mm to 0.1 mm (see figure 1.3).

The Terahertz radiation covers a frequency range between microwaves and infrared which is also known as Terahertz gap whereon intensive research is carried out. THz radiation thus shares some properties of both infrared and microwave radiation. It is a non-ionizing radiation travelling in a line of sight and is able to penetrate a variety of non-conducting objects such as clothing, paper, wood, plastic and etc. However Terahertz radiation is subject to considerable losses when passing through fog and clouds (i.e the absorption of water vapour) and it cannot penetrate liquid water or metal. Due to the presence of water vapour in the air, the usage of

Terahertz radiation is limited within a range of maximum 10 meters.
In particular, THz frequencies have numerous applications in stand-off security scanning, biology and medical sciences and broadband short-range wireless communication systems [38] and one of the prominent topics in this field has been to manipulate the THz incoming wave using meta-surfaces that are designed based on reflectarry antenna concept. Multi-band reflectarray performance in this region will also have its benefits and advantages that were discussed previously.

1.2 The main challenges and objectives

The goal of this thesis, is to develop printed reflectarray antennas with a very high functionality/cost ratio, by proposing multi-band structures that are capable of performing at any polarization i.e. dual-linearly polarized at Ku band (12 - 18 GHz) as well as in THz region(0.3 - 3 THz). More specifically, the thesis concentrates on multi-band reflectarray antennas with closely separated frequency bands since, it can also serve as a solution to the major drawback of reflectarray antennas: narrow bandwidth performance. As such, the multi-band reflectarrays can be considered as the combination of several separate reflectarray antennas sharing one single aperture. So far in the literature various multi-band reflectarrays with linear and/or circular polarization have been reported. However most of the proposed antennas have a multi-layer structure and/or lack dual linear polarization performance.

The main challenge in designing multi-band reflectarray antennas, is then to meet all of the following conditions:
1- The antennas should be constructed on a single-layer in order to minimize complexity and therefore costs.
2- They should be dual-linearly polarized, in order for them to perform at any polarization and thus increase their functionality.
3- They should perform at several closely separated frequencies.
4- In case of THz frequencies, in addition to the above conditions, the reflectarray surface must use high-resistivity silicon as substrate, in order to enable the integration of solid-state devices to achieve reconfiguration.

1.3 Outline and original contributions

Chapter 2: Reflectarray Antennas and their Multi-Band Performance

description: The development history of reflectarray antennas, their limitations and drawbacks are elaborated. This chapter serves as a review on the technologies and advances on reflectarray antennas from microwave to THz, infra-red and optical region.

original contribution: The concepts and results discussed in this chapter are not new.

Chapter 3: Theory and Design of Printed Reflectarray Antennas

description: The theory and design of a typical reflectarray antenna is discussed in this chapter, providing an insight to its limits as well. In addition, the behaviour of an ideal unit-cell for a reflectarray antenna demonstrating an infinite bandwidth (i.e. that of a parabolic reflector) and the existing unit-cells that mimic that behaviour are presented and discussed.

original contribution: This chapter presents the idea of a versatile prism which is a reflectarray surface with a pre-designed frequency-scanning behaviour. An infinite bandwidth reflectarray antenna would therefore be a special case of a versatile prism. In addition, two unit-cell structures are proposed for the implementation of a versatile prism.

Chapter 4: Multiband Reflectarray Antennas in Ku-Band

description: Single-layer, dual-linearly polarized unit-cells are proposed for dual-band and quad-band reflectarray antennas for four closely separated frequencies of 12, 13, 14 and 15.5 GHz. Simulation and measurement results of the prototypes, showing their satisfactory performance, are presented in this chapter.

original contribution: For the first time, a quad-band, dual-polarized and single layer reflectarray antenna is designed and fabricated with a very good functionality/cost ratio. The resulting reflectarray antenna thus satisfies the criteria presented in the previous section.

Chapter 5: Dual-Band, Dual-Polarized Reconfigurable Reflectarray Antenna

description: Single-layer, dual-linearly polarized reconfigurable unit-cells are proposed for dual-band reconfigurable reflectarray antennas with closely separated frequency of 12 and 14 GHz. The resultant reflectarray achieves independent beam-scanning at each frequency.

original contribution: For the first time, a reconfigurable dual-band, dual-polarized, single layer unit-cell has been designed and simulated with satisfactory results. In addition, this chapter presents the chessboard arrangement for reflectarray antennas that use a high cross-polar unit-cells. The theory and limitations of such an arrangement is discussed in this chapter.

Chapter 6: Tri-Band Reflectarray Surface in THz Frequency Band

description: Single-layer, dual-linearly polarized unit-cells are proposed for single-band, dual-band and tri-band reflectarray surfaces with closely separated frequency of 0.7, 1 and 1.5 THz, having with silicon as the substrate. The prototypes have been simulated, fabricated and measured using Terahertz time-domain spectroscopy (THz TDS) and results are discussed.

original contribution: For the first time, a tri-band, dual-polarized, single-layer reflectarray has been designed in THz region. In addition, contrary to prototypes fabricated and reported so far in the literature, high-resistivity silicon has been used as substrate which integration of solid-state devices to achieve reconfiguration.

5

1.4 Publications

1- **Hasani, H**., Peixeiro, C., "Dual-band, Dual-polarized Reflectarray antenna in Ku Band", Proc Loughborough Antennas and Propagation Conf. – LAPC, Loughborough, United Kingdom, Vol. 1, pp. 1 - 4, November, 2012.

2- **Hasani, H**., Peixeiro, C., "Dual-band Dual-Polarized Reflectarray Antenna with close Frequencies in Ku Band", Proc IEEE AP-S/URSI International Symp., Chicago, United States, July, 2012.

3- **H. Hasani**, C. Peixeiro, A. K. Skrivervik, J. Perruisseau-Carrier,"Single-Layer Quad-Band Microstrip Reflectarray Antenna with Dual Linear Polarization ," IEEE Transactions on Antennas and Propagation, May 2015. *Accepted with major revision*.

4- **Hasani, H**.; Perruisseau-Carrier, J.; Peixeiro, C.; Mosig, J.R., "Dual-band dual-polarized reconfigurable unit-cell for reflectarray antenna in Ku-Band," 7th European Conference on Antennas and Propagation (EuCAP), vol., pp.861,862, 8-12 April 2013.

5- **H. Hasani**, M. Tamagnone, S. Capdevila, C. Moldovan, P. Maoddi, A. M. Ionescu, C. Peixeiro, J. R. Mosig, A. K. Skrivervik and J. Perruisseau-Carrier "Tri-Band, Polarization-Independent Reflectarray at Terahetz Frequencies: Design, Fabrication and Measurement," Submitted for publication in IEEE Transactions on Terahertz technology.

6- Michele Tamagnone, Santiago Capdevila, **Hamed Hasani**, Pietro Romano, Anja Skrivervik, Julien Perruisseau-Carrier,Wolfgang Vitale, Clara Moldovan, Adrian Mihai Ionescu, "Performance evaluation of novel technologies for Terahertz reflectarrays" European Microwave Week (EuMW), Paris, France, September 2015.

7- **H. Hasani**, M. Tamagnone, S. Capdevila, C. Moldovan, A. M. Ionescu, C. Peixeiro, J. R. Mosig, A. Skrivervik, "Design, Fabrication and Characterization of Terahertz Reflectarrays Based on a Silicon Substrate", META15 Conference, New York, August 2015.

2 Reflectarray Antennas and their Multi-band Performance

The concept of reflectarray antenna was first introduced by Berry, Malech, and Kennedy [39] in 1963. In the prototype, an array of short-ended waveguides, shown in figure 2.1 were illuminated by a feed horn antenna. The length of each of the waveguides were adjusted so that, once coupled to the waveguide, the incident wave of the feed horn, was reflected by the short-end and re-radiated from the waveguides open-end with phase values depending on the waveguides lengths. By adjusting the length of each waveguide, a desired phase distribution can be made on the array surface and hence, a directed beam can be made in the far-field. However, due to the use of wave-guide plus the feed horn, the whole structure became very bulky and heavy and the concept was not popularized until ten years later with the introduction of microstrip technology.

2.1 Microstrip reflectarray antennas

A microstrip reflectarray antenna was first introduced by Malagisi in 1978 [40] and in the same year, its analysis using infinite array approach was proposed by Montgomery [41]. A decade later, In the late 1980s and early 1990s, various printed elements were proposed in order to achieve a low-profile, low-cost directive antenna. Figure 2.2 shows a typical printed reflectarray configuration along with the various printed element types. The first reported reflectarrays used simple printed patches with different sizes [42] as shown in figure 2.2.c, printed cross-dipoles and rings with different lengths and radius [43, 44] as shown in figure 2.2.b, same size patches with attached stubs having different lengths [45] shown in figure 2.2.a and other elements. In addition to these designs that were targeted for linear polarization performance, microstrip reflectarrays were also developed for circular-polarization applications by using identical circularly polarized elements with different rotation angles [46, 47] as shown for instance in figure 2.2.d. In this reflectarray type, with a circularly polarized incident field and circularly polarized elements, physical rotation of each element creates a phase-shift which is proportional to twice the angle of rotation [46].
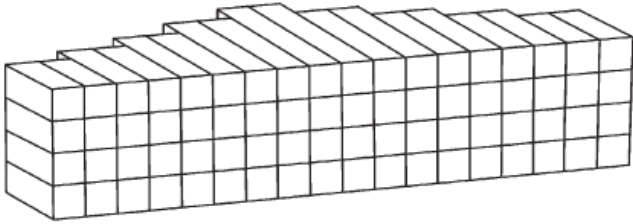
(a) 3D schematic view [1]
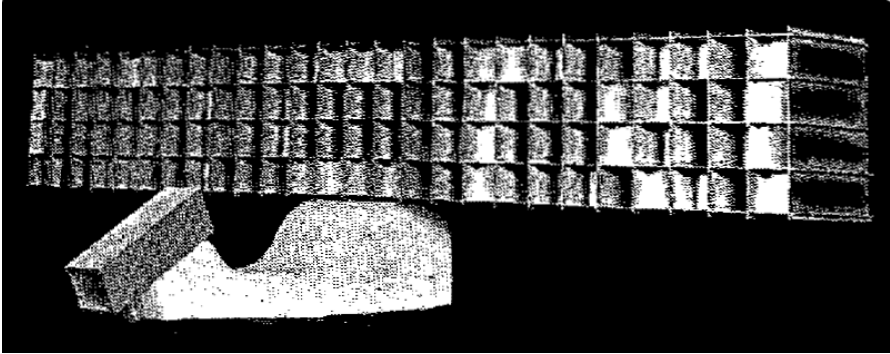
(b) Implemented prototype [39]

Figure 2.1: The first reflectarray antenna using short-ended waveguides as elements [1, 39].
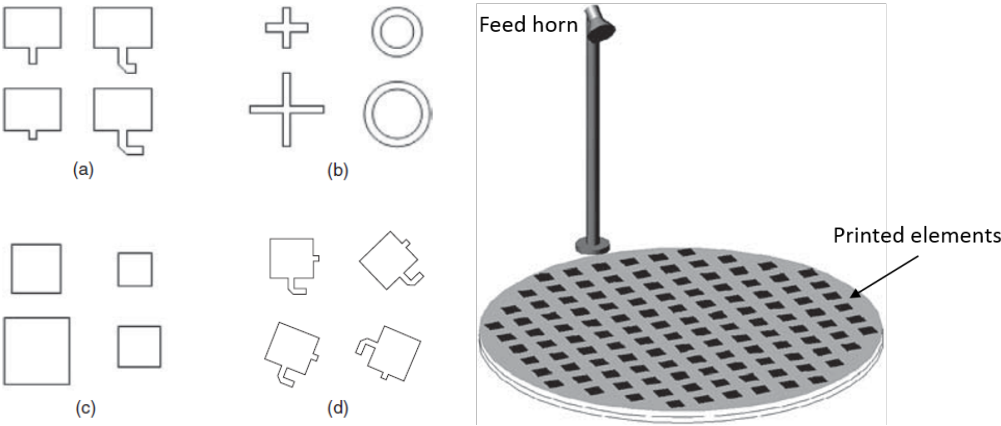
Figure 2.2: Typical geometry of a printed reflectarray antenna and various printed element types, (a) identical patches with variable length phase delay lines, (b) variable size dipoles or loops, (c) variable size patches,(d) variable angular rotations [1].

The main disadvantage of a reflectarray antenna is its narrow bandwidth performance which typically does not go beyond ten percent. It is only in this sense that a parabolic reflector with its inherent theoretical infinite bandwidth has superiority over a reflectarray antenna. Reflectarray bandwidth depends on element design, plate size, focal length and so on. As a result, extensive research on reflectarrays focuses on presenting elements that can overcome this deficiency [48–57].

2.2 Multi-band reflectarrays

In spite of demonstrating a narrow bandwidth performance, a reflectarray antennas with a distinctive potential of being designed for multi-band performance was first reported in [58]. This is of special interest in the case where the communication system requires the coverage of several narrow frequency bands. In addition, a multi-band reflectarray is completely independent at each frequency band, a characteristic that is very difficult to achieve using parabolic reflectors. It should be noted that for the unit-cell of a multi-band reflectarray we would need geometrical parameters inside the cell equal to the number of frequencies so that at each frequency the cell can provide the required reflection phase.

Multi-band reflectarrays can be divided into two major groups: those with largely separated frequency bands and those with closely separated frequencies. A discussion on multi-band reflectarrays structures and the geometry of their unit-cells is provided in chapter 6 of [1]. However we mention next some of their important characteristics and provide some examples reported in the literature.

2.2.1 Reflectarrays with largely separated frequencies

Reflectarrays with largely separated frequencies cover frequencies each belonging to a certain known frequency band e.g C, X, Ku, K, Ka and so on. An example is a reflectarray antenna covering widely separated frequency bands in X (8-12 GHz) and Ka (26-40 GHz) region presented in [59]. The reflectarray consists of two layers each for one of the intended frequency bands. Due to the large separation between the frequencies, each layer performs as a reflectarray at one frequency and becomes almost transparent at the other one (see figure 2.3). This characteristic makes the design procedure straightforward, meaning that since the two layers do not disturb each other's phase profiles, there will be no need for time consuming tuning and/or optimization.

Dual-band reflectarrays can also be designed as single-layer structures. Figure 2.4 shows two single-layer dual-band structures for largely separated frequencies 8 and 16 GHz where small and large cross-dipoles and/or patches are responsible for phase-shift at the higher and lower frequency band, respectively [1]. In these structures, due to the large separation between operating frequencies, size variation of a structure assigned to one frequency, does not affect the phase response of the other frequency. In other words inside the unit-cell, at each frequency the phase-shift depends on only one parameter of the cell. This characteristic
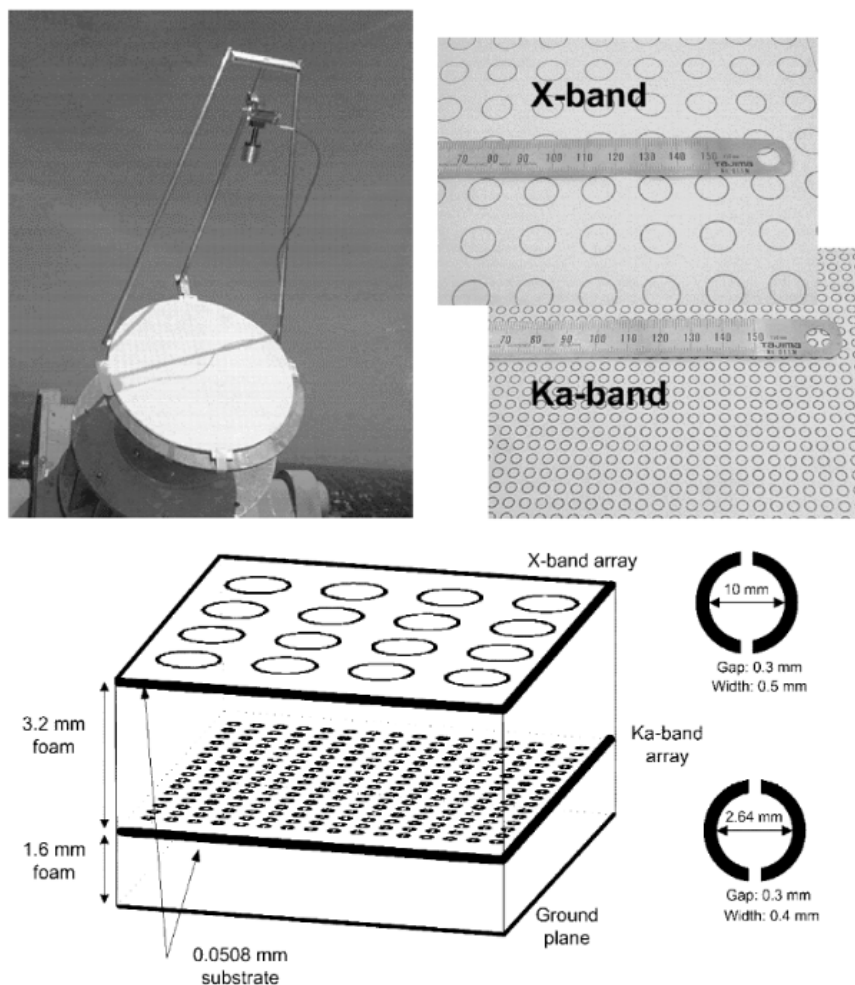
Figure 2.3: Two-layer, X/Ka dual-band reflectarray antenna with the fabricated layers for each band [59].

leads the reflectarray to have completely independent beam shapes at each frequency. It should be noted that these structures benefit also from dual-linearity which allows them to operate at any polarization. As another example, in [60] the single-layer reflectarray antenna covers three separated frequency bands of 7.1 GHz (C-band), 8.4 GHz (X-band) and 32 GHz (Ka-band) for circular polarization performance. The reported reflectarray antenna with its unit-cell as shown in figure 2.5 where every structure assigned to a certain frequency, has a different color.

 Finally, figure 2.6 shows another good example of multi-band cells for reflectarray antennas. The double layer geometry includes many possible configurations for multi-band operation. The cell operates at six frequency bands of 6.6, 18.7, 57.7, 52.5, 166 and 183 GHz [61].

 As shown in the prototypes presented in the literature, the important concern in designing multi-band reflectarrays is how to implement inside a unit-cell structures for different frequencies with their own varying parameters *without* severe mutual coupling and physical
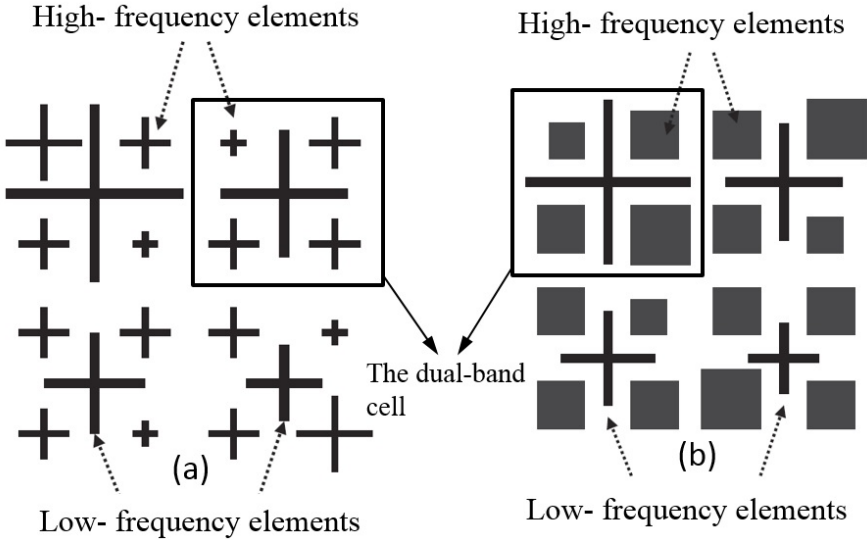
Figure 2.4: Single-layer, simple dual-band structures at 8 and 16 GHz using a) cross-dipoles b) cross-dipoles and patches. The small and large sized elements are responsible for phase-shift at higher and lower frequencies, respectively [1].
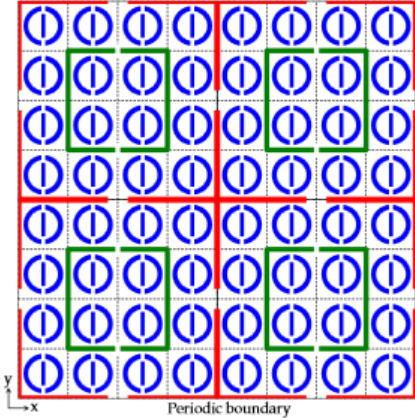
Figure 2.5: C/X/Ka single layer tri-band reflectarray unit-cell [60].

overlapping. We should of course take into account the unit-cell size since large values results in unwanted grating lobes. And as mentioned before, the large separation between operating frequencies is to our benefit for both issues.

Similar multi-band reflectarrays with multi-layer or single layer structures can be found in [62–64].

(a) Top layer configuration

(b) Bottom layer configuration

6.6, 18.7, and 57.5 GHz elements

Foam   52.5, 166, and 183 GHz elements   Substrate

Foam

Ground

(c) Side view
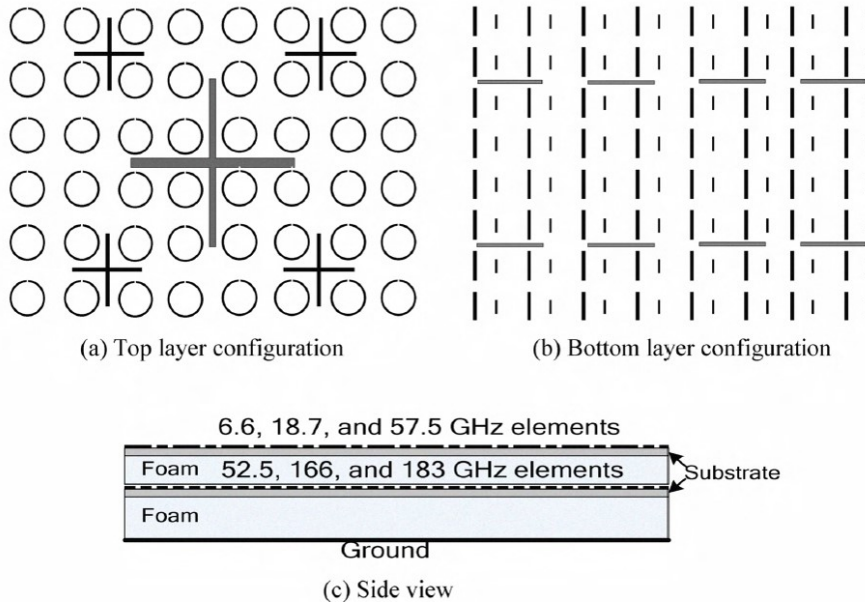
Figure 2.6: A six-band, two-layers cell configuration [61].

2.2.2 Reflectarrays with closely separated frequencies

In some applications the communication system requires the coverage of two closely separated frequency bands. This feature is of interest specially at Ku band (12-18 GHz) where the two frequency bands of 12 and 14 GHz are used for up-link and down-link DBS satellite communications. In these cases the design of a dual-band reflectarray antenna is of notable advantage as suggested by figures 1.1 and 1.2.

Design of reflectarrays for closely separated frequency bands however are more subtle than those for large separation bands. Inside the cell we need structures with a varying parameter to control the phase-shift at a certain frequency. However due to the close proximity of the frequencies, structures for each frequency inside the cell have close sizes. This characteristic makes it difficult to integrate the structures inside the cell without physical overlapping (due to their size variation) or severe mutual coupling, specially for a single-layer geometry. The design becomes even more challenging if dual-polarized structures are required since they have to be vertically and horizontally symmetric.

In the literature various unit-cells are presented for closely separated frequencies. In [65] a two-layer cell geometry with two stacked split rings were proposed for dual-frequency operation in the two closely separated frequencies 7.4 and 8.9 GHz. In the proposed cell shown in figure 2.7, the split rings in each layer are placed orthogonal to each other in order to decouple their phase response at their own operational frequency. In other words the phase responses of the split rings became independent. With this decoupling technique however, the reflectarray becomes single-polarized at each frequency.

Figure 2.8 shows the unit-cell configuration for a dual-band operation at Ku band where two
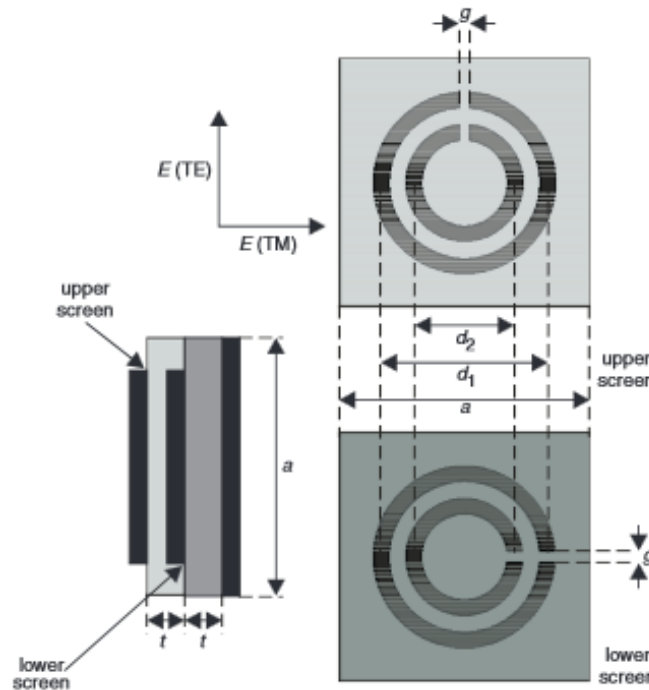
Figure 2.7: Two-layer unit-cell of reflectarray element for dual-band operation at 7.4 and 8.9 GHz. The variable for phase-shift regulation are d_1 and d_2 while other parameters are fixed to $a = 10mm, \epsilon_r = 3.54, t = 1.524mm, g = 0.2mm$. The cell is single-polarized at each frequency band. [65].

separate structures of split cross-loops and split rings are used for transmission centred around 14 GHz and reception centred around 12 GHz, respectively. The cell benefits from a simple single layer geometry and here also the splits are made in both structures and they are rotated 90° with respect to each other in order to minimize their mutual effect. As a result, similar to the example shown in figure 2.7, the reflectarray is single polarized at each frequency. Another example of a reflectarray operating at the close frequencies (12 and 14 GHz) is presented in [67] for DBS (Direct Broadcast Satellite) applications. The unit-cell, as shown in figure 2.9.a, consists of three stacked patches each with a different size. The unit-cell geometry provides the advantage of dual-polarized operation *at both frequency bands* due to both vertical and horizontal symmetry of the cell. However, in this case the patches have strong mutual coupling between them and therefore in the design procedure the patch sizes are optimized so as to fulfil the phase requirement at each frequency band. The fabricated reflectarray is shown in figure 2.9.b. In general, the structures proposed for closely separated frequencies are either multi-layer or lack dual-polarization performance in all the intended frequency bands. On one hand dual-polarization performance is essential for DBS satellites and on the other hand a multi-layer structure needs to undergo a time consuming optimization procedure. In addition, in a multi-layer structure the mechanical aspects of the reflectarray become more crucial which requires the usage of sophisticated substrates as in [67]. As a result, for DBS satellite systems a dual-polarized single layer structure would be of great benefit in terms of cost and
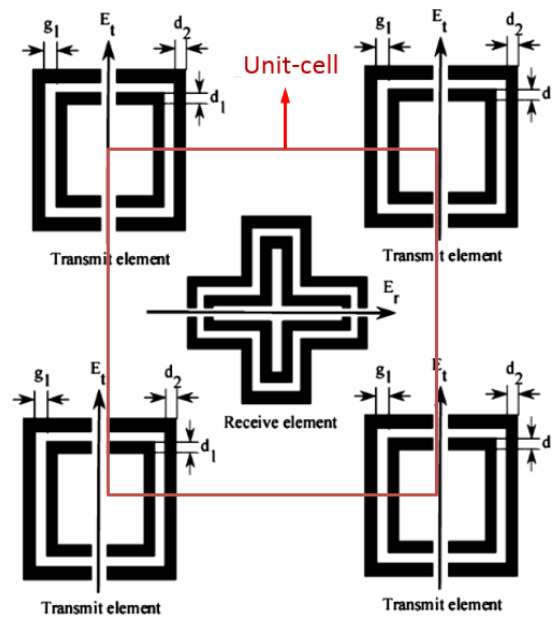
(a)
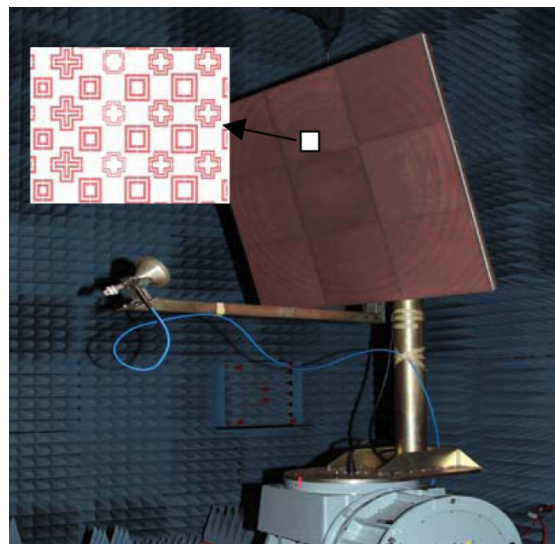
(b)

Figure 2.8: a)Single layer unit-cell for dual-band operation at 12 and 14 GHz b)The fabricated reflectarray [66].

mechanical stability.

2.3 Reflectarrays in THz, infrared and visible spectrum

In recent years, together with the increasing sophistication of designs enabled by the progress in the nanofabrication technology, the concept of reflectarray antenna has led to the design

(a)

(b)
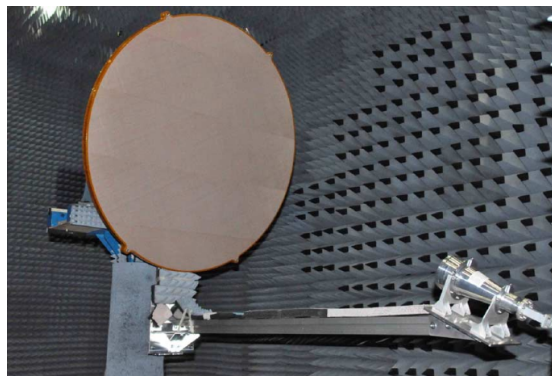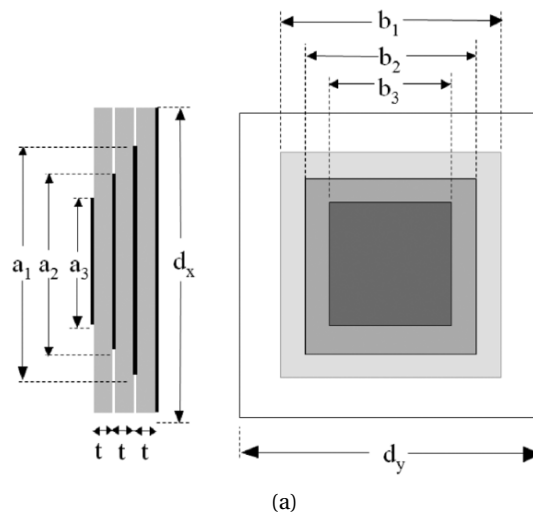
Figure 2.9: a)reflectarray element based on three-staked varying-sized patches for coverage at 12 and 14 GHz b)The fabricated reflectarray [67].

and fabrication of reflectarrays that are capable of deflecting an impinging plane wave to an arbitrary angle in Terahetz (0.3-3 THz), near infra-red (214-400 THz) and visible spectrum (430-790 THz).

Examples on the design, simulation and fabrication of reflectarrays at infrared can be found in [19–25] . The major issue in designing reflectarrays at these frequencies is the material losses which has been the focus of reported papers in the literature treated in more detail in [24]. Figure 2.10 shows a segment of the fabricated reflectarry reported in [20] which is composed of metallic patches performing at the wavelength 10.6 μm.

In the visible spectrum, the concept of reflectarrays have also been applied and their design and experimental results have been reported in the literature [26–28]. Figure 2.11 shows the schematic view and the fabricated sample of such a reflectarray antenna using cylindrical dielectric resonators with variable height as unit-cells [28]. The realized reflectarray creates beam deflection at the specular direction at the wavelength 633 nm corresponding to red light. As mentioned earlier, the DRA (Dielectric Resonator Antenna) cells are used due to their low
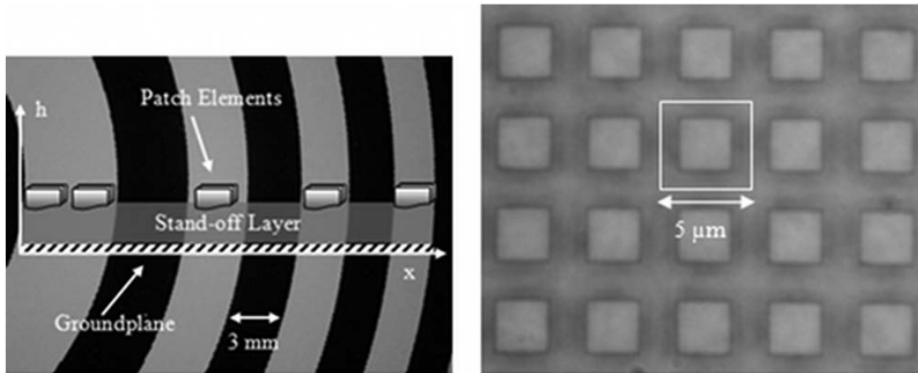
Figure 2.10: Fabricated reflectarray at infrared [20].

loss and hight efficiency at these frequencies as compared to the rapid efficiency degradation of metallic antennas at high frequencies. As such, for the cylindrical DRA the material TIO_2 is chosen with relative permittivity of 8.29 along the planar axes and 6.71 along the cylindrical axis and an estimated loss tangent lower than 0.01.

It should be noted that many reflectarrays in the optical region have been developed as a family of meta-surfaces which are planar arrays with sub-wavelength periodicity that enforce abrupt change in both the amplitude and the phase of an impinging plane wave. In [29] the wave deflection in reflection and transmission has been demonstrated under the name of anomalous reflection and refraction. The reflectarray/transmitarray uses V-shaped dipoles as unit-cell as shown in figure 2.12. The resulting device manipulates the polarization and the direction of the out-going wave both in reflection and transmission. Based on the same idea, out-of-plane reflection and refraction by meta-surfaces has been reported in [30–33].
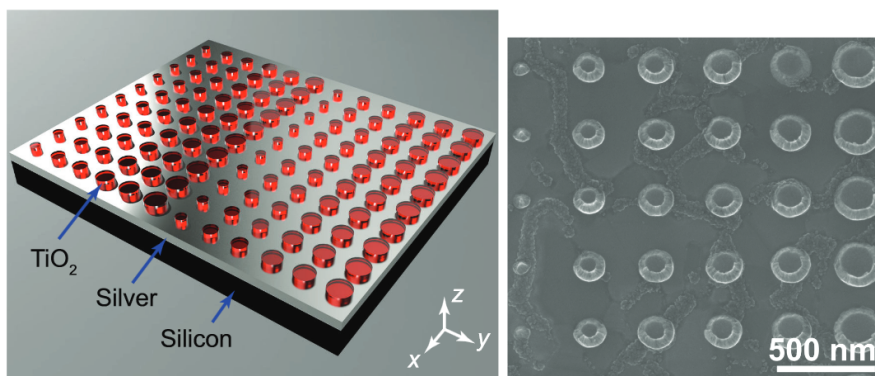
Figure 2.11: Fabricated reflectarray at visible frequencies (at wavelength 633 nm) [28].

Reflectarrays at THz

Terahertz (THz) technology has rapidly become the focus of recent research in electromagnetism, due to its numerous applications in stand-off security scanning, biology and medical
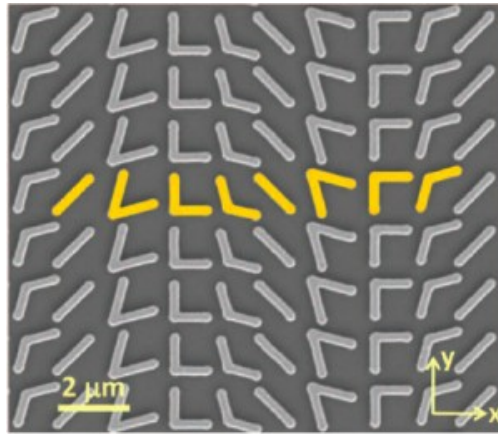
Figure 2.12: Fabricated meta-surface using V-shaped dipoles [29].

sciences and broadband short-range wireless communication systems [38]. One of the prominent topics in this field has been to manipulate the THz incoming wave using reflectarray surfaces. In the THz region, the performance of reflectarray antennas has experimentally been demonstrated in [2, 34, 35] using a planar array of golden patches and dipoles on a polydimethylsiloxane (PDMS) substrate with platinum as the ground plane.

The devices are capable of deflecting the incoming wave to a pre-designed direction and/or to decompose the incoming wave into its orthogonal TE and TM polarizations and deflect each of them to an arbitrary direction (see figures 2.14 and 2.13).

Recently, in [36] it has been shown that, with the proper choice of the cell parameters, one can control the deflection angle versus frequency (see figure 2.15). The unit-cell is composed of a thin aluminium film, a BCB (Benzocyclobutene) dielectric layer with thickness 120 μm and an aluminium pattern on top. As shown in the figure 2.15.a, the unit-cell is composed of two rectangular rings and a thick dipole at the center. By properly choosing the cells parameters, at 250 GHz a linearly phase response can be obtained. With the optimized cell parameters, the device radiation pattern will have the frequency dependent behaviour shown in figure 2.15.b. However, the resultant device has limitations in terms of angle-vs-frequency relation due to the high inter-element coupling inside the cell. In other words, the device cannot achieve a completely independent deflection angle at each frequency.

2.4 Conclusion

In this chapter we reviewed some of the important reported multi-band reflectarrays in the literature. It was shown that reflectarrrays can provide a low-cost solution by performing independently at different frequencies, a characteristic that is very difficult to achieve with conventional parabolic reflectors. In particular, multi-band reflectarays with closely separated operational frequency bands are of interest in satellite communication systems, specially at

(a)

(b)
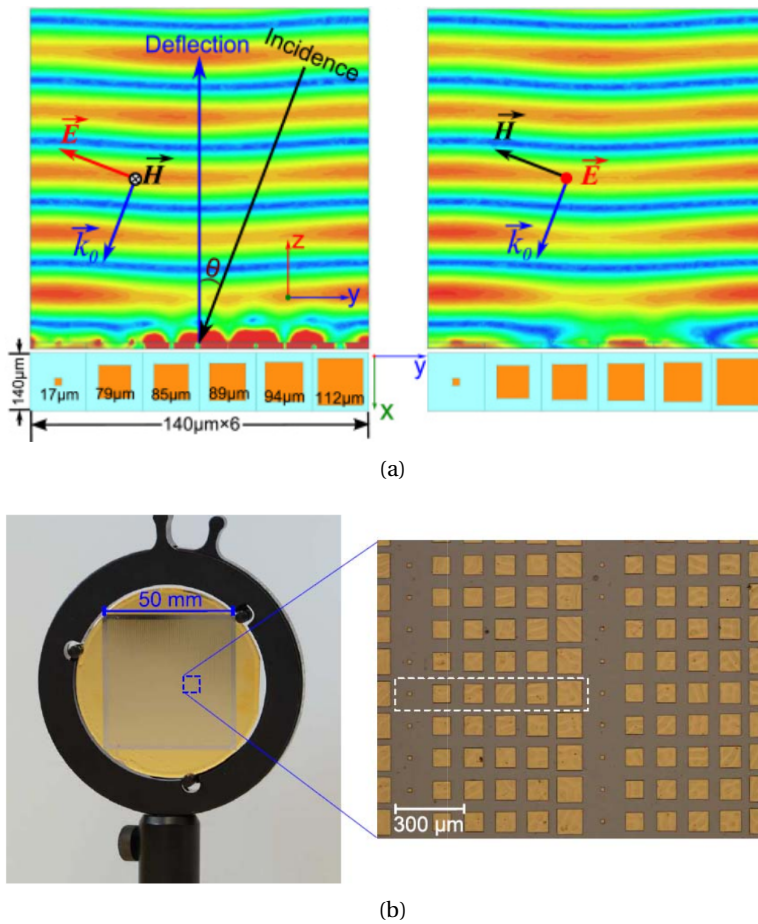
Figure 2.13: Fabricated reflectarray at 1 THz. a) The reflectarray deflects a plane wave with incidence angle of 30° to broadside direction for both TE and TM polarized waves. b) The fabricated prototype [34].

Ku band where we have DBS geostationary satellites. A multi-band, dual-polarized reflectarray antenna at Ku band would be able to establish simultaneous wireless connections with several satellites at different positions operating at different frequencies.

Finally, this chapter presented existing reflectarrays (or meta-surfaces) performing at THz, infrared and visible light. It was shown that, reflectarrays at these frequencies are in fact the down scaled version of those at microwave frequencies except that, we have a plane wave as a source instead of a feed-horn. In addition, the material losses are the major concern for reflectarrays performing at higher frequencies.
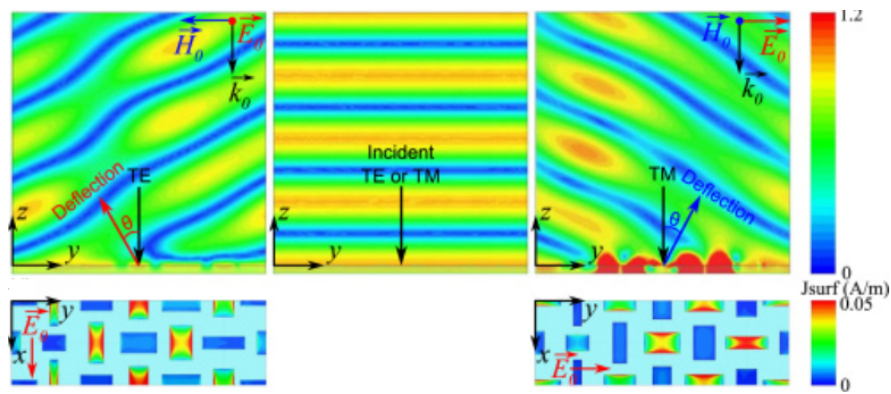
(a)
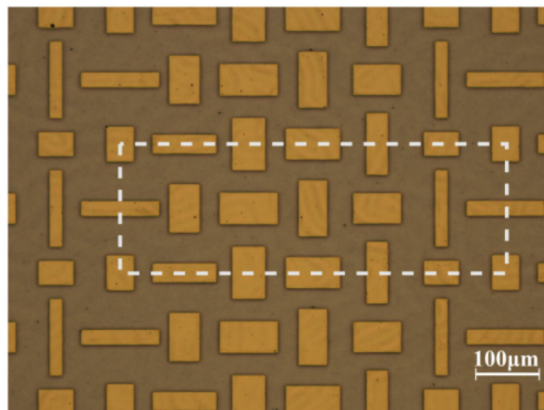
(b)

Figure 2.14: Polarizing beam splitter reflectarray at 1 THz a)When the incident wave is impinging normally to the surface of the reflectarray, the TE and TM polarized wave are deflected into two different directions with the angles of -30° and +30°. b) Fabricated reflectarray. [2].
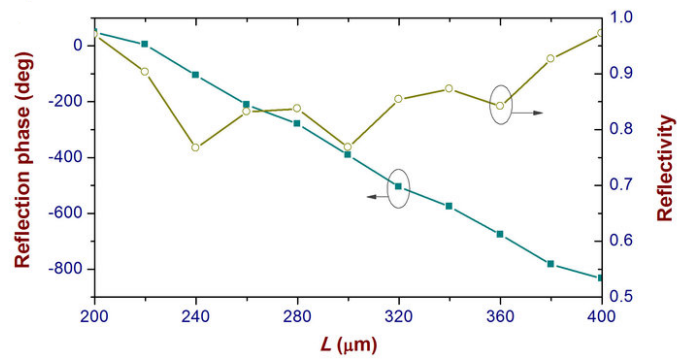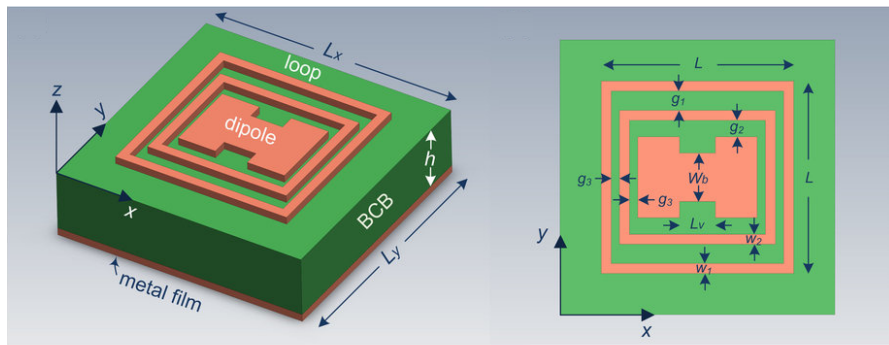
(a)
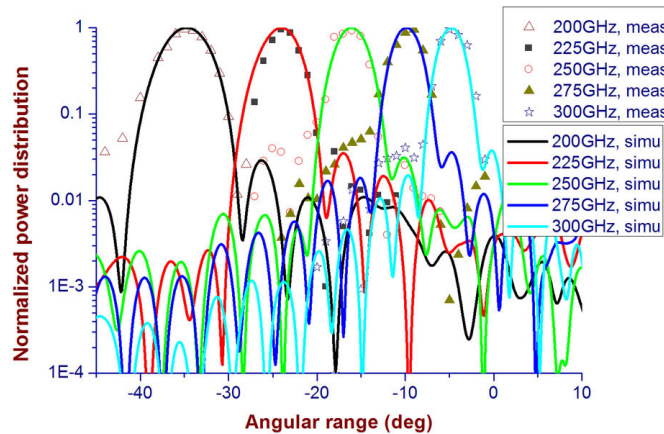
(b)

Figure 2.15: THz reflectarray with frequency dependent beam deflection. a) The unit-cell is composed of two rectangular rings and a thick dipole in the center. By proper selection of the cell parameters, a linear phase response is obtained based on the varying parameter of the cell L at 250 GHz b) With the above phase response, the reflectarray antenna demonstrates a frequency dependent deflection versus frequency [36].

3 Theory and Design of a Printed Reflectarray Antenna

This chapter deals with the general procedure towards designing a printed reflectarray antenna, either with a feed horn or an impinging plane wave as the source. The main disadvantage of a reflectarray antenna is its narrow bandwidth performance. This issue is discussed in section 3.3 where the behaviour of an ideal cell for theoretical infinite bandwidth (i.e that of a parabolic reflector) is described. As state-of-the-art, subsections 3.4.1 and 3.4.2 present unit-cells that approximately mimic the behaviour of an ideal cell and those that can solve the narrow bandwidth issue with multi-band performance. Furthermore, application, advantages and disadvantages of each type of unit-cell will be explained. In addition, this chapter presents the versatile prism, which is basically a frequency-scanning reflectarray antenna whose outgoing beam direction has a pre-designed relationship with frequency. It is evident that, a broadband reflectarray would be a special case of a versatile prism. Challenges and suitable unit-cells will be discussed for the realization of such devices.

3.1 Performance principle of a printed reflectarray

As schematically shown in figure 3.1, a printed reflectarray antenna is an array of elements (also known as cells) on a grounded substrate and illuminated by a radiating point source (usually a horn antenna). A particular parameter of each cell is chosen in order to manipulate the phase of the reflected wave. This parameter can be the length of a printed dipole, size of a patch, the permittivity of the grounded substrate, the length of a slot, the element's rotation angle (in case of circular polarization), etc. As a special case, if simple printed patches are used, by the proper selection of the size of each patch, an arbitrary phase distribution is created on the array surface and hence, a desired beam shape can be obtained at the antenna far-field. Later we will explain how to obtain the phase-shift versus element size relationship. In most cases we want to direct the antenna beam to a specific direction. According to the phased-array antenna theory [8], in order to have the outgoing beam directed to $(\theta_{out}, \phi_{out})$ at the antenna far-field, the array must have the following reflection phase distribution on its

surface:

$$\phi_R(x_i, y_i) = -k_0 sin\theta_{out} cos\phi_{out} x_i - k_0 sin\theta_{out} sin\phi_{out} y_i \tag{3.1}$$

Where k_0 is the propagation constant in vacuum, and (x_i, y_i) are the coordinates of the ith element. Additionally, if we have a point source as the feed, we know that the reflection phase off an element equals the summation of the phase change due to the propagation from feed to each element and the reflection phase of the element itself:

$$\phi_R(x_i, y_i) = -k_0 d_i + \phi_E(x_i, y_i) \tag{3.2}$$

Where d_i is the distance between the feed and the ith element , and $\phi_E(x_i, y_i)$, is element's reflection phase which depends on its structure parameters (ex: length of dipole in case of using printed dipoles). From 3.1 and 3.2 the required element phase reflection denoted by $\phi_E(x_i, y_i)$ can be obtained:

$$\phi_E(x_i, y_i) = k_0 d_i - k_0 sin\theta_{out} cos\phi_{out} x_i - k_0 sin\theta_{out} sin\phi_{out} y_i \tag{3.3}$$

From $\phi_E(x_i, y_i)$ the corresponding parameter of the ith element can be specified. As an example, figure 3.2 shows a typical element phase reflection for a reflectarray consisting of 30×30 elements arranged in a rectangular grid in order to point the beam to broadside direction at the far-field. The surface is illuminated by a point source placed 290 mm above and perpendicular to the array center (i.e. a center-fed reflectarray) and the grid spacing is $\lambda/2$ at 12 GHz. In case we limit the phase-shift to $0° < \phi_E < 360°$, the required phase-shift becomes as shown in figure 3.2.b.

On the other hand, if we have a plane wave with an incident angle of (θ_{in}, ϕ_{in}) as the illuminating source, and we desire to deflect the outgoing beam to $(\theta_{out}, \phi_{out})$, the reflection phase, $\phi_R(x_i, y_i)$, will then be the summation of the phase due to the incident plane wave and the element's reflection phase. In this case, the required element reflection phase will become:

$$\phi_E(x_i, y_i) = -k_0 x_i(sin\theta_{in} cos\phi_{in} + sin\theta_{out} cos\phi_{out}) - k_0 y_i(sin\theta_{in} sin\phi_{in} + sin\theta_{out} sin\phi_{out}) \tag{3.4}$$

Figure 3.3 shows a 2D schematic view of a reflectarray having the illuminating source as an incident wave from $(\theta_{in}, \phi_{in} = 180°)$ and with designed deflected (or outgoing) beam to $(\theta_{out}, \phi_{out} = 0°)$. Since in this case $\phi_E(x_i, y_i)$ and hence the size of the elements, does not depend on y_i, the array is shown in the xz plane. Through out the thesis, reflectarray surfaces with an incident wave as illuminating source, are treated and designed based on this view.
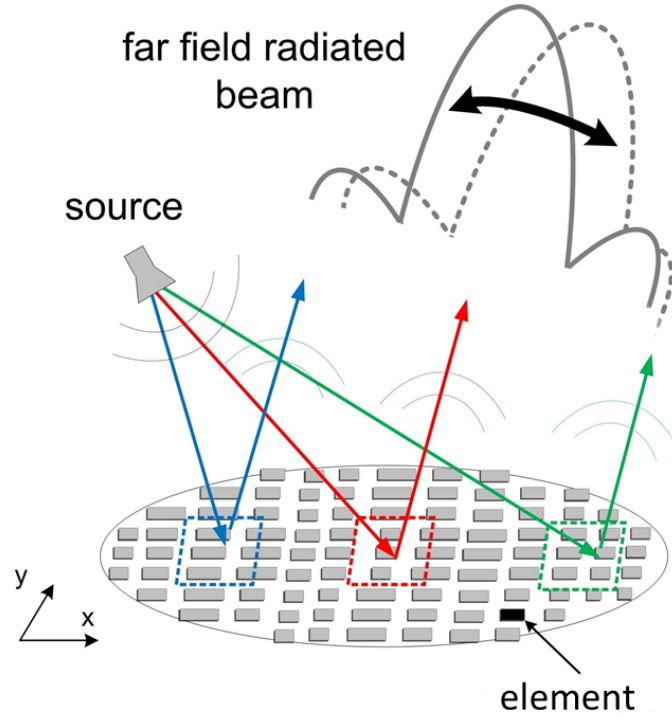
Figure 3.1: Schematic view of a reflectarray antenna. The size of each element is specified in a way so as to compensate the element-to-feed phase-shift and produce the required phase distribution on the array.

3.2   Elements reflection phase: unit-cell design

As mentioned in the previous section, once the required $\phi_E(x_i, y_i)$ is obtained, we only need to place at (x_i, y_i) an element which has such a reflection phase. In order to obtain the relationship between an element's size and its reflection phase, i.e. element phase response, we can impinge a plane wave upon the element with a certain size and numerically (or if possible analytically) calculate the phase of the reflected wave with respect to the phase of the impinging wave. However, since the element is going to be placed in an array, one must consider the effect of the surrounding elements as well. To this aim, we assume that each element on the array is surrounded by an infinite array of elements with the exact size of its own which gives rise to an infinite periodic structure. The analysis of a periodic structure in electromagnetism is carried out using Floquet's Theory [68] in particular for structures known as Frequency Selective Surfaces (FSS) first introduced in [69] and on which a through discussion is provided in [70]. Therefore, in order to obtain the elements reflection phase, we deal with an FSS implemented out of the same element. As an example, consider figure 3.4 where a periodic array (FSS) of arbitrary shaped elements in a rectangular grid are illuminated by an impinging plane wave with wave number denoted by $\vec{k}$, i.e. :

$$\vec{E}_{in} = \vec{E}_0 e^{j\vec{k}.\vec{r}}, \qquad \vec{k} = k_0(sin\theta_{in}cos\phi_{in}\vec{e}_x + sin\theta_{in}sin\phi_{in}\vec{e}_y + cos\theta_{in}\vec{e}_z) \tag{3.5}$$
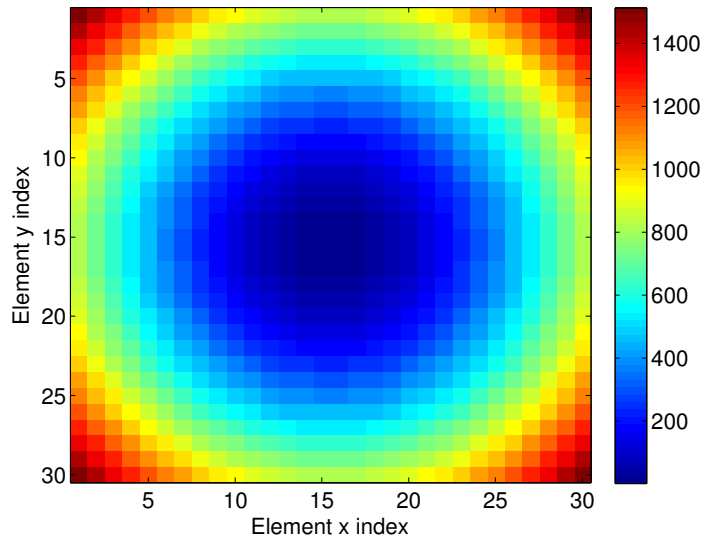
(a)
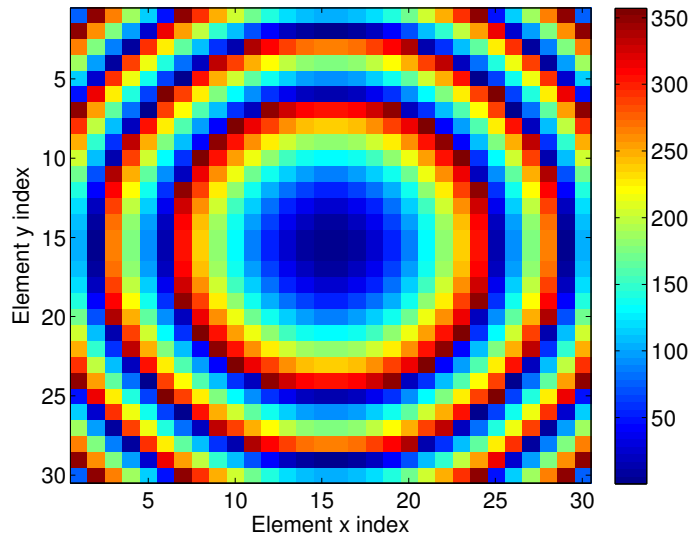
(b)

Figure 3.2: Typical required phase-shift for the elements of a reflectarray antenna. a) un-wrapped phase b) phase limited to 0° to 360°.

wherein (θ_{in}, ϕ_{in}) are the angle of incidence. In this case, since the structure is assumed to be infinite, the fields are periodic along the x and y axis with phase shift of $\Delta\phi_x = d_x sin\theta_{in} cos\phi_{in}$ and $\Delta\phi_y = d_y sin\theta_{in} sin\phi_{in}$, respectively. The reflection characteristic of such an array can therefore be analysed by putting a single element inside a waveguide with Periodic Boundary Condition (PBC) as shown in Figure 3.5 representing the unit-cell. The PBC will force the fields on each of the two lateral walls of the waveguide facing each other along the x and y directions
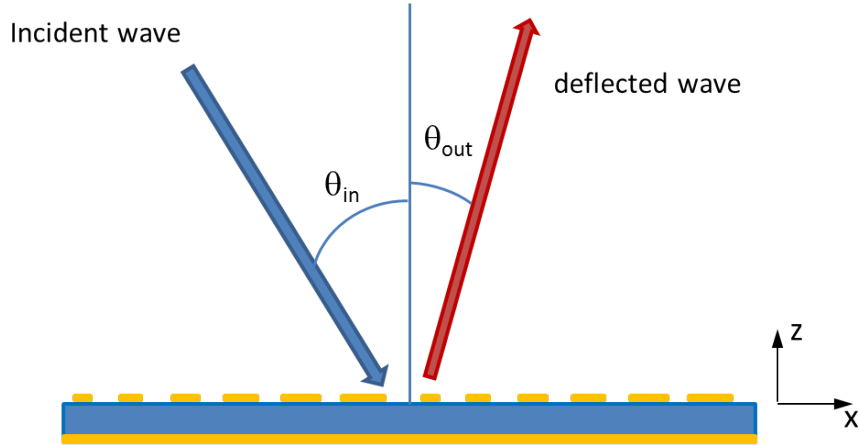
Figure 3.3: 2D schematic view of a reflectarray surface. The principle of the deflection is the same as that of a reflectarray antenna except that here we have a plane wave as the illuminating source.

to be equal except for the above mentioned phase-shifts. In other words for the lateral walls along y axis we have:

$$\vec{E}(x,0) = \vec{E}(x,dy)e^{j\Delta\phi_y}, \qquad \Delta\phi_y = d_y sin\theta_{in}sin\phi_{in} \qquad (3.6)$$

and for the lateral walls along x axis we have:

$$\vec{E}(0,y) = \vec{E}(dx,y)e^{j\Delta\phi_x}, \qquad \Delta\phi_x = d_x sin\theta_{in}cos\phi_{in} \qquad (3.7)$$

The analysis of such a waveguide is beyond the scope of this thesis and interested reader is referred to [70] where more elaboration is performed. However we simply consider important out-comes of the PBC waveguide for reflectarray antenna design. The unit-cell of figure 3.5 supports the propagation of evanescent and non- evanescent TE_{pq} and TM_{pq} Floquet modes, where p and q denote the mode number. For the reflectarray design purposes we are only interested in non-evanescent TE_{00} and TM_{00} modes which are in fact simple plane waves with orthogonal polarizations with respect to each other. Furthermore, according to periodic structures theory, the cut-off frequency for the onset of the second pair of (TE/TM) non-evanescent modes, are in fact the cut-off frequency for the onset of unwanted grating lobes for a reflectarray antenna. In other words, propagation of higher order non-evanescent modes in a unit-cell must be avoided, since it will result in appearance of grating lobes in the reflectarray far-field region. As a result, in the design process of reflectarray antennas, we should follow the conventional condition established for phased-array antennas in order to rule out the unwanted grating lobes:

$$d < \frac{\lambda}{1 + sin\theta_{out}} \qquad (3.8)$$

where we assume $d_x = d_y = d$, and θ_{out} is the angle of the outgoing beam.
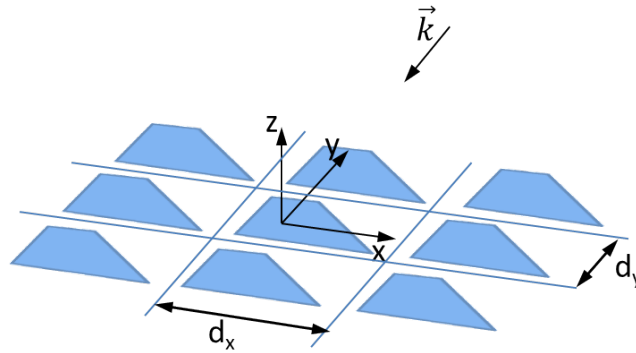
Figure 3.4: Schematic view of an FSS with arbitrary shaped elements illuminated by a plane wave.
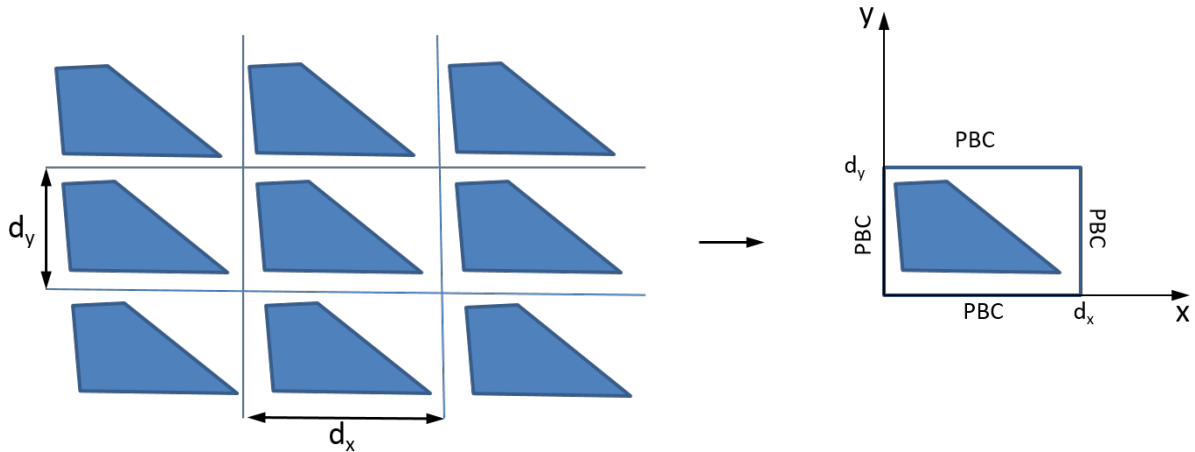
Figure 3.5: Schematic view of an FSS with arbitrary shaped elements represented by its equivalent unit-cell.

Unit-cell simulation

In order to analyse the unit-cell, we will employ a Finite Element Method (FEM) [71] embedded in CST Microwave studio [72]. Figure 3.6.a shows an example for simulation of a unit-cell in order to obtain its reflection phase versus the element size, denoted here by L, at 12 GHz. A periodic boundary condition is assigned to the lateral walls. The element is a simple cross-dipole printed on a grounded substrate with 0.787 mm of thickness and a relative permittivity of 2.33. The unit-cell can be excited by different Floquet modes with different incident angles. However, since we are always following the condition of the equation 3.8, the unit-cell is always excited with the TE_{00} and TM_{00} orthogonal Floquet modes, each of which in fact corresponds to a simple plane wave. The reflection coefficient of such a cell is shown in Figure 3.6.b in which, the green curve, combined with equation 3.3, is used to determine the

size of each element on the reflectarray surface. The blue curve stands for the losses of the cell which ideally is 0 dB. However due to the losses in the substrate and the metallic losses of the element(s), it is always less that 0 dB. A through discussion about the cell losses and how to reduce them can be found in [73].

(a) 3D view
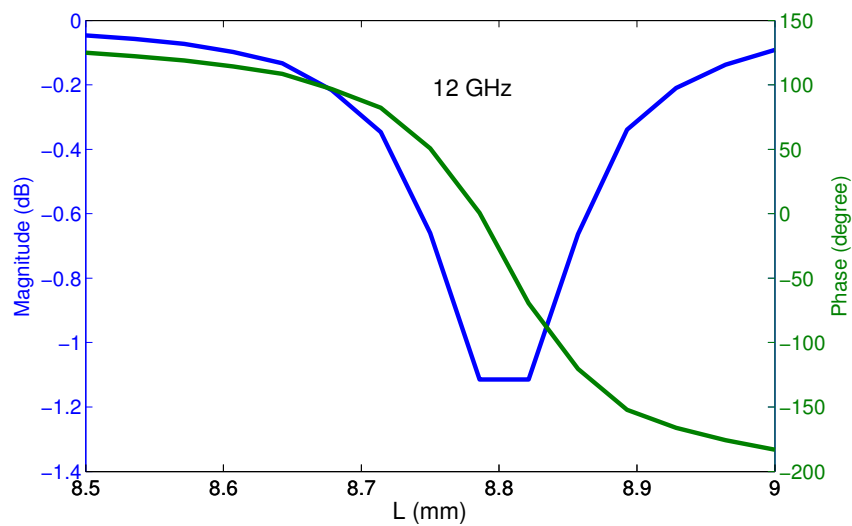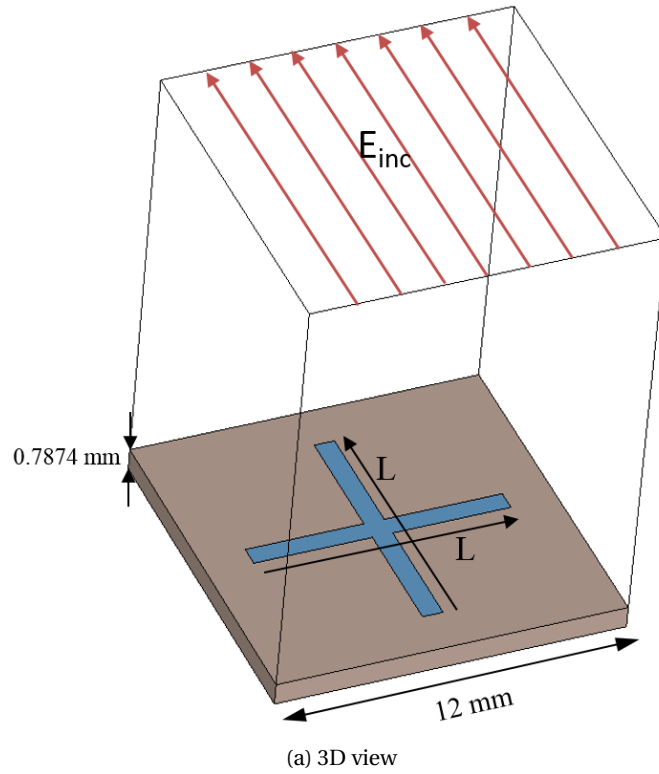
(b) phase and amplitude response of the unit-cell

Figure 3.6: Unit-cell simulation setup along with its phase and amplitude response. The blue curve is interpreted as the unit cell's losses which is due to the substrate losses.

3.3   Ideal unit-cell for broadband operation

As mentioned in the previous chapter, the main concern in reflectarray antennas, has been to enhance their operational bandwidth. By broadband performance, we mean that, the out-going beam's direction would not change with the frequency, and as a result reflectarray would demonstrate the performance of a parabolic reflector with its inherent theoretical infinite bandwidth. In reflectarry antennas the bandwidth is determined by the gain-vs-frequency curve of the antenna in the designed direction. A 3 dB bandwidth would be the frequency span between the minimum and maximum frequency where 3 dB gain drop occurs with respect to the antenna gain at the designed frequency. In order to investigate more closely this issue, we consider a simple 2D reflectarray surface with an incident plane wave as the illuminating source as shown in figure 3.3. (Note that the following arguments applies as well to a reflectarray antenna illuminated by a feed-horn and it is out of shear clarification that a 2D reflectarray surface is chosen). If we choose the parameters as $(\theta_{in}, \phi_{in} = 180°)$ and $(\theta_{out}, \phi_{in} = 0°)$, we obtain the required reflection phase of each cell:

$$\phi^i_{cell} = -k_0 x_i (\sin\theta_{out} - \sin\theta_{in}) + \phi^0_{cell} \tag{3.9}$$

Wherein, ϕ^0_{cell} is the phase of the 0th element (reference element) placed at $x_0 = 0$. This term has been added since the required phase of each element is obtained with respect to a reference element on the array surface. The above equation shows that, if we desire to keep the direction of the out-going beam invariant with respect to the frequency (an infinite bandwidth), the reflection phase of the cell must vary linearly with frequency. Suppose that we have such a cell with the following phase response in terms of frequency f:

$$\phi_{cell} = Af + B \tag{3.10}$$

where A and B depend on the cell's structure. If the design of the reflectarray is based on this ideal cell, then we only have to find A and B for the ith cell (denoted by A_i and B_i):

$$\phi^i_{cell} = A_i f_0 + B_i \tag{3.11}$$

if we designate the reference cell with ϕ^0_{cell} on the reflectarray surface then by equating 3.11 and 3.9 we get:

$$A_i f + B_i = -k_0 x_i (\sin\theta_{out} - \sin\theta_{in}) + \phi^0_{cell}, \qquad \phi^0_{cell} = A_0 f + B_0 \tag{3.12}$$

Knowing that $k_0 = \frac{2\pi f}{c}$, we can obtain the values of A_i and B_i for the ith cell placed at x_i on the surface:

$$A_i = \quad A_0 - \frac{2\pi}{c} x_i (\sin\theta_{out} - \sin\theta_{in}) \tag{3.13}$$

$$B_i = \quad\quad\quad B_0 \tag{3.14}$$

where c is the speed of light. This kind of cell, is also called a true-time delay cell in analogy to phased-array antennas in which true-time delay phase-shifter are used to avoid beam squint with frequency.

3.4 State of the art

3.4.1 True-time delay cells

True-time delay cells are used in reflectarray antennas for broadband operation in [48], [89] and [49]. In the cell introduced in [49], the phase regulation is accomplished by varying the length of the delay line (i.e. the transmission line). The cell with its phase response is shown in figure 3.7. It was shown that, in a certain frequency band, the phase response of the cell has the following linear relationship with frequency:

$$\phi_{cell} = -2\beta L + \phi_0, \qquad \phi_{cell} = (-2\frac{2\pi\epsilon_{eff}}{c}L)f_0 + \phi_0 \qquad (3.15)$$

where L and ϵ_{eff} are the length and effective permittivity of the transmission line, respectively. In this case since the value of ϕ_0 is the same for all the delay line lengths, for equation 3.3, we have:

$$A = \quad (-2\frac{2\pi\epsilon_{eff}}{c}L) \qquad (3.16)$$
$$B = \quad \phi_0 \qquad (3.17)$$

Therefore, for each cell, the corresponding length can be obtained. It should be noted that, this linearity holds for a certain bandwidth, since the coupling of the incident wave through the slot into the transmission (delay) line, is only feasible in a certain frequency band. Based on the above elaboration, in general cells with a rather smooth phase response i.e. loosely linear, will exhibit a broadband performance.

3.4.2 Resonant cells

Resonant cells are the most commonly used cells in the design of reflectarray antennas. They are usually single-layer (or multi-layer) structures consisting of elements (dipole, cross-dipole, ring, patch, etc) printed on a grounded substrate. A simple single-layer cell using patch elements was first introduced in [42]. However, the cell demonstrates a non-linear S-shaped phase response (figure 3.6) with respect to its varying parameter which limits the operational bandwidth to 4-5%. In order to increase the bandwidth for resonant cells, one could increase the substrate thickness which results in smoother phase response at the expense of reduced phase range. Now in order to increase the phase range, one can increase the number of layers as proposed in [50] and [51]. One example [50] is shown in figure 3.8 where a two layer structure is used resulting in a linear phase response and thus a broadband performance.

(a) true-time delay cell
structure

(b) true-time delay cell phase response
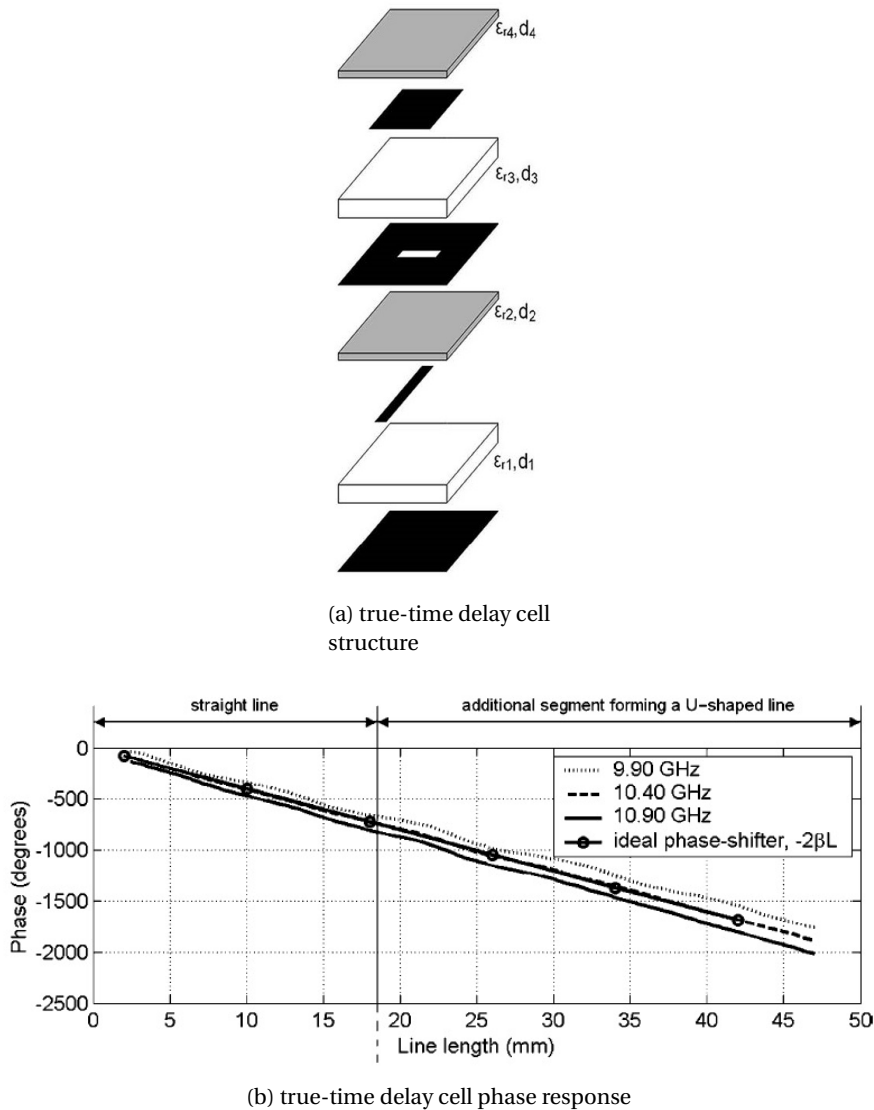
Figure 3.7: True-time delay, aperture-coupled cell with linear phase response for broadband reflectarray antennas [49].

Here the varying cell parameter for phase regulation is $a_2(= 1.42a_1)$ so that, when the size of the lower patch i.e. a_2 is growing, its resonance at the frequency f_0 will immediately be followed by the resonance of the upper smaller patch with the size a_1, which in the end results in the rather linear phase response shown in figure 3.8.b. Another method, which avoids a multi-layer structure, would be to employ several resonant elements on a thick substrate in the cell as proposed in [55], [52], [53] and [54]. In practice, these are cells containing elements that have very close resonance frequencies. This fact, combined with a thick substrate generates a rather linear phase response with adequate phase range as shown, for example, in figure3.9. In this work [55], the regulating parameter is designated as l_0 based on which, other dipoles lengths are chosen as $l_0 = 2l_2 = 1.53l_1$. The resultant reflectarray exhibits 1 dB gain bandwidth

of 35.41% which for a reflectarray antenna, is very satisfying. It should be mentioned that, the fact that the out-going beam is in the broadside direction and the design is center-fed, positively contributes to the bandwidth improvement according to [74].
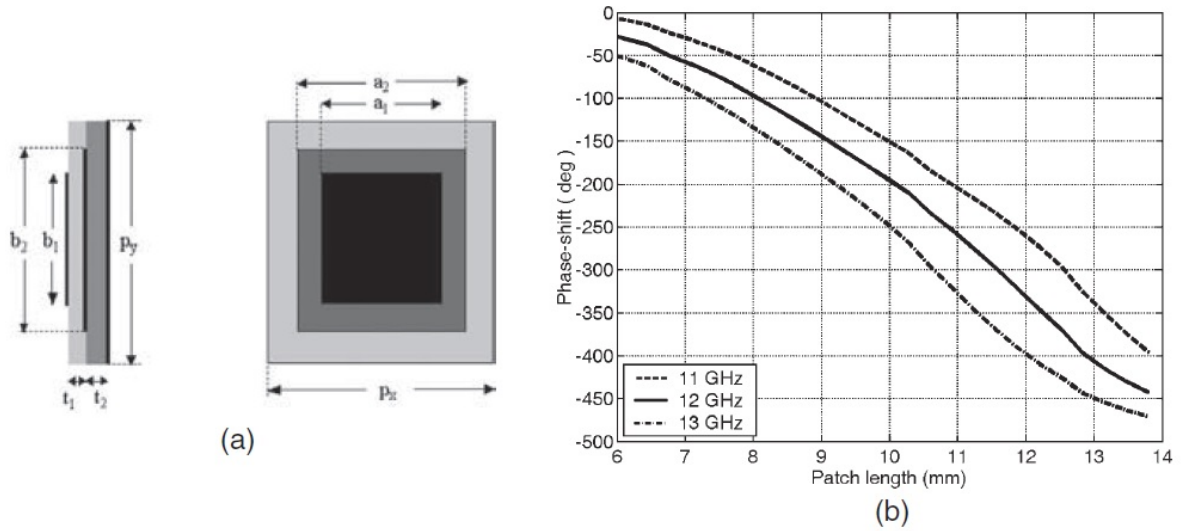
Figure 3.8: Two-layer stacked patch cell with linear phase response for broadband reflectarray antennas. a) the structure with parameters ($a_1 = b_1, a_2 = b_2, P_x = P_y = 14mm, t_1 = t_2 = 3mm, a_1 = 0.7a_2$) b) Resulting phase response [50].

3.5 The versatile flat prism

A versatile prism is in fact a reflectarray surface for which, the out-going beam direction has a pre-designed relationship with frequency. In this section we intend to introduce a cell that can be used for such a device. However before going onto the details of the challenges and requirements of such a device, the mechanisms that demonstrate the frequency agility behaviour are presented. However none of them can be designed in such a way to demonstrate a completely arbitrary frequency-vs-angle profile. This has been the main motivation to use the reflectarray antenna concept to extract any arbitrary frequency-vs-angle profile from the resultant flat device specially at microwave frequencies. In other words, the current devices will become each an special case of a versatile flat prism.

3.5.1 State of the art

The most typical device with frequency-agile behaviour is a prism. In optics a prism (figure 3.10) is a transparent optical element with flat polished surfaces that refracts light. It is typically made from any material that is transparent to the wavelengths for which it is designed. Typical materials include glass, plastic and fluorite. Due to the dispersive nature of its materials, a prism can be used to decompose a white light into its constituent wave lengths

(a)

(b)
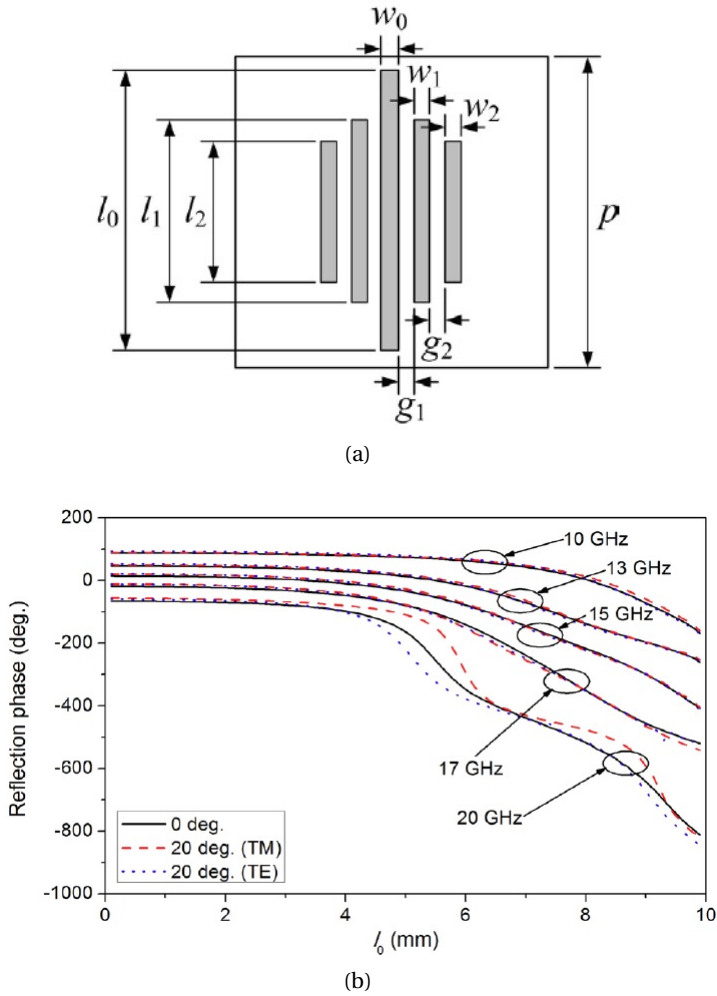
Figure 3.9: A multi-resonant single layer a) The structure b) phase response. ($g_1 = g_2 = w_0 = w_1 = w_2 = 0.5mm, l_1 = 0.65l_0, l_2 = 0.5l_0, f_0 = 15GHz, \epsilon_r = 2.2, h = 3.175mm$) [55].

(i.e. colors). Depending on the shape of a typical prism, and the relationship of the refractive index of its material ($n(\lambda)$), the angle of refraction-vs-frequency,(angle-vs-color) can easily be obtained by tracing a sample ray through the dispersive prism and using Snell's law at each interface. As an example, consider figure 3.11 where a dispersive prism with refraction index $n(\lambda)$ is surrounded by air. In this case, if we have an impinging wave with incidence angle θ_{in}, the out-going beam direction θ_{out} versus frequency, for this particular prism geometry, is obtained as follows:

$$\theta_{out}(\lambda) = arcsin\left(n(\lambda)\sin\left[\alpha - arcsin\left(\frac{1}{n(\lambda)}\sin\theta_{in}\right)\right]\right) - \alpha \tag{3.18}$$

Although with different prism structures and geometry, many different frequency-vs-angle profiles can be achieved, but not *any* relationship. In addition a prism becomes very bulky and difficult to handle in microwave frequencies.

Interested reader is referred to [75] for more detailed discussion on the principles of a dispersive prism as well as gratings that demonstrate similar behaviour.
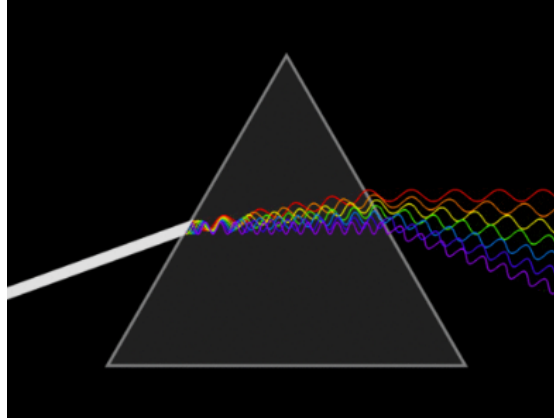
Figure 3.10: A typical dispersive prism.
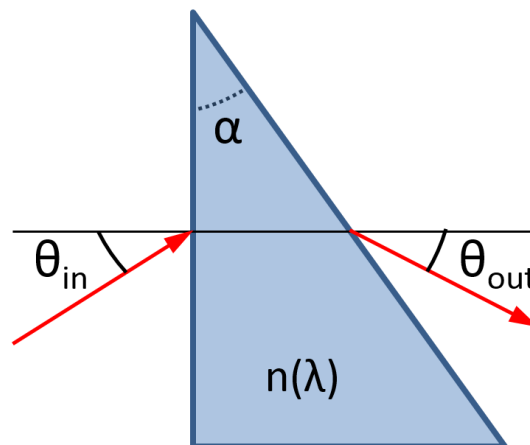
Figure 3.11: Schematic view of a typical dispersive prism in the air.
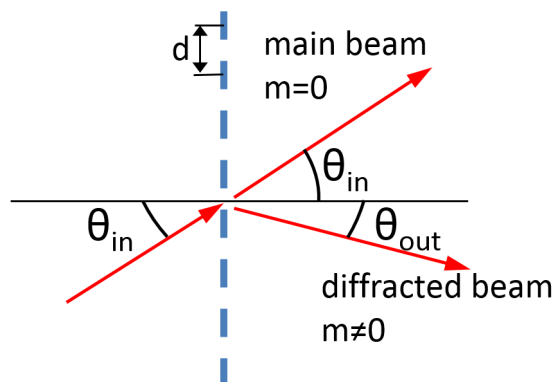
Figure 3.12: Schematic view of a simple grating.
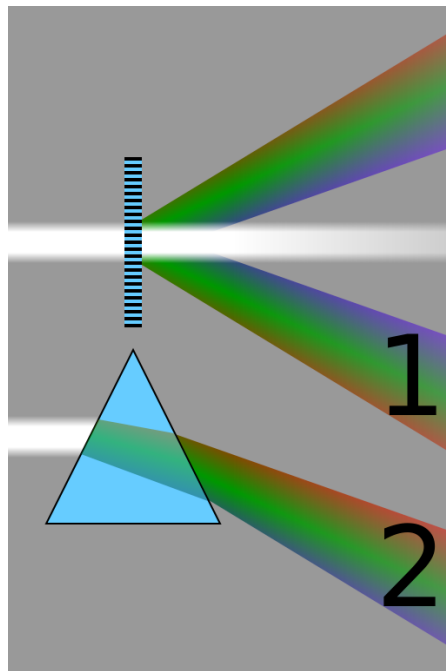
Figure 3.13: Comparison of the spectra obtained from a diffraction grating (1) and a prism (2).

Figure 3.14: The grooves of a compact disc act as a diffraction grating.

A similar device to a prism that demonstrates frequency agile behaviour is a diffraction grating. A diffraction grating in optics, is a periodic structure which, by proper choice of its periodicity d, can split the impinging light and break it into its colors, diffracted to different directions. A schematic view of a simple grating is shown in figure 3.12 where the elements are separated by the periodic distance d. In this case for the out-going diffracted beam we have:

$$\theta_{out}(\lambda) = arcsin\left(\frac{m\lambda}{d} - \sin\theta_{in}\right)$$
(3.19)

Where m is an integer number that can take up any integer number as long as the absolute value of the argument of $arcsin(*)$ is smaller than or equal to unity. As shown in figure 3.12, in addition to the main beam containing all the frequencies (when $m = 0$ in 3.19), there is a diffraction where each frequency has a different direction (correspondin to $m \neq 0$). Figure 3.13

compares a conventional prism and a diffraction grating when illuminated by white light with a normal incidence ($\theta_{in} = 0$). As shown, contrary to a dispersive prism, here lower frequencies (e.g red light) are more *refracted* than higher frequencies (e.g violet) with respect to the broadside. We should note that, the diffracted colors in case of a grating are equivalent to the grating lobes of array antennas that have a frequency dependent angle and where the out-going white light in the broadside direction corresponds to the main beam of an array antenna. Figure 3.14 shows an ordinary compact disk which is an every-day example of diffraction grating due to the fact that, the grooves of a compact disk act as a grating. The effect can easily be verified by reflection of sunlight from a compact disk onto a white wall.

In the literature, there has been many attempts to achieve non-conventional diffraction/refraction using various methods and technologies. In [76], the photonic crystals fabricated on Silicon (shown schematically in figure 3.15), demonstrate an extremely wavelength dependent beam steering such that, with only a 1% shift of incident wavelength at around $1\mu m$, the scanning span reaches 50°. The resulting angular dispersion is two orders of magnitude larger than that achieved with conventional prisms or gratings.
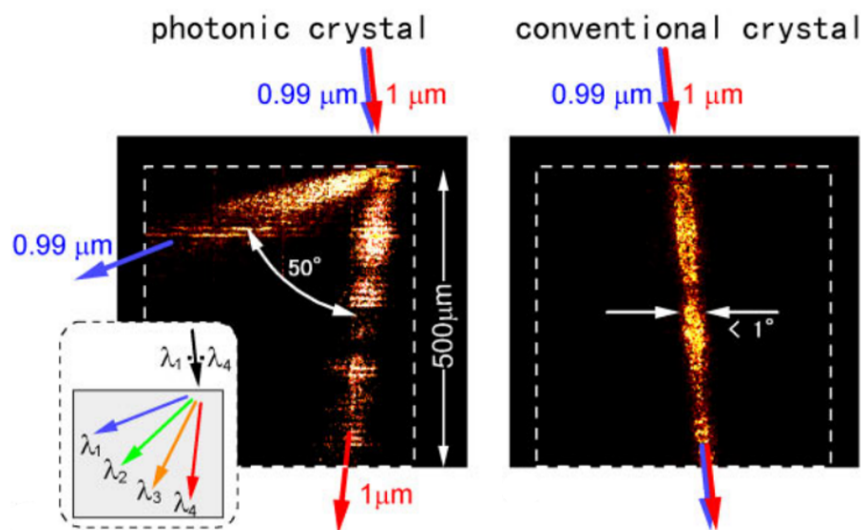
Figure 3.15: Photonic crystal fabricated on Silicon with extreme wavelength dependent steering behaviour. Two incident waves of wavelengths $0.99\mu m$ and $1\mu m$ are refracted with angular difference 50° [76].

In [77], a metamaterial lens is introduced with a reverse chromatic aberration, i.e. a lens with a focal length increasing with frequency in the 83-130 GHz range. As shown in figure 3.16, the lens is a flat multi-layer structure with capacitive and inductive printed elements similar to a transmit-array. In the design process, each printed element size is optimised in order to achieve a desired transmission phase response in terms of frequency. With this procedure, the proper transmittal phase distribution at each frequency can be obtained on the lens surface and hence a desired frequency-vs-focal length profile can be achieved.

Another interesting example of frequency agile devices is presented in [78] where based on
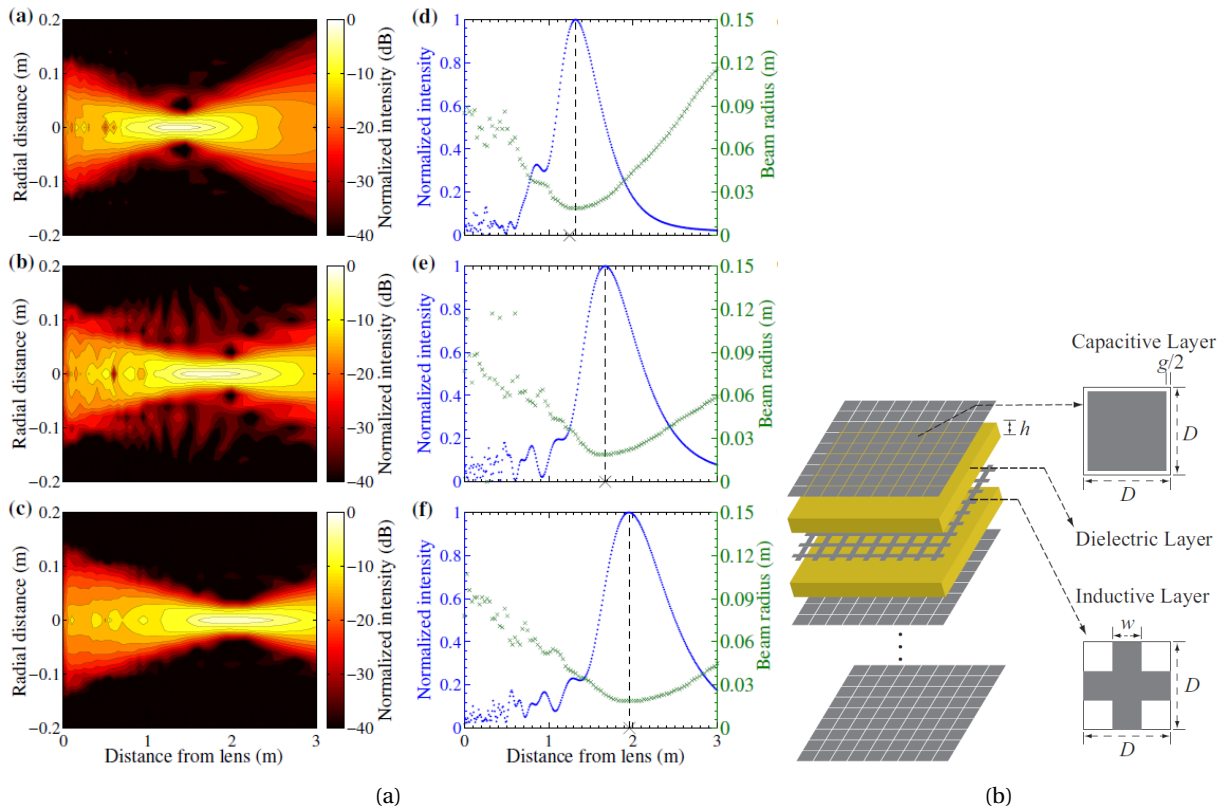
Figure 3.16: Meta-material lens with an frequency dependent focal length. a) simulation results show the increase of focal length with frequency b) Multilayer structure along with its capacitive and inductive printed elements [77].

metamaterial microstructures, a prism is designed with reverse behaviour, that is, contrary to the conventional prism, higher frequencies are less refracted than lower frequencies (see figure 3.17). The device is designed based on meta-material micro-structures.
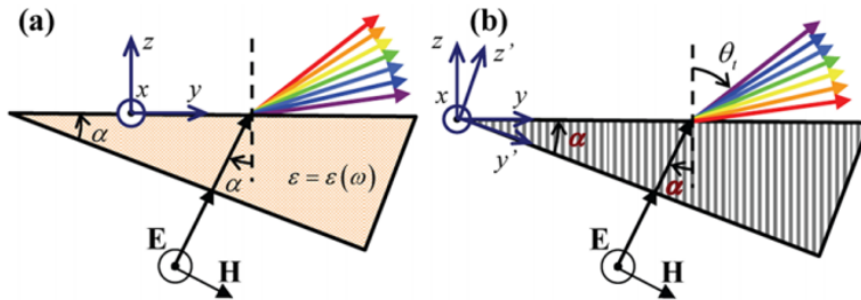
Figure 3.17: A non-conventional prism with reversed refraction-vs-frequency profile. a) conventional prism. b) Meta-material prism with reversed refraction-vs-frequency [78].

3.5.2 Design challenges of a versatile prism

In the previous section, example of devices were presented that possessed a frequency dependent performance in terms of diffraction, refraction, focusing, etc. However no device has been presented so far that can be designed in such way that it demonstrates a *completely arbitrary* performance in terms of frequency. In this subsection, we introduce a versatile prism based on the reflectarray antenna concept, that is to demonstrate a pre-designed arbitrary frequency-vs-deflection profile. The challenges and limitations as well as potential solutions are also presented in this subsection.

Let's consider the simple case of the 2D reflectarray surface of figure 3.3 with a normal incident wave i.e. $\theta_{in} = 0$. It is desired to direct the beam to $\theta_{out}(f)$, f being the frequency. In this case the required phase of the ith cell writes:

$$\phi_{cell}^{i}(f) = -k_0 x_i \Big(\sin\theta_{out}(f)\Big) + \phi_{E0}(f), \qquad \phi_{E0} = \phi_{cell}^{0} \tag{3.20}$$

It is observed that, a broadband reflectarray is a special case of a versatile prism in which $\theta_{out}(f)$ is a constant. Equation 3.20 implies that in fact in order to realize a versatile prism, ideally we should find a cell that could demonstrate an arbitrary phase-shift in terms of frequency since $-90° < \theta_{out}(f) < 90°$ is an arbitrary function. Here we present an example that provides insight concerning the versatile prism. Let's consider an array of 20 cells, at the design frequency of f_0 =15 GHz, with spacing $d = \frac{\lambda_0}{2}$, performing at the frequency span of 9-15 GHz. Let's choose the angle-vs-frequency profile as follows:

$$\theta_{out}(f) = \theta_{max} sin\Big(\frac{\pi}{f_{max} - f_{min}}(f - f_{min})\Big) \tag{3.21}$$

with this particular profile, the beam direction has a sinusoidal behaviour in terms of frequency. As shown in figure 3.18, at f_{min} =9 GHz the out-going beam is pointed to broadside direction. As the frequency increases, the beam will point towards $\theta_{max} = 30°$ at around 12 GHz, and then the beam moves backwards and points again to broadside direction at f_{max} =15 GHz.

This particular beam direction has been chosen since it best shows the general issues of the flat versatile prism. With this behaviour, figure 3.19.a shows the phase response of each of the cells in terms of frequency. By assuming a constant phase response of $\phi_{E0} = 0°$ for the reference cell, as shown in figure 3.19.a, we encounter phase responses that increase with frequency, that is, they have a positive slope with respect to frequency. This is a characteristic that is indeed unachievable in physics without significant reflectivity degradation. However, the positive slope can be avoided by choosing a negative-slope linear phase response for the reference cell as shown in figure 3.19b where it is observed that the issue of the positive slope phase response is solved at the expense of large phase delays (around 5000°). Therefore, the main issue in the implementation of a flat versatile prism is the enormous phase range.

The two types of cells that can give us rather smooth phase response with a large phase-shift are stacked patches and single-layer multi-resonance cells with a thick substrate. Given the phase range, it will be required to have many layers in case of multi-layer structures and
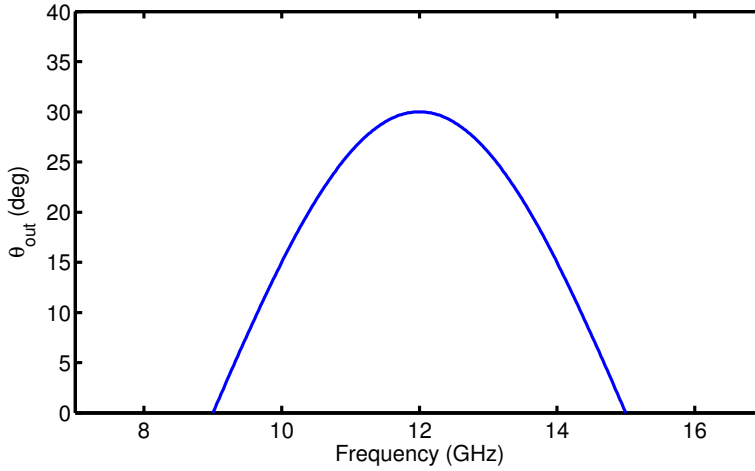
Figure 3.18: Sinusoidal beam direction with frequency.

enormous amount of resonators in case of single-layer cells with a thick substrate.

3.5.3   Circuit model solution

The unit-cell phase response issue for a versatile prism can be solved by reducing it from an electromagnetic model to a circuit model. Consider the cell shown in Figure 3.20 where we have a loaded dipole. Our goal is to find the value of the load in order to achieve a given phase response. As shown in the figure, in fact by extracting the S-parameter matrix of the structure, knowing the reflection coefficient of port No.1 (the single mode Floquet port), and hence its input impedance, we can simply obtain the values of the load impedance for different frequencies. Figure 3.20b shows the simplified circuit model of the unit-cell. Using this model, once we know the value of Z_{in} (extracted from the required phase response) and the impedance matrix of the structure $[Z]$ (extracted by simulation), the value of Z_L can simply be obtained as follows:

$$Z_L = \frac{Z_{12} * Z_{21}}{Z_{11} - Z_{in}} - Z_{22} \tag{3.22}$$

As an example, we consider that the dipole has a length of 6 mm and width of 0.25 mm printed on a grounded substrate of thickness 0.7874 mm and permittivity of 2.33. If we know already the phase of the reflection coefficient of the port no.1 (i.e. cell's phase response), we can obtain the input impedance value seen from port no. 1 for each cell and hence the impedance values to be loaded at port no. 2. Figure 3.21 shows the obtained values of the components of the impedance matrix using HFSS. All of the values are purely imaginary. Now we desire to obtain three different reflection coefficients for three different cells having the phases shown in figure 3.22a and absolute value of unity assuming that the unit-cell is lossless. Figure 3.22b
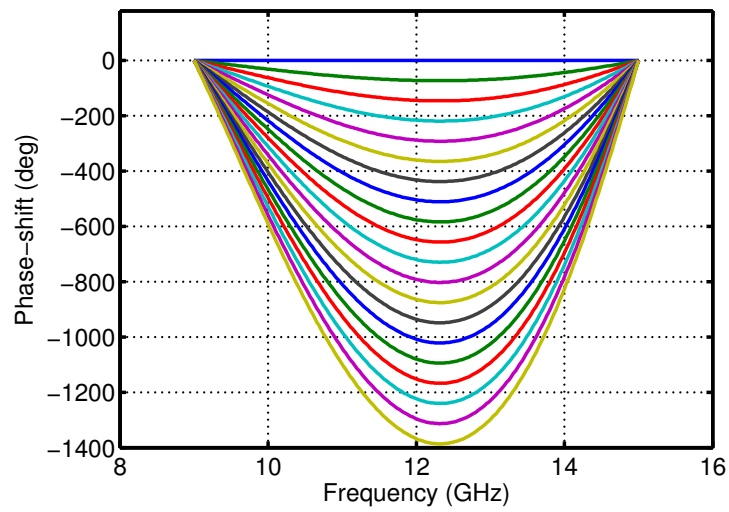
(a) phase response of each cell containing curves with positive slope
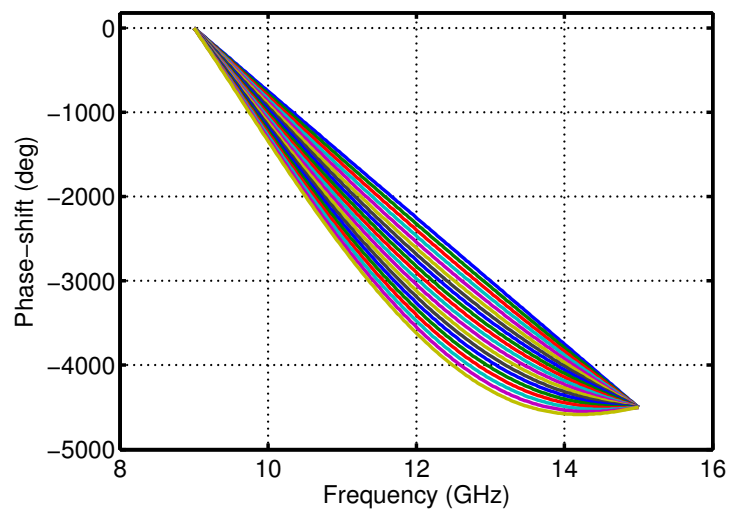
(b) phase response of each cell with negative slope

Figure 3.19: Phase response of each cell for a particular case of a versatile prism. The out-going beam is deflected according to 3.21 a) Phase responses by assuming constant zero phase for the reference element b) Phase responses all with negative slope using a negative slope phase response for the reference cell.

shows the value of the load impedances required for each cell. As mentioned before, in this stage the problem is now merely a circuit synthesis with combination of inductors, capacitors and/or transmission lines with open/short termination so as to obtain a desired behaviour in terms of frequency.

(a)

(b)
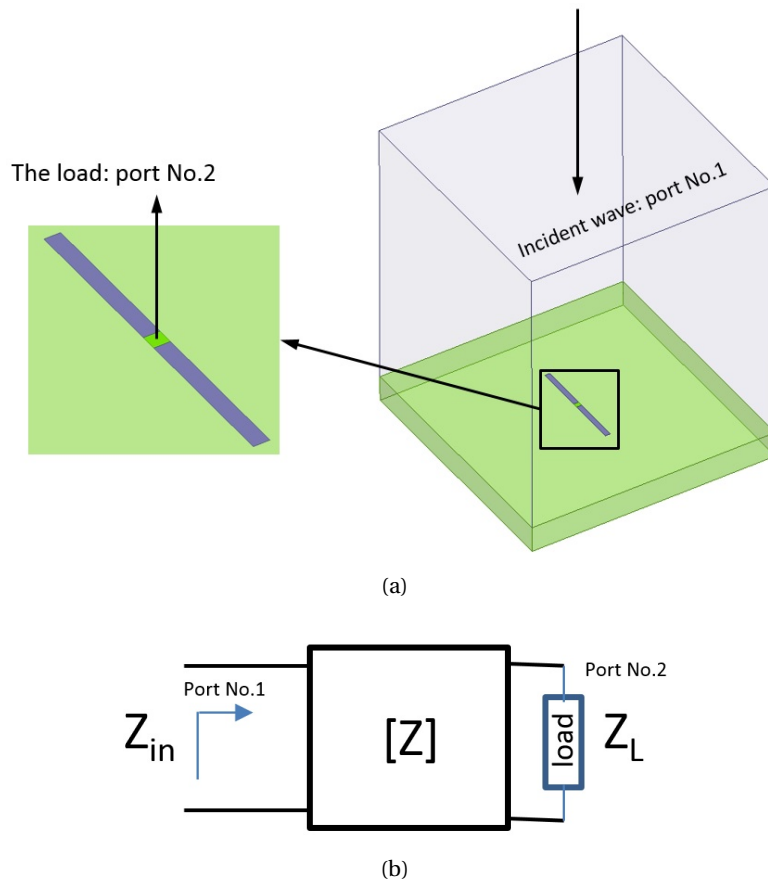
Figure 3.20: a) Unit-cell with a loaded printed dipole b) the equivalent circuit of the unit-cell in which the $[Z]$ is the impedance matrix between port no.1 and port no.2. With a known Z_{in} we can obtain the desired load impedance

3.5.4 Other solutions

We should mention that, it is possible to design a versatile prism using cells with limited phase range. However in that case, the prism will become in fact a multi-band reflectarray antenna. In other words, the reflectarray antenna will follow the relation of $\theta_{out}(f)$ only at certain discreet frequencies. As mentioned before, one possible solution would be to place as many parallel dipoles as possible inside the unit-cell i.e. as much as the cell size allows us. The lengths of dipoles can then be optimized such that at each frequency we get the desired reflection phase. Another solution would be to employ a Genetic Algorithm optimization method [79] starting with a simple patch inside the cell, which results in the so-called fragmented patch element. Figure 3.23 shows a typical patch with the method employed on. The pattern can be modified until the desired phase response is obtained. The disadvantages are the high level of cross-polarization due to the element's non-symmetrical shape and enormous optimization time since the procedure should be repeated for all the cells of the reflectarray. Since the design details of such a cell is beyond the scope of this thesis,
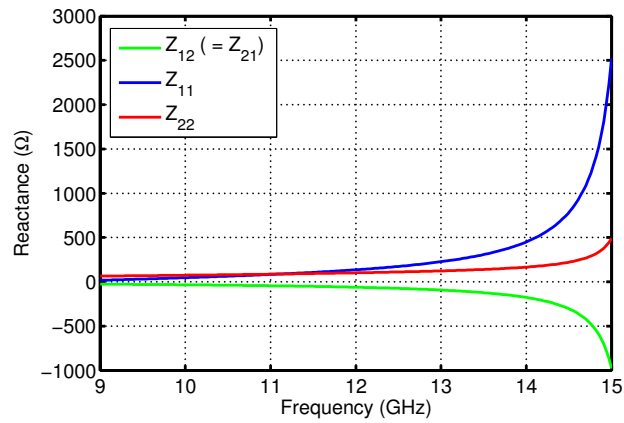
Figure 3.21: Components of the impedance matrix according to the structure of the figure 3.20 with cell size 9 mm, dipole length and width 6 mm and 0.25 mm respectively, printed on a grounded substrate of thickness 0.7874 mm and permittivity of 2.33. All of the components are purely imaginary.

the interested reader is referred to [79–81] for more details.
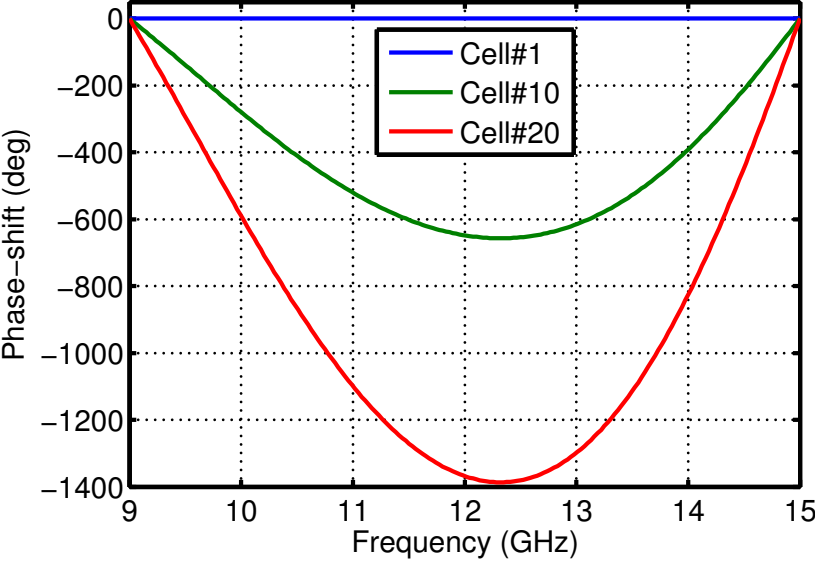
(a)
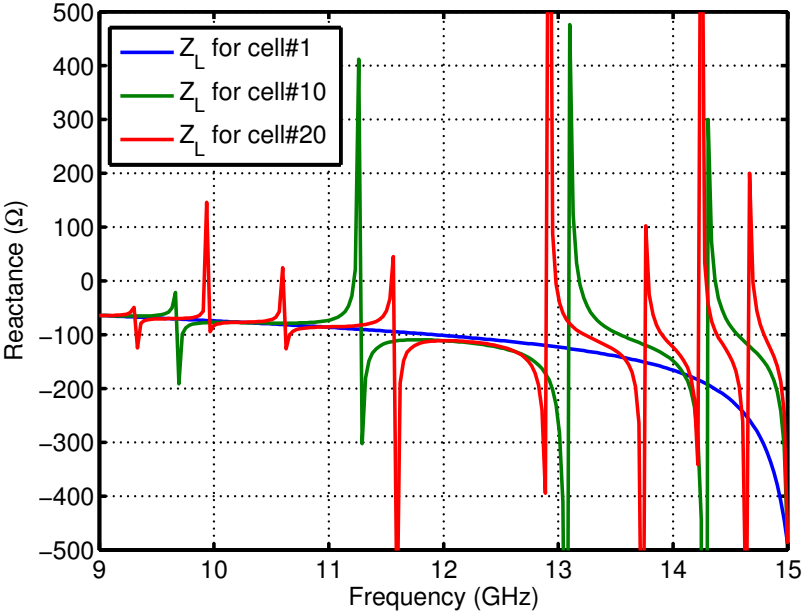
(b)

Figure 3.22: a) Required phase response for three random cells b) The corresponding load impedance for each cell obtained according to equation 3.22.

$Genome = \begin{bmatrix} 1111111...111111111 \end{bmatrix}$ $Genome = \begin{bmatrix} 1001111...0110100101 \end{bmatrix}$
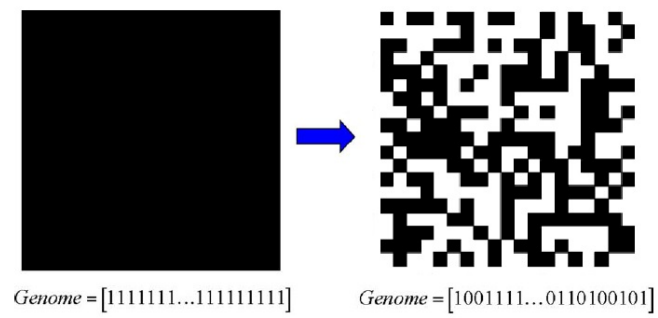
Figure 3.23: Fragmented patch synthesis showing the starting patch element and the synthesized fragmented element. The iteration will be continued until the element demonstrates the desired phase response [79].

4 Multi-Band Reflectarray Antennas in Ku-Band

4.1 Introduction

In this chapter we describe a dual-band and a quad-band reflectarray antenna with closely separated frequency bands in the range 12-15.5 GHz. The multi-band unit-cells are designed as single-layer structures composed of printed elements etched on a thin dielectric substrate with thickness 0.7874 mm and permittivity 2.2 and 2.33 for dual-band and quad-band design, respectively. In addition, the unit-cells are dual linearly polarized which makes the antennas capable of performing in circular polarization as well. The proposed unit-cells have as many regulating parameters as the number of bands and they have the important feature of independent phase-shifts for each frequency. In other words, the phase-shift at each frequency depends on only one regulating parameter of the unit-cell. Thus, the resultant multi-band reflectarray antennas can be considered as the superposition of several reflectarray antennas with their specific pattern shape, sharing one aperture. Here lies the main contribution to the reduction of the cost/functionality ratio. Note that the aim of the chapter is only to prove the concept and that is why small dimensions are chosen for the reflectarray surfaces since the efficiency is not a concern. It is clear that, with a proper choice of the feed horn and antenna dimension, satisfactory performance in terms of gain can easily be achieved. In this chapter, for each multi-band antenna we start with the description of the corresponding unit-cell and its phase response at each frequency, continue with the full array simulation and finally present the measurement results.

The design methodology and results presented in this chapter have been published in [82, 83]. There is thus a certain overlapping between the materials of this chapter and [82, 83].

4.2 Dual-band reflectarray antenna

4.2.1 The unit-cell

As shown in figure 4.1, the unit-cell consists of a cross dipole (for the lower band) and a rectangular split ring (for the upper band) printed on a substrate with permittivity 2.2 and thickness

(a) top view.   (b) 3D view.
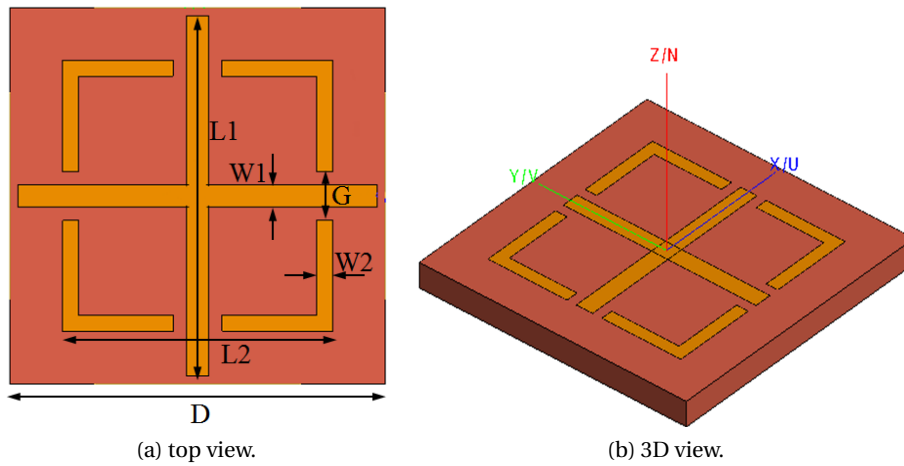
Figure 4.1: The dual-band unit-cell [83].

(a) 12GHz.   (b) 14GHz.

(c) 12GHz.   (d) 14GHz.
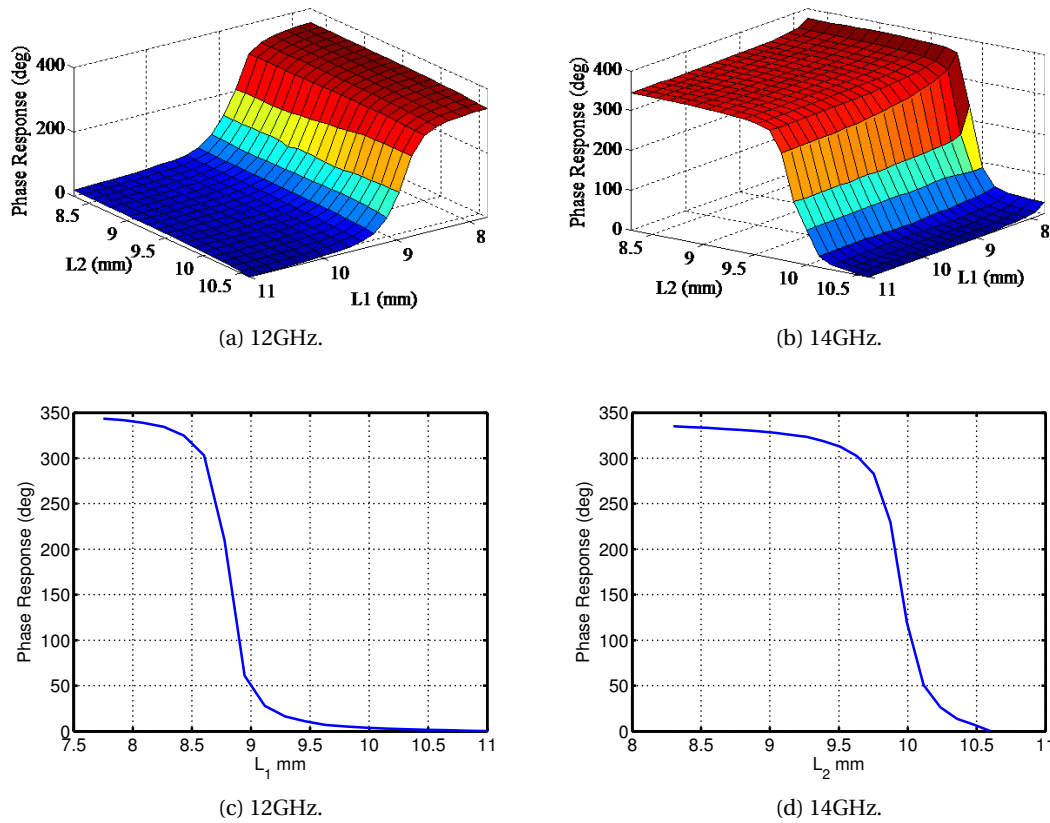
Figure 4.2: Dual-band unit-cell phase response. At each frequency the phase response depends on only one parameter. [83].

0.787 mm. The idea behind the splits in the rectangular ring is to avoid physical contact with the cross-dipole element. With this configuration the phase controlling parameters of

Table 4.1: Dual-band unit-cell parameters (unit: mm).

D	W2	W1	G
11.5	0.5	0.7	1.5

both upper and lower band, that is L_1 and L_2, can have any value inside the unit-cell. The unit-cell fixed parameters are listed in Table 4.1. The phase response of the cell was obtained by impinging a normal plane wave on a finite 5×5 periodic array of the unit-cell since in FEKO [84] environment this configuration is much less time consuming and as accurate as if we used periodic boundary conditions. The reason is that, FEKO allows the utilization of embedded Green's function of an infinite grounded substrate which in it's turn circumvents the meshing of the substrate and hence results in a fast numeric computation.

As illustrated in figure 4.2, the simulated unit-cell phase responses in the two frequencies [83] are almost completely independent from one another owing to the negligible coupling between the two elements in the unit-cell. As a result, the reflection phase at 12 GHz is controlled only by variations in L_1 which is between 7.75 - 11 mm and at 14 GHz it is controlled only by variations of L_2 between 8.3 - 10.6 mm. This feature makes it possible to obtain independent functionalities in each frequency band.

4.2.2 Reflectarray antenna simulation scenario
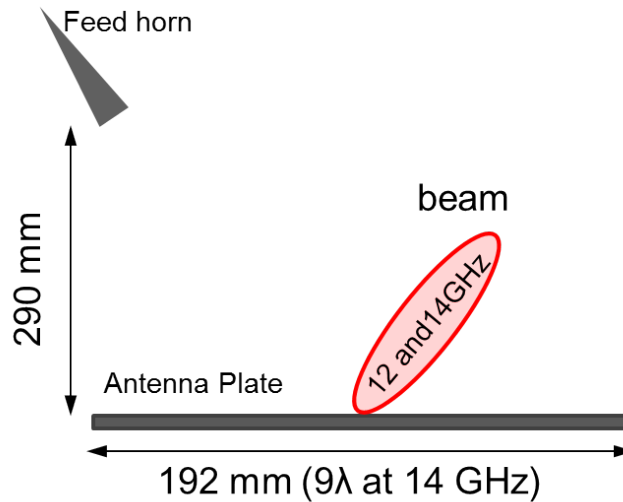
Figure 4.3: General configuration of the dual-band reflectarray antenna.

The dual-band simulation of the reflectarray is carried out in FEKO, a MoM-based full-wave commercial software [84]. The main challenge in the full-wave simulation of a reflectarray antenna is always the large electrical size of the antenna plate. This problem becomes more severe if we consider that, as in the present case, a fine meshing is required owing to the high Q-factor nature of the elements and the strong mutual coupling between neighbour

cells. This section provides a detailed scenario for a fast and accurate simulation of the proposed reflectarray antenna which indeed can be applied to the majority of reflectarray antennas. For the present case, shown schematically in figure 4.3, the elements are printed on an available standard 20×20 cm^2 substrate plate which, considering the unit-cell spacing of 11.5 mm, incorporates 17×17 cells. Owing to the symmetry of the reflectarray plate, there is the possibility of applying a magnetic symmetry plane. However, in the simulation process, it appeared that even with the incorporation of a magnetic symmetry plane, the simulation requirements remained huge, leading to unacceptable simulation time and memory. As a result we used another technique to simulate the structure. The idea is that, in addition to the symmetry plane, to further facilitate the simulation and reduce the simulation time, the following assumptions can be made:

A) *The antenna plate is at the far-field of the feed horn*

The outcome of this assumption is that, the feed antenna can be replaced by its far-field radiation pattern arising from a point source situated at the antenna focal point, optimally obtained at Zp = 290 mm for a given feed horn pattern and feed horn position in y axis (Yp = -96 mm) which, corresponds to the antenna plate edge (see figure 4.3). In order to obtain the optimum performance in terms of radiation pattern [74], the reflectarray antenna is designed to point the beam to 19° off broadside at both frequencies:

$$\theta = \tan^{-1}\left(\frac{-Y_p}{Z_p}\right) \cong 19° \tag{4.1}$$

The feed horn used is a standard gain horn with nominal gain of 15 dBi and a beamwidth of about 37° in both E and H planes. It is obvious that, the horn blockage effects will be ignored as a consequence of this simplification. However, the feed horn blockage has also a minor effect on the radiation pattern owing to the off-set configuration.

B) *The grounded substrate is extended to infinity*

This assumption provides the main contribution to the numerical model simplification by significantly reducing the simulation time. By applying this assumption, it is possible to use predefined multilayer Green's Functions, available in many integral equation based commercial softwares and avoid meshing the whole substrate, as required by finite-difference or finite-element algorithms. This assumption has proven to be accurate in predicting the antenna performance in terms of directivity and beamwidth as will be shown later in the measurement results. A potential drawback of this assumption is that the spurious reflection from the infinite grounded substrate could influence the far-field radiation pattern. However, since the majority of the incident power from the feed horn is concentrated on the antenna plate, the contribution of the waves reflected from the virtual portions of the infinite substrate

(a) 12GHz.

(b) 14GHz.

(c) Simulated antenna structure in FEKO [83]
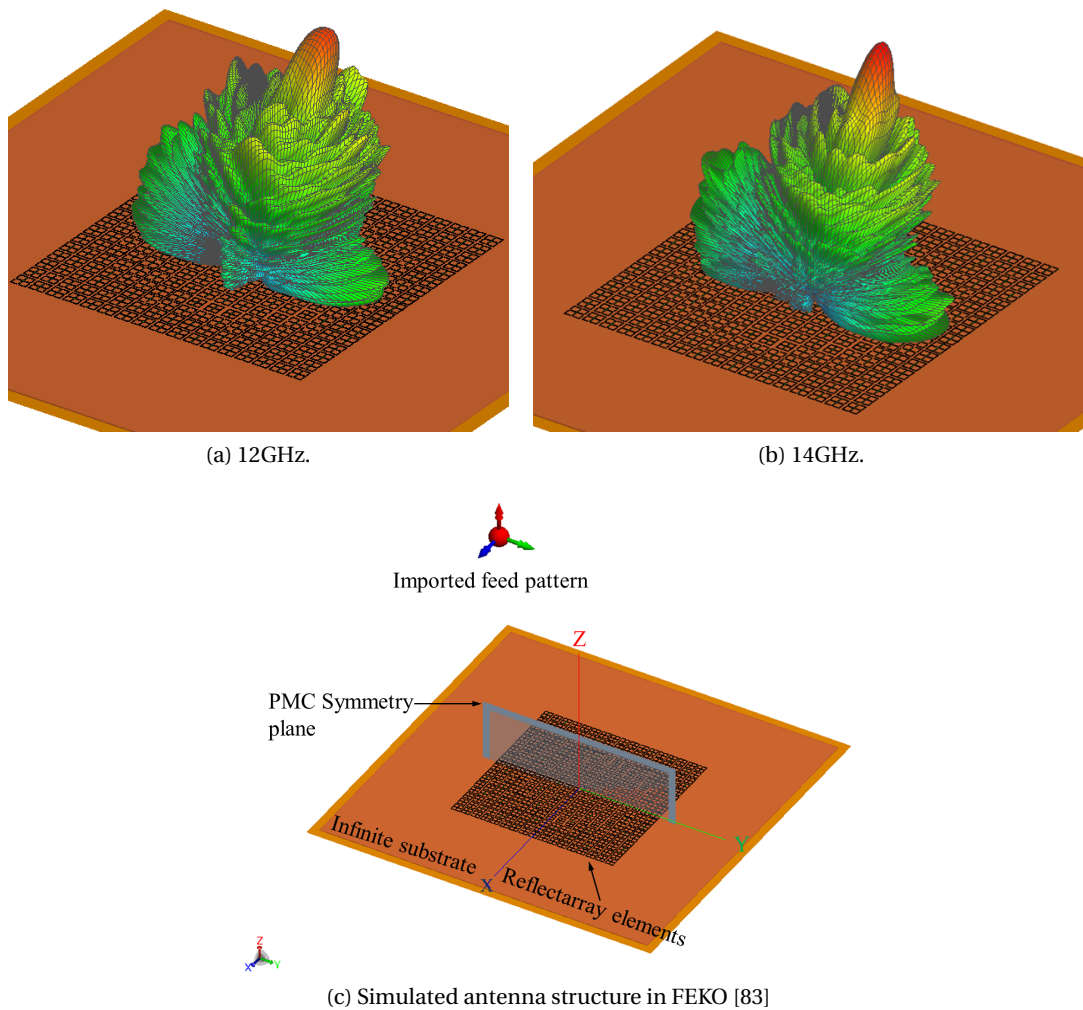
Figure 4.4: Simulated antenna structure in FEKO and 3D radiation patterns at 12 and 14 GHz.

extending to infinity is minor. Another possible drawback of the infinite grounded substrate hypothesis is that it prevents a correct description of the back radiation of the reflectarray antenna. A well tested way out exploits the fact that the main contribution to the antenna back radiation comes from the diffraction from the edges of the antenna plate. Back radiation can then be easily estimated by replacing the reflectarray antenna plate by a PEC plate with the same size and position with respect to the feed horn.

4.2.3 Simulation and measurement results

The normalised 3D patterns at 12 and 14 GHz along with the structure itself are shown in figure 4.4. However, in order to obtain the antenna gain, the structure is simulated separately in two frequency bands i.e. from 11 to 13 GHz and from 13 to 15 GHz and thus it is fine meshed

with a $\lambda/16$ mesh size in which λ corresponds to the higher frequency in each simulation (13 and 15 GHz). Copper with 35 μm of thickness is considered as the printed elements material. The antenna prototype shown in figure 4.5 has been measured in an anechoic chamber of $8\times4\times4\text{m}^3$. Simulated and measured far-field radiation patterns at both central frequencies of 12 and 14 GHz, are compared in figure 4.6. It can be seen that the antenna is showing satisfactory behaviour in terms of both beamwidth and sidelobe levels. Beamwidths of 8 and 6 degrees and sidelobe levels of -13 and -15 dB are measured at 12 and 14 GHz, respectively. While the figures demonstrate an overall agreement between measured and simulated radiation patterns, especially in terms of beamwidth, some differences are noticeable in the sidelobe levels. It is believed that this discrepancy between measured and simulated values is simply due to the tolerances in the measurement setup, especially the horn deviation and its distance from the plate. The effect of these tolerances is more apparent in figure 4.6.a, in which the measured radiation pattern has its maximum at $17°$ while it should be $19°$ according to simulations. In addition to the tolerances, the absence of the antenna plate surroundings (holders, cables, etc) in the simulation might be another cause of the differences between measured and simulation results. As for backside radiation, limitations in the measurement setup at angles close to $\pm180°$ (see figure 4.5) prevented accurate gain measurements at those angles. For both frequencies, the cross-polarization level in E-plane remained below -30 dB for all the angles. Simulated and measured reflectarray antenna gain versus frequency are compared in figure 4.7. In good agreement with simulations, the antenna is showing two overall gain peaks at 12 and 14 GHz in spite of a narrow bandwidth performance caused by the thin substrate used. As shown in figure 4.7, the -3 dB bandwidths are estimated to be 5% and 4% for the lower and the upper band respectively. This bandwidth performance can be easily improved if needed by increasing the substrate thickness. The theoretical aperture efficiency of the antenna is estimated to be around 23% for the lower band and 30% for upper band. Efficiency has been calculated as the ratio of the antenna measured gain over the maximum broadside gain that can theoretically be obtained for a uniformly illuminated aperture area of 20×20 cm^2:

$$\eta = \left(\frac{G_m}{G_{max}}\right), G_{max} = \left(\frac{4\pi A}{\lambda^2}\right) \tag{4.2}$$

Wherein G_m is the antenna measured gain and A (equal to 20×20 cm^2) is the antenna plate area. The small size of the antenna plate, elements metallic losses and substrate losses are the main causes for efficiency reduction. We should mention that, in addition to the off-set fed reflectarray, a center-fed design was also fabricated and measured. However, because of the feed blockage effect, the antenna demonstrated poor efficiency and therefore was discarded. Figure 4.8 shows the gain of the center-fed reflectarray compared to the simulation results. Note that in the simulations the feed blockage effect is ignored since the feed pattern is imported.
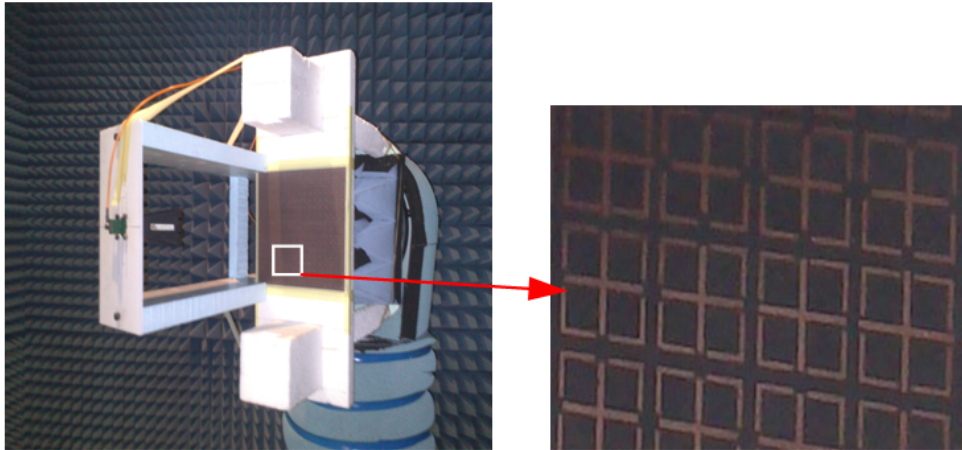
Figure 4.5: Dual-band antenna prototype with measurement setup [83].

4.3 Quad-band reflectarray antenna

This section is considered as a continuation to the dual-band reflectarray antenna. As will be later described in detail, with careful engineering of the unit-cell, it is possible to obtain phase regulation at the *four* frequencies 12, 13, 14 and 15.5 GHz while maintaining the advantages of the dual-band design (dual-polarization performance and single-layer structure) without any additional cost. In the following, we will describe the geometry of the quad-band cell, present the simulation results of the full array and finally, the full array performance will be demonstrated by presenting the measurement results.

4.3.1 The unit-cell

Figure 4.9 shows the general configuration of the quad-band cell. However, before presenting the details of the unit-cell geometry, we explain the idea that led to such a geometry. The first step can be seen in figure 4.10.a, showing a simple dual-band unit-cell with interlaced crossed dipoles [85] along with a portion of its corresponding 3 × 3 array sample (only for demonstrative purposes). In this dual-band structure the regulating parameters for the phase response are the lengths of the cross-dipoles shown in light blue and red designated to perform at 12 and 13 GHz, respectively. In the second step shown in figure 4.10.b, we have designed a tri-band unit-cell by introducing four equal-length tilted dipoles (in light green) in order to obtain the phase-shift at 14 GHz.

It should be noted that at each step we verify that the phase responses are independent from one another and are thus function of only one parameter of the unit-cell. In order to add the fourth parameter for the phase regulation at 15.5 GHz, we introduce a second structure similar to the second stage (in violet) and arrive to the third stage shown in figure 4.10.c. However, at this stage the strong mutual coupling between the parallel dipoles prevents us from obtaining independent phase responses at 14 and 15.5 GHz meaning that at each of
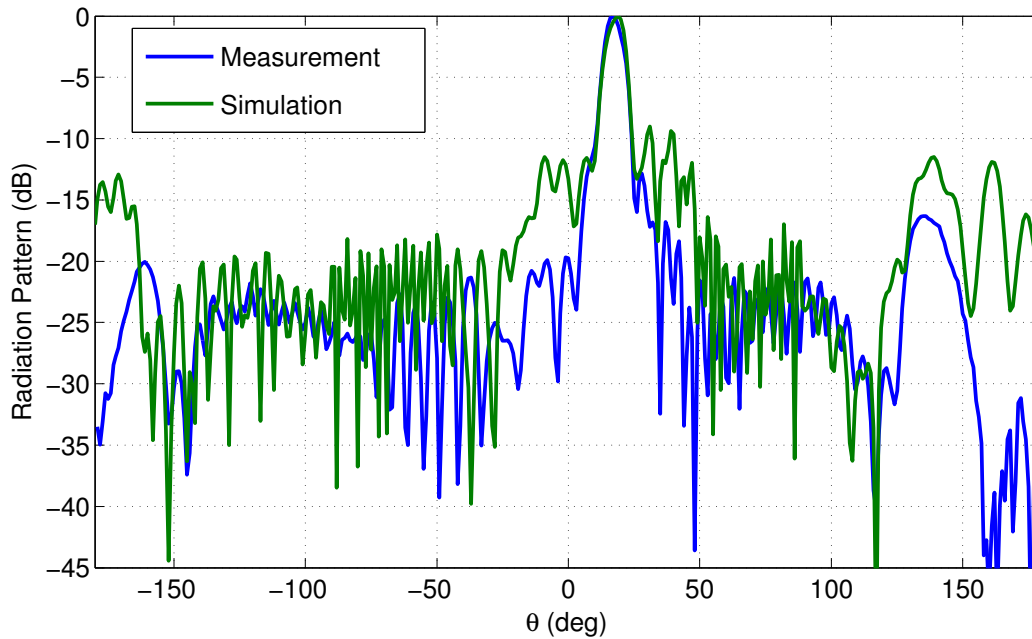
(a) 12GHz.
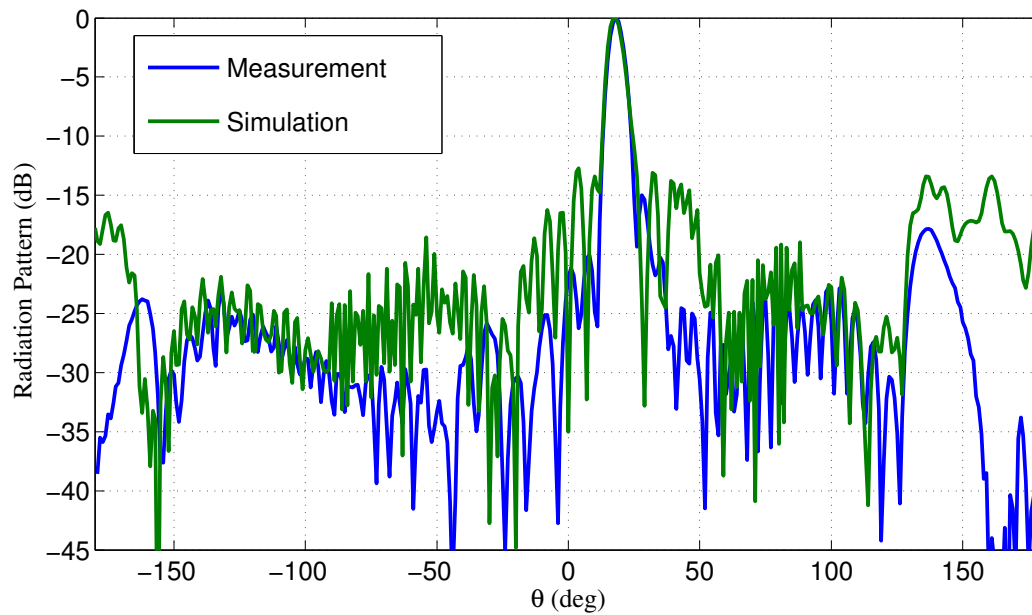
(b) 14GHz.

Figure 4.6: Dual-band reflectarray simulated and measured far-field radiation pattern at a) 12 GHz b) 14 GHz. The simulated pattern in the range of -180< θ <-90 and 90< θ <180 is obtained by putting a PEC plate size of the reflectarray in front of the feed horn [83].
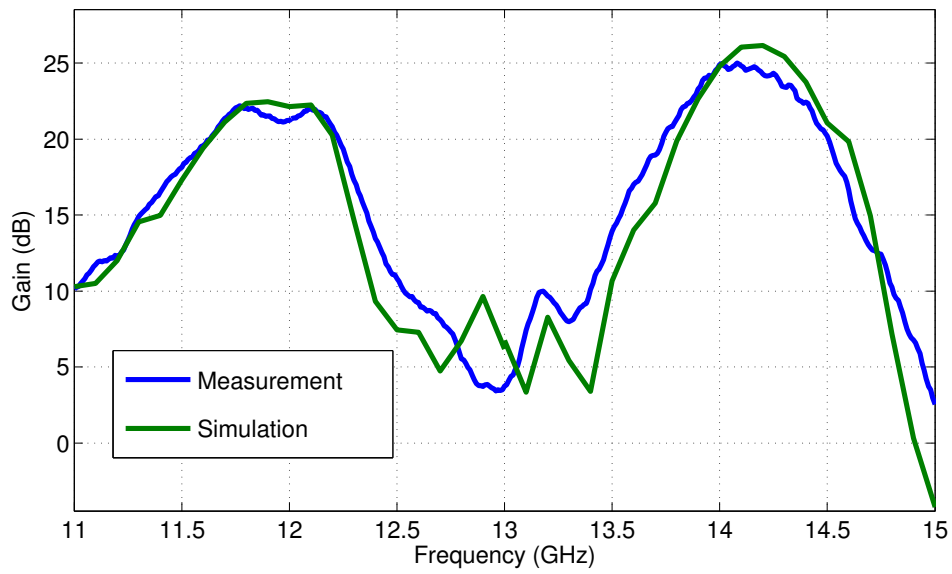
Figure 4.7: Offset dual-band reflectarray simulated and measured gain versus frequency at 19°
off broadside. The two peaks in antenna gain occurs at 12 and 14 GHz as intended [83].
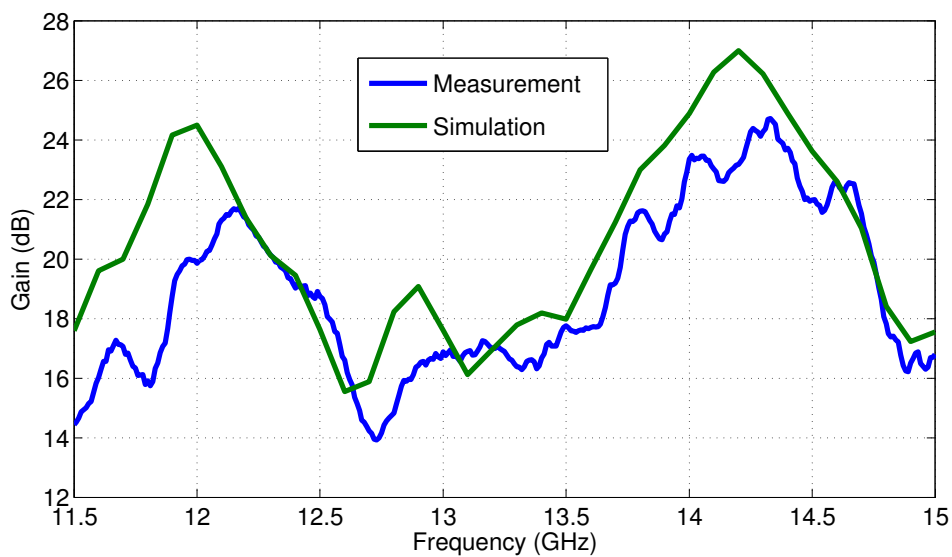
Figure 4.8: Center-fed dual-band reflectarray simulated and measured gain versus frequency
at broadside direction. Note the feed blockage's negative effect on the measured gain with
respect to the simulated one where this effect has been ignored.
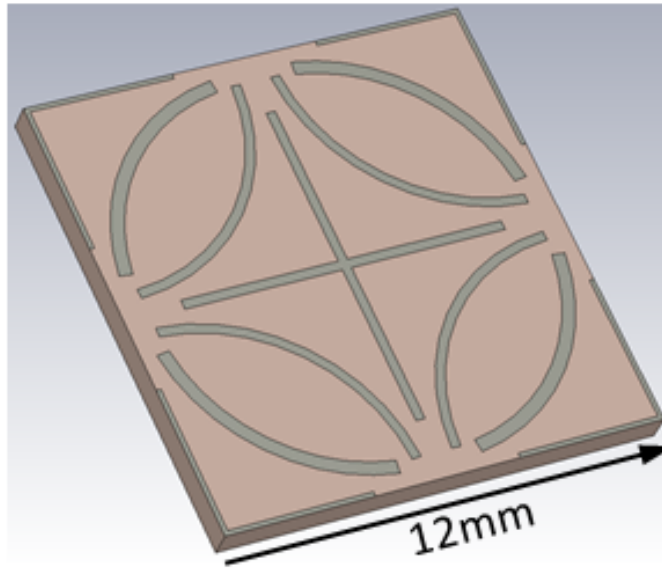
Figure 4.9: The final quad-band unit-cell performing at 12, 13, 14 and 15.5 GHz [82].

these frequencies the phase response will be dependent on the lengths of both parallel tilted dipoles. Moreover, avoiding physical interference with the cross-dipoles will make the design complicated. One possible solution is to curve the tilted dipoles and arrive to the final stage shown in figure 4.10.d. With this solution, as will be shown later, phase-shifts at 14 GHz and 15.5 GHz will become independent with an acceptable tolerance and physical interference will also be avoided.

The constructing structures of the final unit-cell are shown separately in figure 4.11 with geometrical details along with their phase response at each frequency assuming an incident angle of 20°. This value is the incident angle of feed to the central cell due to the off-set design of the reflectarray as shown in figure 4.3. Note that the structure for the phase-shift at 13 GHz are the same as that of 12 GHz, i.e. cross-dipole of width 0.25 mm. Table 4.2 summarises the corresponding parameters and their variation limit for each frequency. As for the substrate, the structures are printed on a grounded substrate with 0.787 mm of thickness and a relative permittivity 2.33. It should be noted that the phase-shifts are obtained with the

Table 4.2: Quad-band unit-cell parameters [82].

Parameter name	Frequency (GHz)	Variation range
$Ł_1$	12 GHz	8.5 - 9 mm
$Ł_2$	13 GHz	7.8 - 8.3 mm
θ_1	14 GHz	80° - 88°
θ_2	15.5 GHz	70° - 77°

presence of all other unit-cell structures. However for the sake of clarity, at each frequency only the corresponding structure is shown. Simulations are carried out in CST Microwave

Studio environment. The phase responses at each frequency are obtained by varying the corresponding parameter with three different values (first, middle and last) of the other three parameters resulting in $3 \times 3 \times 3 = 27$ curves. The solid black curve is the phase response, for the case where the other three parameters are kept at their resonant size.

(a) Initial dual-band unit-cell

(b) Tri-band unit-cell

(c) Quad-band unit-cell

(d) Modified quad-band unit-cell
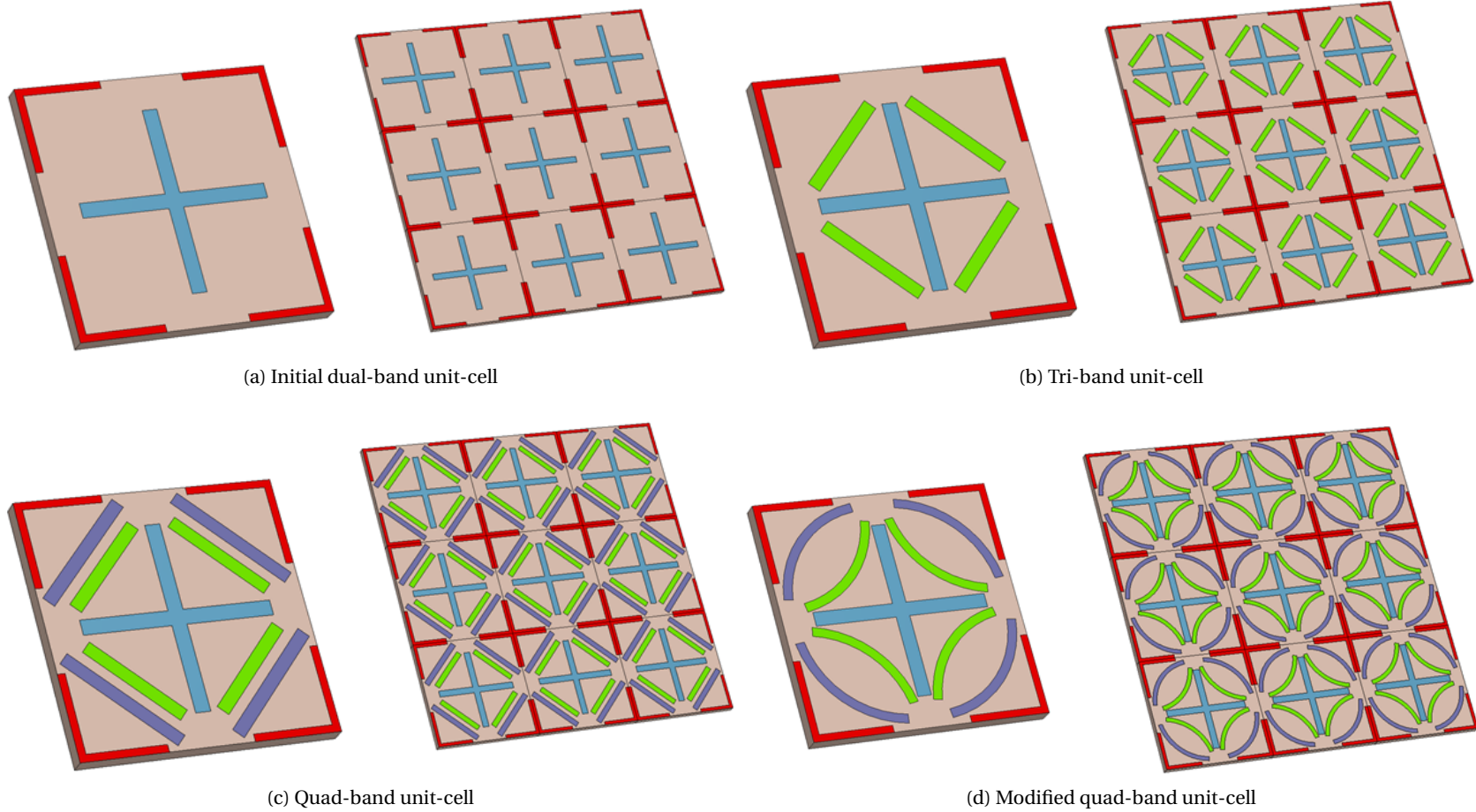
Figure 4.10: Quad-band unit-cell evolutionary stages and the resultant FSS. At each stage. a) simple dual-band structure with interlaced cross-dipoles for 12 GHz (in light blue) and 13 GHz (in red) b) a tri-band unit-cell with the help of four tilted dipoles (in light green) for 14 GHz c) a quad-band unit-cell with added tilted dipoles (in violet) for 15.5 GHz. Mutual coupling and physical interference between structures is an issue d) final quad-band structures with curved tilted dipoles [82].

As mentioned earlier, the important characteristic of the unit-cell is that, at each frequency the phase-shift depends only on one parameter. This implies that the phase-shift at each frequency remains almost unchanged when the other three parameters vary within their limits. This advantage will simplify the reflectarray design since it eliminates the need for building a huge database by sweeping all the parameters at all the frequencies for a multi-frequency phase-matching method. Simulation results show that, of all the phase-shifts, at 14 GHz we have the highest (yet slight) sensitivity with respect to θ_2 only, as shown in figure 4.12. As shown, the phase response is only a function of θ_1 except for the two final values of θ_2 where slight distortion occurs and where we have a 100° phase difference. By selecting an average of these curves as the final phase-shift at 14 GHz (the black solid curve shown in figure 4.11), we can neglect this tolerance since the error on the reflectarray surface occurs only for a few combinations of θ_1 and θ_2. As will be verified later by full wave simulation and measurement results, it has a minor effect on the overall reflectarray performance.

4.3.2 Quad-band reflectarray simulation and measurement results

As a proof-of-concept, we have designed two reflectarray prototypes with 17×17 cells on a 20×20 cm^2 plate. Each antenna has different and arbitrary beam directions for each frequency. It should be noted that the size of the unit-cell (= 12 mm) is larger than $\lambda/2$ at 15.5, 14 and 13 GHz. Therefore, in order to avoid the apparition of grating lobes, the maximum beam deviation at 15.5, 14 and 13 GHz should not exceed 40°, 50° and 68° respectively. At 12 GHz there is no limitation in the beam direction since the unit-cell electrical size is smaller than $\lambda/2$. The beam direction at each frequency and its exact values for the first and second prototypes are shown in figure 4.13. For the first prototype the beams at all the frequencies are pointing to an elevation angle of $\theta = 10°$ off broadside and azimuth angles of ϕ=45°, 135°, 225° and 315° at 12, 13, 14 and 15.5 GHz respectively. The second prototype is similar to the first except that there are only two beam directions. At 12 and 14 GHz the beam is pointed to (θ=10°, ϕ=45°) and at 13 and 15.5 GHz the beam is pointed to (θ=10°, ϕ=135°). The values of the beam directions are chosen in an arbitrary manner merely to show the antennas performances. The antenna plate is illuminated by a standard feed horn antenna placed at zp = 290 mm and yp = -96 mm according to the coordinate system shown in figure 4.13. The feed horn has an aperture size of 31×41.5 mm^2 and its gain vs frequency is shown in figure 4.14. One of the characteristics of the proposed unit-cell is that it can also be viewed as the superposition of two dual-band structures each composed of a cross-dipole and four symmetric arcs. This concept is better shown in figure 4.15 where we have shown a segment of the infinite periodic array represented by the proposed unit-cell. In figure 4.15 the blue elements construct a reflectarray antenna performing at 13 and 15.5 GHz, and the red elements at 12 and 14 GHz. In the middle of the figure one can recognize the proposed unit-cell having the boundaries shown in green coloured solid lines. It is based on this arrangement that the two reflectarray prototypes are designed.
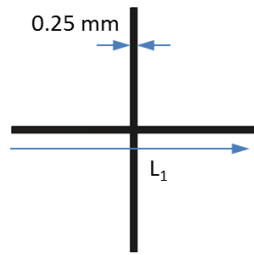
(a) structure for 12 GHz.
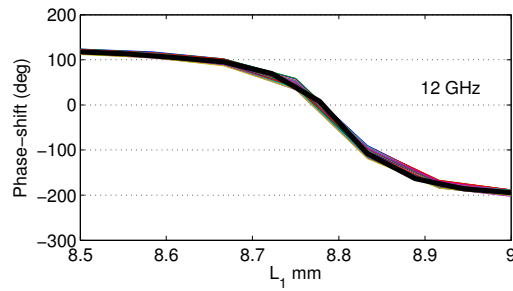
(b) Phase response at 12 GHz
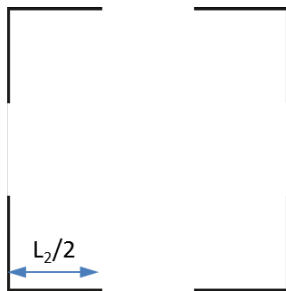
(c) structure for 13 GHz.
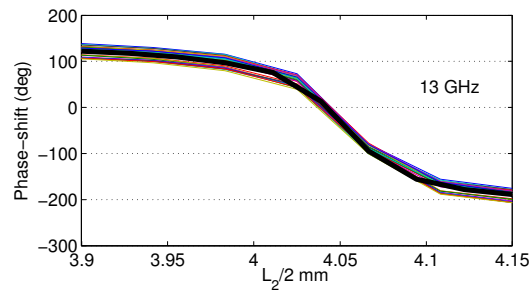
(d) Phase response at 13 GHz
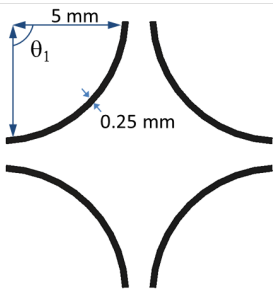
(e) structure for 14 GHz.
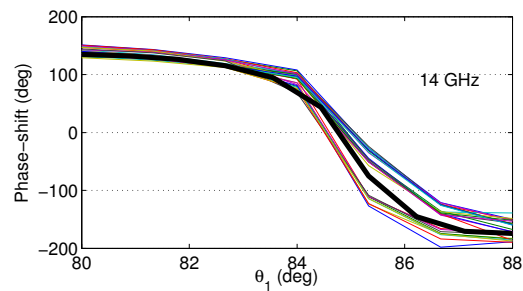
(f) Phase response at 14 GHz
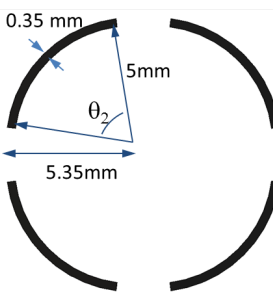
(g) structure for 15.5 GHz.
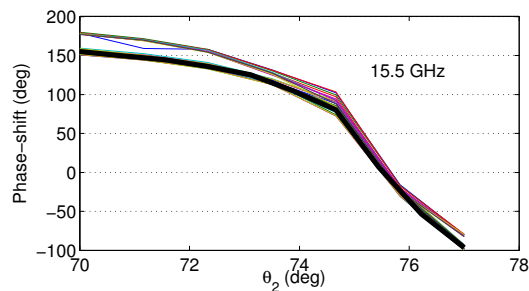
(h) Phase response at 15.5 GHz

Figure 4.11: Structures of the final unit-cell with their geometrical details. The important feature is that, at each frequency, the phase response is only a function of one unit-cell parameter meaning that, it is independent of the variation of the other three parameters. The final unit-cell is the superposition of all these structures [82].
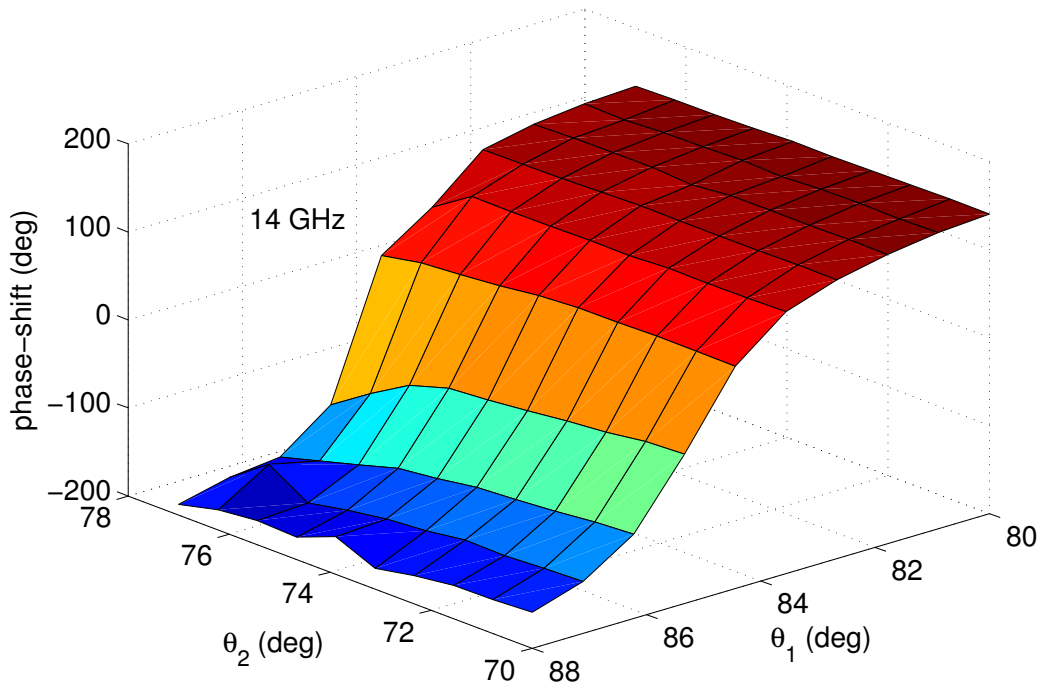
Figure 4.12: Simulated sensitivity of the phase-shift at 14 GHz on different values of θ_2. This slight dependency is negligible for the reflectarray design. An average of these curves has been taken for the final phase response at 14 GHz.

(a) first prototype.
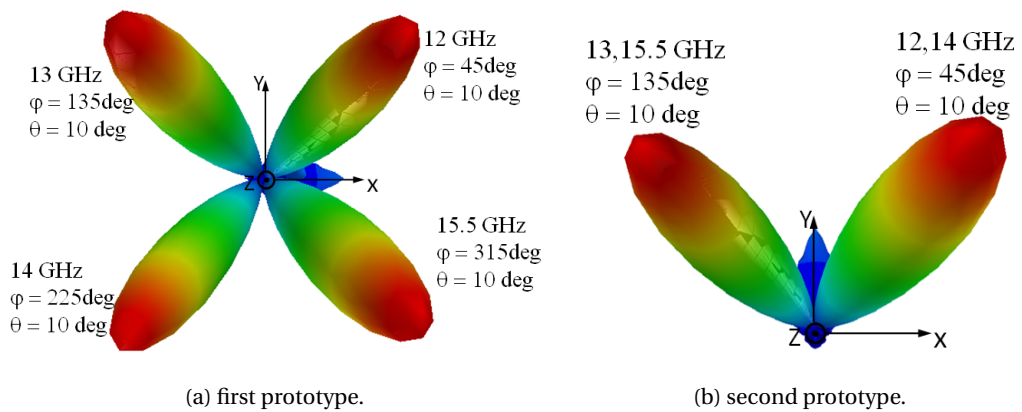
(b) second prototype.

Figure 4.13: Schematic of beam direction for the first and second quad-band reflectarray antenna prototypes. The choice of the beam direction versus frequency is only to show quad-band performance with arbitrary beam-shape at each frequency [82].
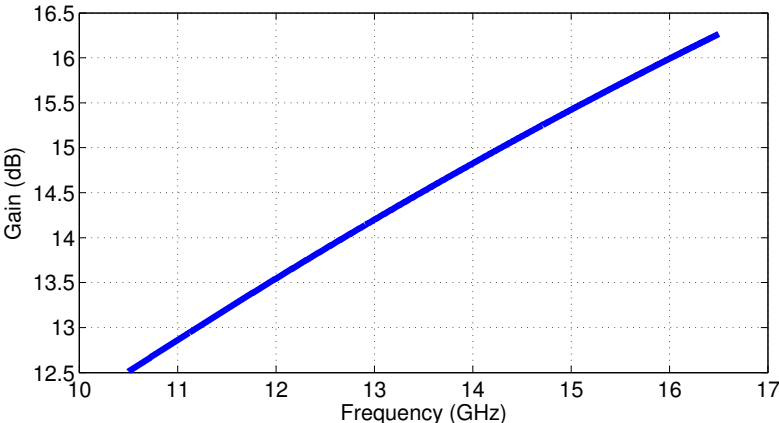
Figure 4.14: Measured feed horn gain versus frequency [82].
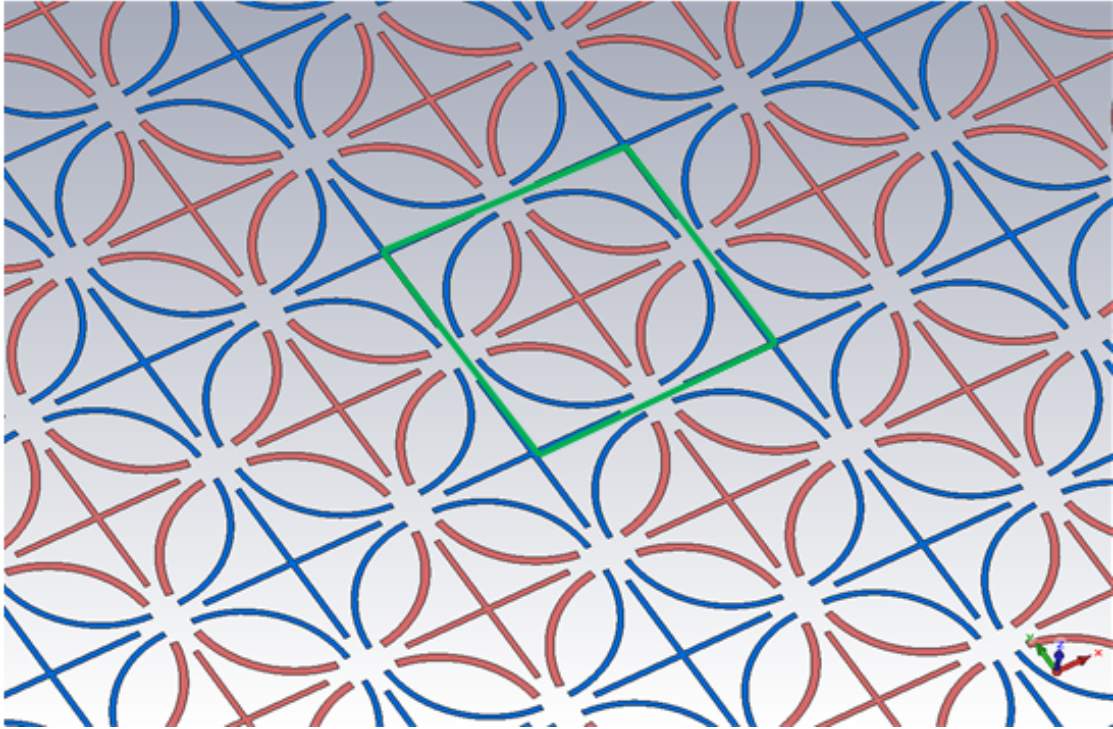
Figure 4.15: Quad-band reflectarray viewed as two dual-band reflectarray antenna at 12 and 14 GHz (in red) and at 13 and 15.5 GHz (in blue). The unit-cell can be distinguished in the middle [82].

(a) fabricated prototype.   (b) measurement setup.   (c) fabricated prototype.

(d) measurement setup.
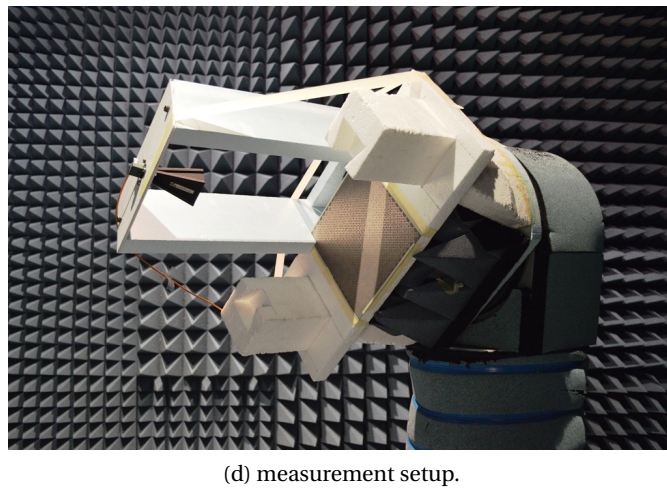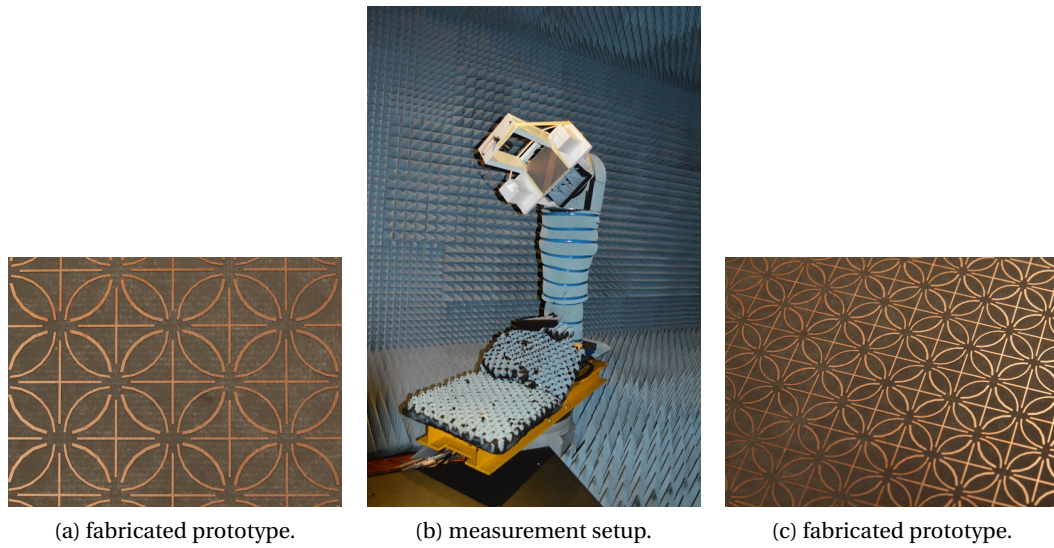
Figure 4.16: fabricated prototype and measurement setup [82].
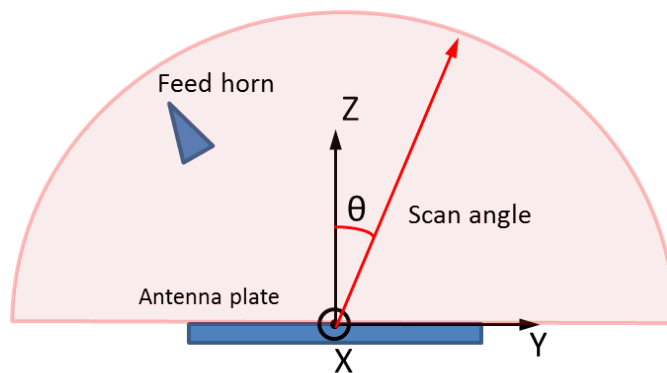
Figure 4.17: Schematic view of the measurement setup to obtain specular radiation pattern at yz plane [82].

Full-array simulation results

In order to estimate the performance of the whole reflectarray antenna, we have simulated the first quad-band antenna in the previous section however with 13 × 13 cells in order to reduce the simulation time as well as achieving precise results. The full-array simulations are carried out in HFSS environment (see figure 4.18.a), having the feed (always placed at zp = 290 mm and yp = -96 mm) as an imported radiation pattern. The simulations are only carried out in order to verify the proposed idea and are considered as the final step towards the fabrication of larger prototypes. The simulated patterns (see figure 4.18.b) also reveal that, there is noticeable radiation in specular direction (yz plane) and this is the motivation for measuring the radiation pattern in this plane for side lobe level estimation. The highest specular radiation with level -10 dB with respect to the maximum gain, occurs at 14 GHz. However, as will be verified in the measurement results, for larger prototypes containing 17 × 17 cells on the plate, at 14 GHz, the specular radiation will be reduced.

Full-array measurement results

The two reflectarray prototypes have been fabricated and measured in an anechoic chamber. Figure 4.16 shows the final fabricated prototype with its printed elements on the plate along with the measurement setup. The elements are printed on a Rogers Duroid RT5870 substrate with 0.787 mm thickness and a relative permittivity of 2.33. Antenna radiation patterns have been measured at ϕ =constant planes namely at ϕ=45°, 135°, 225° and 315°, where the beams are to be found. The radiation pattern has also been measured in the yz plane which is prone to specular radiation [86] due to the existence of the feed on this plane, shown schematically in figure 4.17. According to the configuration, it is clear that the specular radiation will have its highest values around $0° < \theta < 20°$ as it will be seen later in the measured specular radiation patterns. The performance of the prototypes are discussed separately as follows:

A) *First prototype*

The radiation pattern for each frequency is measured at its corresponding ϕ =constant planes and at the specular plane, shown in figure 4.19, where it can be seen that all the beams are directed to θ=10° with a tolerance of ±0.7°. The radiation patterns at each frequency are all normalised to the maximum directivity of the antenna at that frequency. The antenna demonstrates a satisfactory performance in terms of side-lobe level except at 13 GHz where rather high side lobe level and high radiation level in the specular direction are observed. This issue is due to the frequency shift that occurs particularly at 13 GHz which is more obvious in the antenna measured gain curves (figure 4.20). In order to measure the antenna gain, a frequency sweep has been carried out at each of the four specified directions and, as shown in figure 4.20, the gain reaches its maximum at the intended frequency. As mentioned, we have a frequency shift at $\theta = 10°, \phi = 135°$ where the maximum gain occurs at 13.14 GHz instead of 13 GHz. It is believed that this frequency shift is principally due to printed elements under-etching causing the elements to be slightly shorter than what they should be. A slight
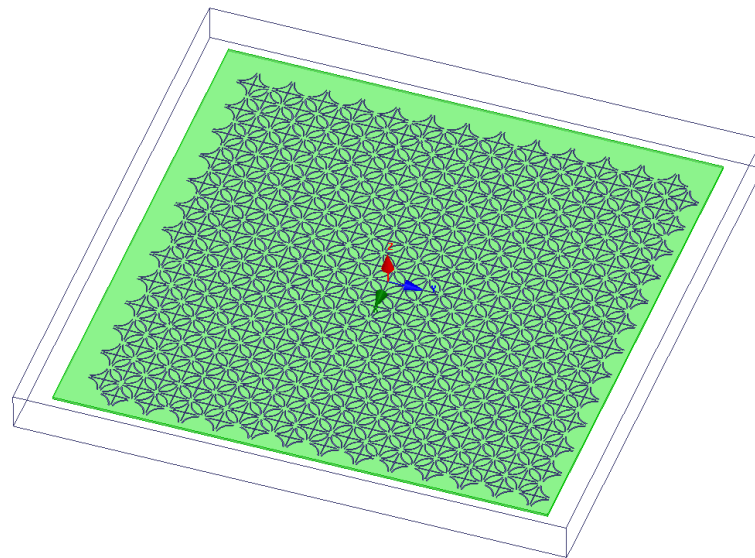
(a) Simulated structure in HFSS environment.
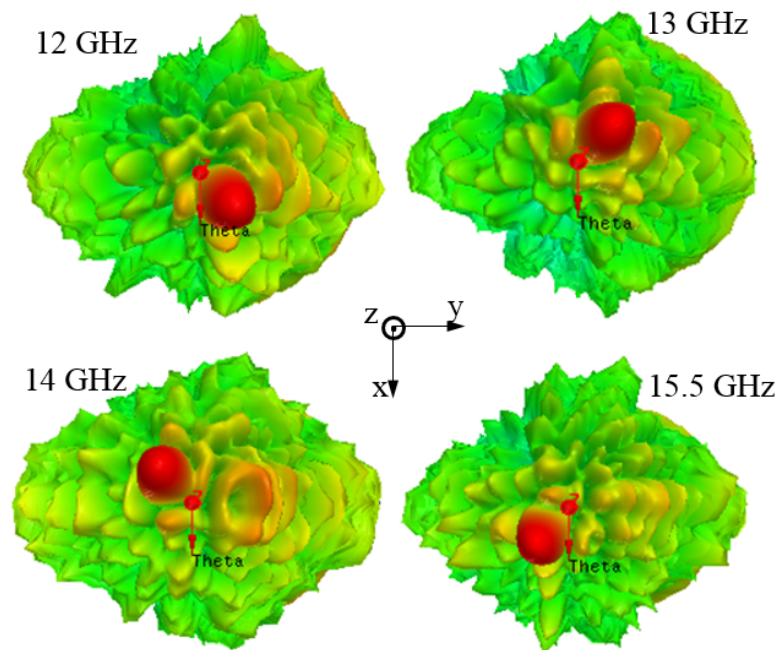
(b) Simulated radiation pattern.

Figure 4.18: a) Simulated quad-band reflectarray in HFSS environment. The feed horn has been considered as an imported radiation pattern. b) 3D simulated far-field pattern of the first quad-band reflectarray antenna with 13×13 cells. The antenna has a gain of 21.8, 23.1, 22.1 and 24.6 dB at 12, 13, 14 and 15.5 GHz, respectively. The cross-polarization level is below -30 dB in all the cases. The antenna has the maximum gain at the intended direction for each frequency [82].

upward frequency shift in the other directions supports this argument. Lack of homogeneity in the permittivity of the substrate could also be one of the frequency shift causes. Tabel 4.3, summarises the first quad-band reflectarray performance.

Table 4.3: First quad-band reflectarray performance [82].

Frequency (GHz)	Beam width	Side-lobe level (dB)	X-pol level (dB)	Bandwidth	Gain (dB)
12	6.6°	18	<-30	2.5%	22.63
13	6.4°	10	<-30	2.5%	20.29
14	6.2°	16	<-30	3.45%	23.45
15.5	5.7°	16	<-30	4.16%	24.61

B) *Second prototype*

Similarly, for the second prototype, the radiation pattern at each frequency has been measured on the corresponding ϕ-constant plane and normalised to the maximum directivity at that frequency (figure 4.21.a). It can be seen that all the beams are directed to $\theta=10°$ as designed. In addition, measured specular radiation at each frequency, normalised to the maximum antenna directivity at that frequency, is shown in figure 4.21.b. The antenna demonstrates a satisfactory performance in terms of side-lobe level at all the frequencies and unlike the first prototype, it has undergone no frequency shift as it is confirmed as well in gain curves shown in figure 4.22. In order to measure the antenna gain, a frequency sweep has been carried out at each of the two main specified directions and as shown in figure 4.22 the gain reaches its maximum at the intended frequencies. Tabel 4.4, summarises the second quad-band reflectarray performance.

Table 4.4: Second quad-band reflectarray performance [82].

Frequency (GHz)	Beam width	Side-lobe level (dB)	X-pol level (dB)	Bandwidth	Gain (dB)
12	6.8°	12.47	<-30	2.5%	23.24
13	6.7°	15.7	<-30	2.5%	22
14	5.8°	16.8	<-30	3.45%	25.38
15.5	5.7°	20	<-30	4.16%	26

In the both cases, the side lobe level at each frequency has been taken as the maximum value between the side lobe level of the radiation pattern on the diagonal planes and the specular radiation level. In comparison, one notices that the second prototype demonstrates better performance due to the reduction of the frequency shift.
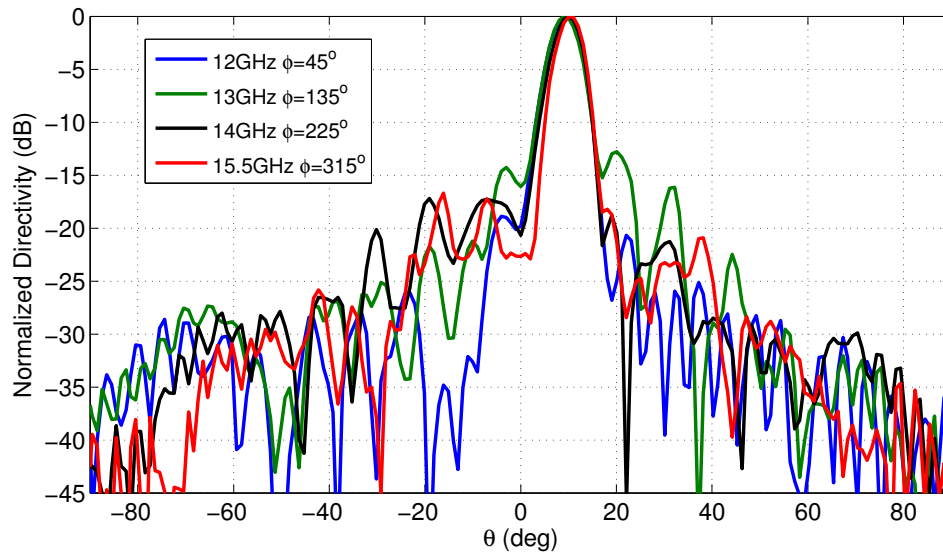
(a) Radiation pattern on ϕ =constant planes.
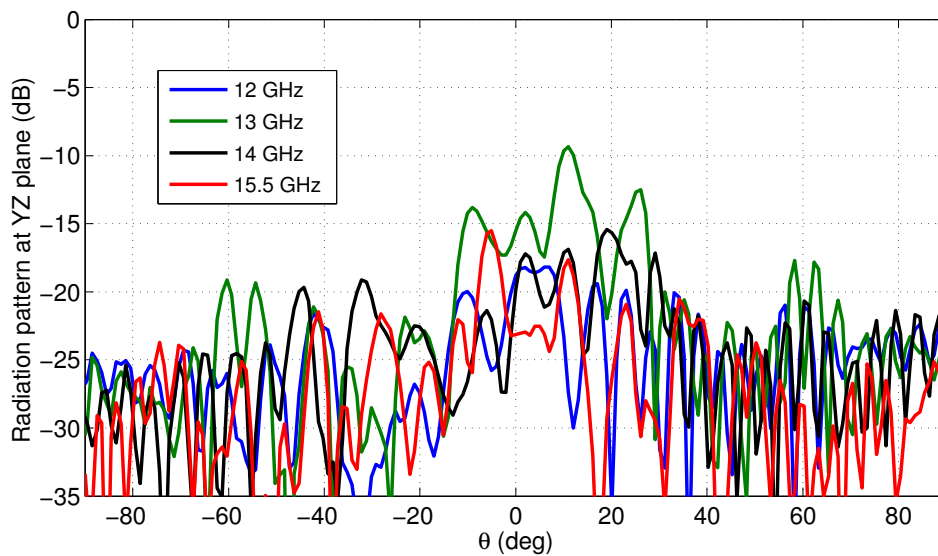
(b) Radiation pattern on yz plane (specular radiation).

Figure 4.19: Measured co-polar radiation pattern of the first prototype at different frequencies on a) ϕ =constant planes b) yz plane (specular radiation). Relatively high side-lobe levels at 13 GHz seen on both figures are due to the antenna frequency shift [82].

4.4 Conclusion

In this chapter we have presented a low-cost and multi-functional quad-band reflectarray antenna operating at four closely separated frequencies namely at 12, 13, 14 and 15.5 GHz. The reflectarray antenna unit-cell has the advantage of being a single layer dual linear polarized
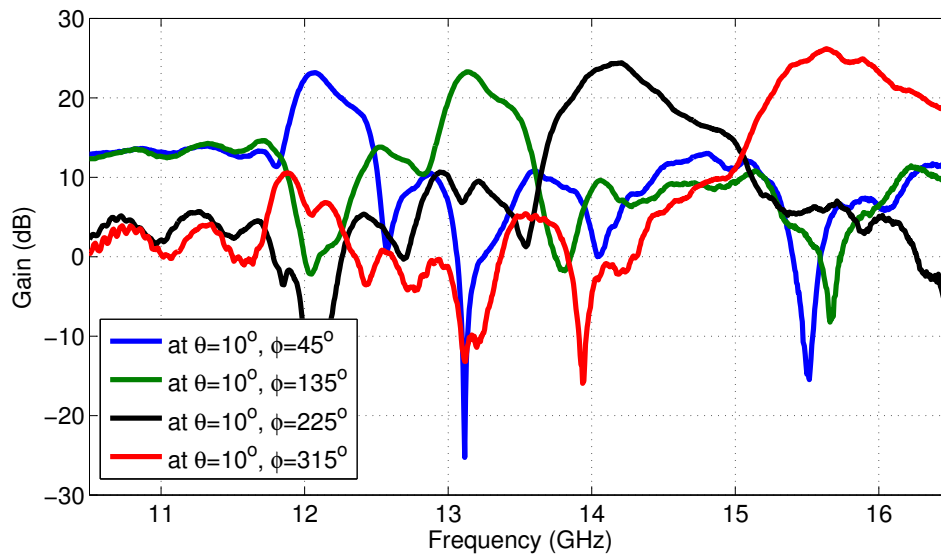
Figure 4.20: Measured gain of the first quadband reflectarray. A general frequency shift is noticeable specially at $\theta = 10°, \phi = 135°$ where the peak occurs at 13.14 GHz instead of the intended 13 GHz [82].

structure. This enables the reflectarray to operate at circular polarization as well. Based on the new unit-cell two reflectarray antenna prototypes having specific beam directions for the four frequency bands were fabricated and measured as proof-of-concept. Measurement results show a satisfactory performance of the two prototypes in spite of using an electrically small antenna plate. It should be noted that since the phase-shift of the unit-cell at each frequency depends on only one parameter, the array design becomes very simple.
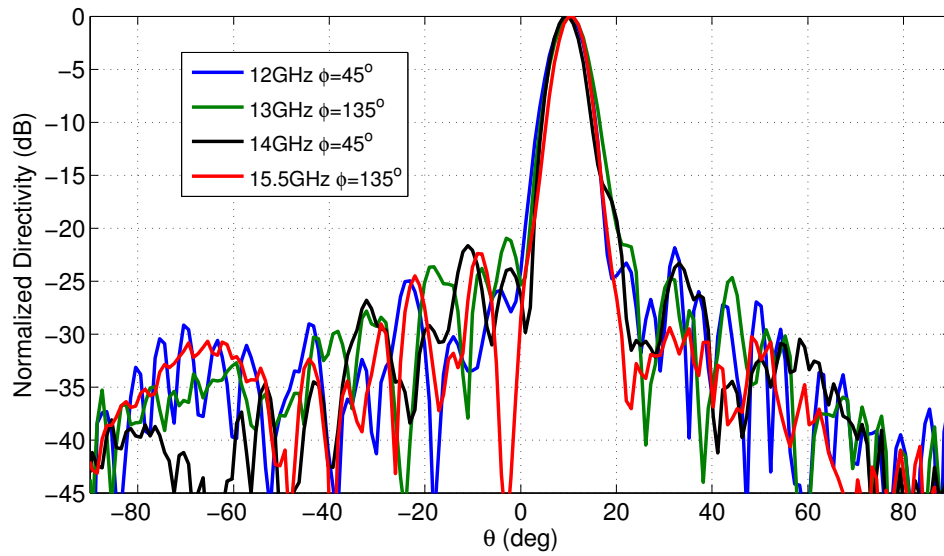
(a) Radiation pattern on ϕ =constant planes.
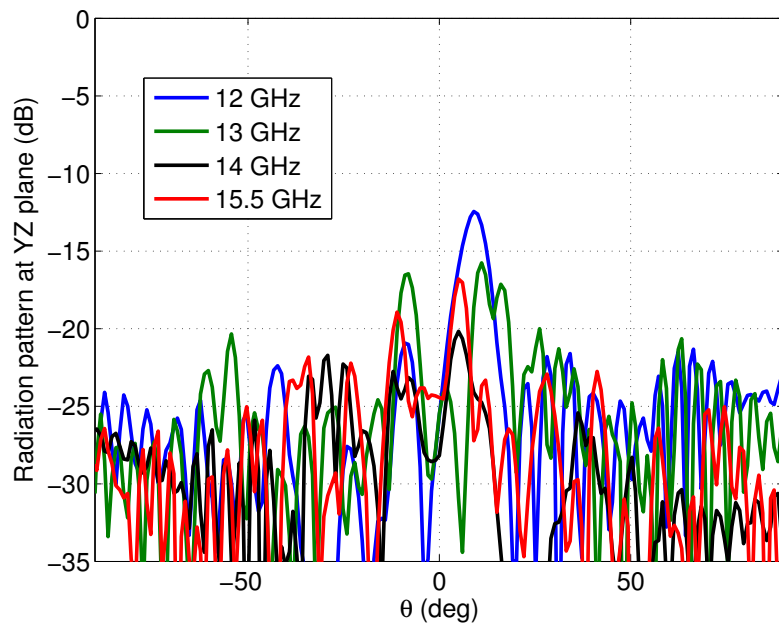
(b) Radiation pattern on yz plane (specular radiation).

Figure 4.21: Measured co-polar radiation pattern of the second prototype at different frequencies on a) ϕ =constant planes b) yz plane (specular radiation) [82].
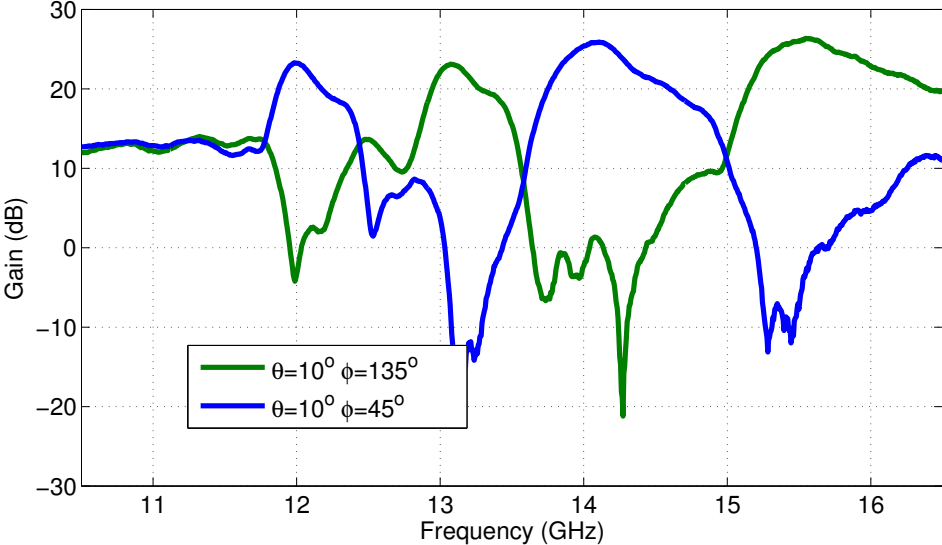
Figure 4.22: Measured gain of the second quadband reflectarray. As designed, for each specific direction, gain has its peak at the two intended frequencies [82].

5 Dual-Band, Dual-Polarized Reconfigurable Reflectarray Antenna

5.1 Introduction

One of the most prominent advantages of reflectarray antennas, is their capability to provide electronic beam scanning, in a cost-effective, simple and efficient way, by using unit-cells integrated with discreet elements such as varactor and PIN diodes [11, 12], ferro-electric devices [13] and MEMS [14–16]. Electronic beam scanning is feasible with the conventional phased-array antennas however, since each radiating element has to be assigned with a sophisticated transceiver module, the implementation cost will become very high. In addition, the usage of transmission line feeding network in phased-array antennas will degrade their efficiency because of the losses that occur at high frequencies while these disadvantages have been avoided in reconfigurable reflectarrays.

In addition, reconfigurable reflectarrays have proven to demonstrate advanced capabilities in terms of operating frequency and polarization. In other words, it has been shown that simultaneous phase control over several frequency bands and/or the polarization is possible. Such additional capabilities are of high interest in many radar, satcom and cognitive radio applications. The most prominent examples for multi-band and polarization-flexible reconfigurable reflectarrays can be found in [17] and [18], respectively. In [17] the proposed cell is a dual linearly polarized cell which is also capable of controlling independently the phase of each TE/TM linear polarization at single frequency. It is evident that the proposed cell can be also used for circular polarizations. In [18], the reflectarray antenna possesses the capability of independent beam scanning at two frequencies of 24 and 35 GHz. The proposed unit-cell operates however only for circular polarization and thus fails at linear polarization beam-scanning. It's worth noting that in the majority of applications a common beam for both of the polarizations is desired and in addition cells with dual-linear polarizations have the advantage of performing as well for circular polarizations.

This chapter introduces a topology for a reconfigurable dual-band dual-polarized reflectarray cell at Ku band centred around 12 and 14 GHz. The novel unit-cell is composed of a printed cross-dipole element with a rectangular split-ring element. In order to achieve reconfigurable capability, 5 varactor diodes controlled by only two voltages- one for each frequency- are

employed to control the phase response of the unit-cell. Simulated results show that at each frequency band the phase response is dependent on only one of the applied voltages. This means that a single layer printed reflectarray antenna could be realized possessing independent beam scanning capability in two closely separated frequency bands. The main issue in the design is the unit-cell high cross polarization level because of its non-symmetrical geometry. In order to circumvent this issue, cells are arranged on the array surface in a particular way namely chessboard arrangement. Fullwave simulation results along with the developed theory for the proposed arrangement, show the effectiveness of the chessboard arrangement.

5.2 The unit-cell

Figure 5.1 shows the schematic view of the unit-cell with the varactor diodes and the high-value resistors for biasing. As shown in figure 5.1, at the lower band, i.e. 12 GHz, for both polarizations the phase response is controlled by voltage V_1 applied to the diode D_1. As for the upper band, i.e. 14 GHz, the phase response is controlled by four similar diodes having voltage V_2 applied to them. It is obvious that, due to the series configuration of the D_2 diodes, in order to have the desired voltage, say Vp_2, across each D_2 diode, the applied voltage should be $2 \times Vp_2$. As for the diodes DC biasing, the voltages are applied to the diodes through vias which are themselves connected to the unit-cell elements through high-value resistors of value $1 k\Omega$ denoted in the figure by R_b. It should be noted that the proposed unit-cell is an extension to the dual-band, dual-polarized unit-cell introduced in the previous chapter. In the unit-cell simulation, diodes have been replaced by their equivalent capacitances in series with a 0.3Ω resistor representing diode ohmic losses and a $0.4nH$ inductor for the packaging effect. For the used MGV125-09 Hyperabrut GaAs varactor diode from Aeroflex-Metelics [87], the capacitance varies from 0.8 to $0.07pF$ corresponding to an applied voltage of 2 to $20V$.

5.3 Unit-cell high cross-polarization level: chessboard arrangement

In the course of simulation it was found out that the unit-cell suffers from high cross-polarization levels. This issue is attributed to the presence of the the non-symmetrical cross-dipole designated for 12 GHz. Figure 5.2 shows the phase and amplitude response of the unit-cell with periodic boundary conditions where it is observed that the unit-cell at 12 GHz lacks the required phase-range and suffers from high level of cross-polarization at its resonance. The responsible element for this deficiency is also shown in figure 5.2 on which the co-polar and cross-polar currents are shown with red and blue arrows respectively, for the element illuminated by a vertically polarized electrical field. The solution to avoid the cross-polarization level in the resultant reflectarray would be to use a chessboard configuration.

In chessboard configuration, cells are arranged is a way that each one is the mirror of its immediate neighbour. Figure 5.3 compares two reflectarray cell arrangements, a conventional and a chessboard arrangement. In figure 5.3a it can be observed that, by using a conventional arrangement, the induced cross-currents (shown with red arrows) would give rise to a high-level
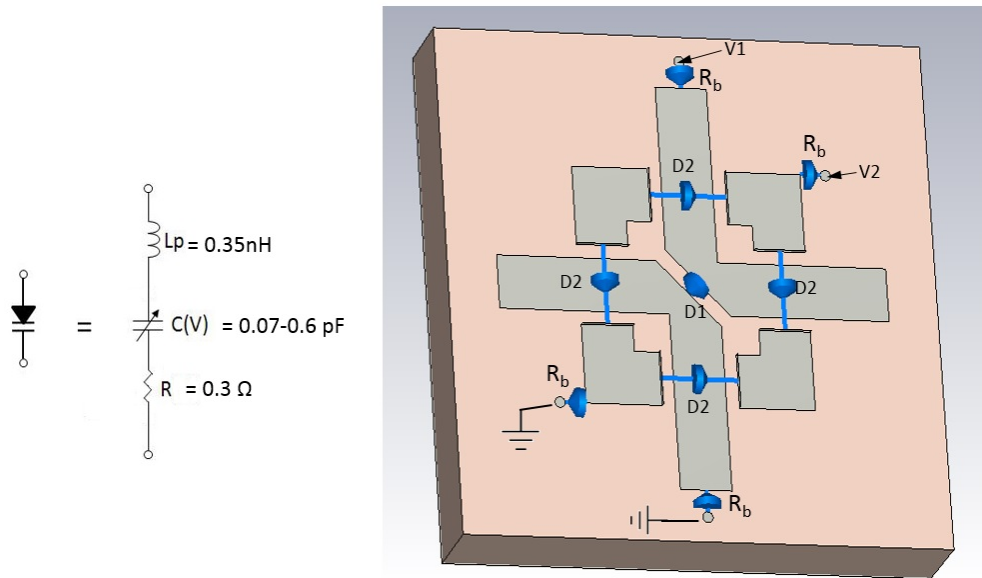
Figure 5.1: Proposed topology for the dual-band, dual-polarized unit-cell. On the left, the equivalent circuit of the varactor diode is shown.

of cross-polarization, when illuminated by a vertically polarized electrical field. Figure 5.3b shows on the other hand a chessboard arrangement where each cell/element is the mirror of its immediate neighbour. With this arrangement, the cross-polar field-components generated by the cross-currents will cancel each other out in the antenna far-field. The phase response of the cell, in case of a chessboard arrangement can be in fact obtained by simply putting the cell inside an E-H wall waveguide [1]. By doing so, figure 5.4 shows the phase and amplitude responses of the unit-cell for perpendicular wave incidence at 12 and 14 GHz in terms of varying capacitance C1 and C2 of the diodes D1 and D2 respectively. As shown, for each frequency we achieve sufficient phase range which is dependant on one of the capacitances while almost independent from the other one. As for amplitude responses, the maximum amount of loss due to the varactors is estimated to be maximum 2 dB in both frequencies. The size of the unit-cell is 9.5 mm corresponding to 0.44λ at 14 GHz which rolls out the presence of grating lobes at any scan angle in the upper hemisphere region.

5.4 Theory of the chessboard arrangement

For a reflectarray antenna the chessboard arrangement was first proposed in [88] for a particular case where the beam was directed to broadside direction while the reflectarray had a center-fed configuration. This technique proved to be more effective than a previous method introduced in [89]. Experimental results showed a 1 to 12 dB reduction in cross-polarization level and a notable increase in the antenna's overall gain. This subsection however will treat such an arrangement in more detail and for the case when we have beam steering. To begin
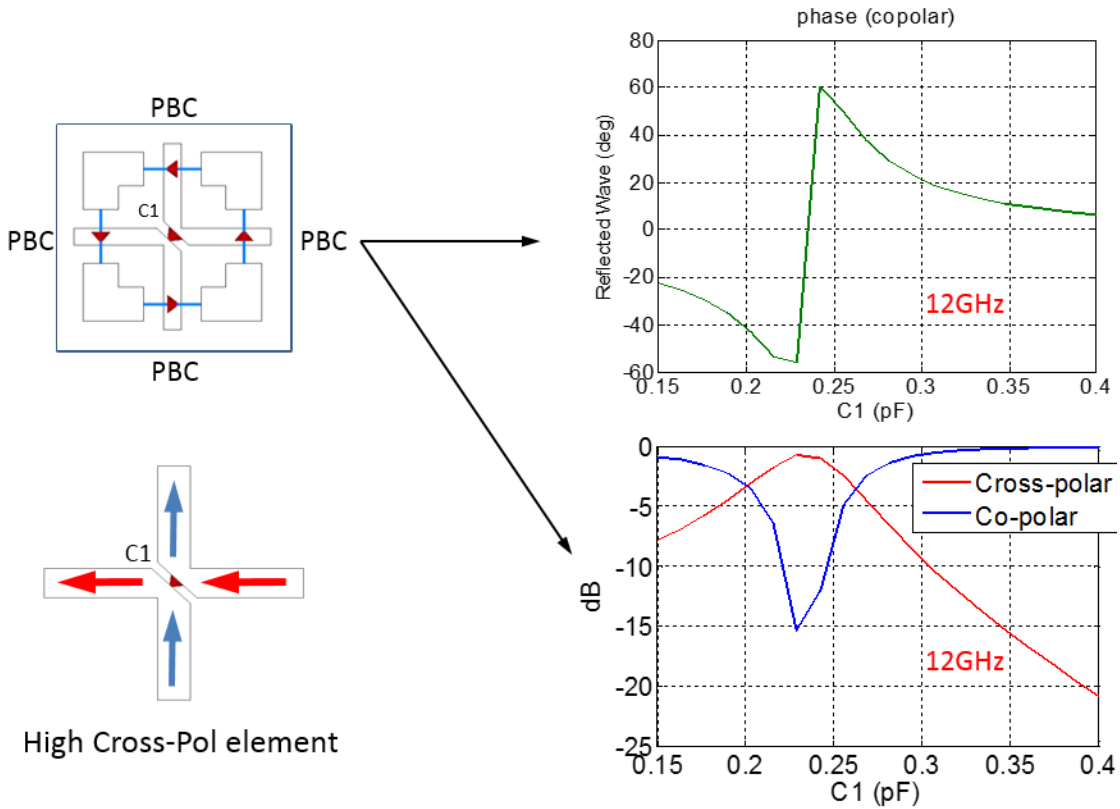
Figure 5.2: Cross-polarization issue of the dual-band reconfigurable unit-cell. The proposed cell lacks phase range and suffers from high levels of cross-polarization when simulated with periodic boundary condition. This deficiency is due to the cross-dipole of 12 GHz shown in the left-bottom of figure. The incident vertically polarized electrical field, will induce horizontal cross-currents that give rise to high cross-polarization level.

with, we consider the reflectarray antenna shown in figure 5.3b which uses the high cross-pol cross-dipoles. The goal here is to determine the behaviour of the cross-polarization pattern when we steer the beam to the angle of (θ_0, ϕ_0). To this aim, following assumptions are made:

1- The amplitudes of the reflected co-polar and cross-polar fields are uniformly distributed on the array surface. In addition, each cell reflects both components with the same amplitude (see figure 5.3b).
2- Same phase distribution is assumed for both components with the exception that cross-polar currents at each cell are 180 out of phase with respect to their immediate neighbour (see figure 5.3b).

With the above assumptions, referring to figure 5.3b, we are in fact dealing with two reflectarray antennas, one for co-polar fields (blue arrows) and one for the cross-polar ones (red arrows)

72
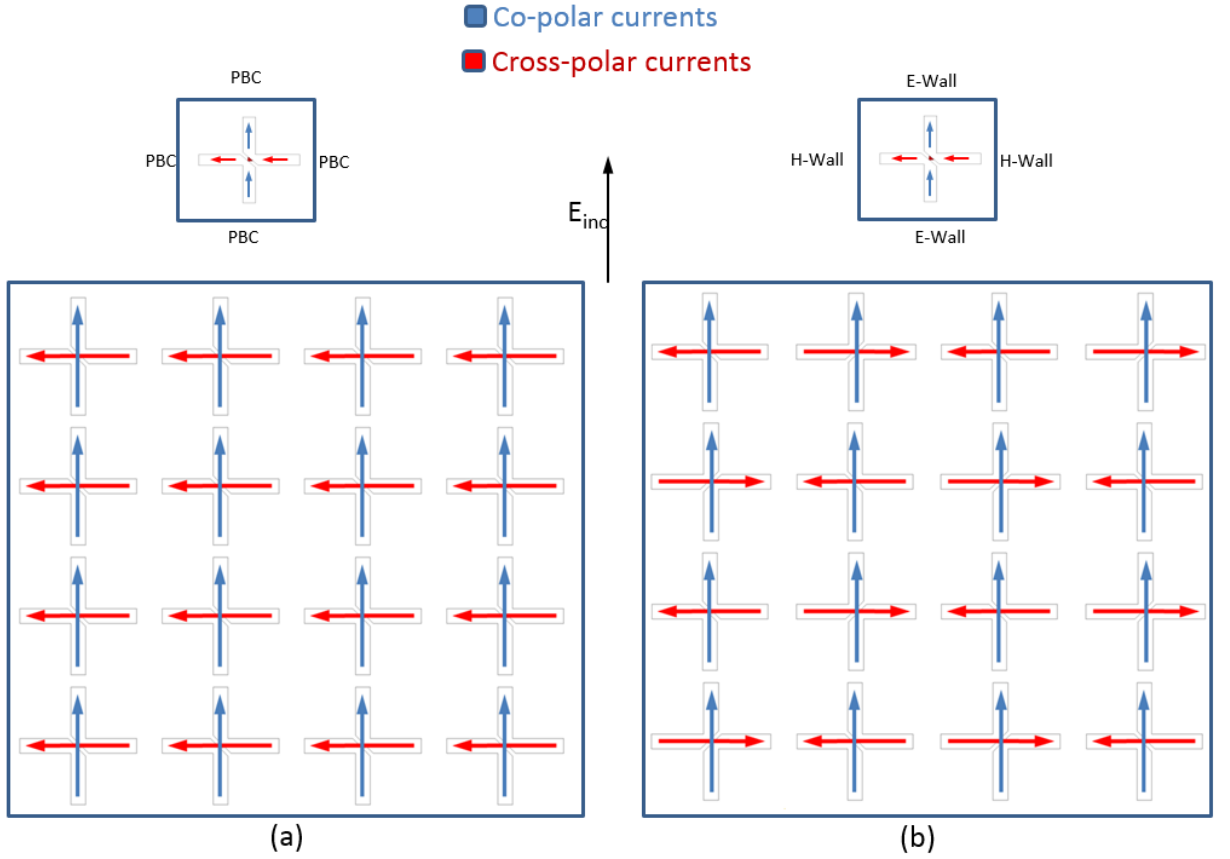
Figure 5.3: Chessboard arrangement and its comparison with a conventional one. a) By using a conventional arrangement constructed as a result of assigning periodic boundary condition, the induced cross-currents (shown with red arrows) would give rise to a high-level of cross-polarization, when illuminated by a vertically polarized electrical field. b) In a chessboard arrangement, constructed by using an E-H wall wave-guide, each cell/element is the mirror of its immediate neighbour. With this arrangement, the cross-polar field-components generated by the cross-currents will cancel each other out in the far-field

that are radiating simultaneously. Therefore, according to the phased-array antenna theory, the following normalised array factors will be obtained for each of the co and cross-polar arrays:

$$F_{co}(\theta,\phi) = \frac{sinc(\frac{Md_x(u-u_0)}{\lambda})}{sinc(\frac{d_x(u-u_0)}{\lambda})} \frac{sinc(\frac{Nd_y(v-v_0)}{\lambda})}{sinc(\frac{d_y(v-v_0)}{\lambda})} \tag{5.1}$$

$$F_{cross}(\theta,\phi) = \frac{sinc(\frac{Md_x(u-u_0)}{\lambda} + \frac{M}{2})}{sinc(\frac{d_x(u-u_0)}{\lambda} + \frac{1}{2})} \frac{sinc(\frac{Nd_y(v-v_0)}{\lambda} + \frac{N}{2})}{sinc(\frac{d_y(v-v_0)}{\lambda} + \frac{1}{2})} \tag{5.2}$$
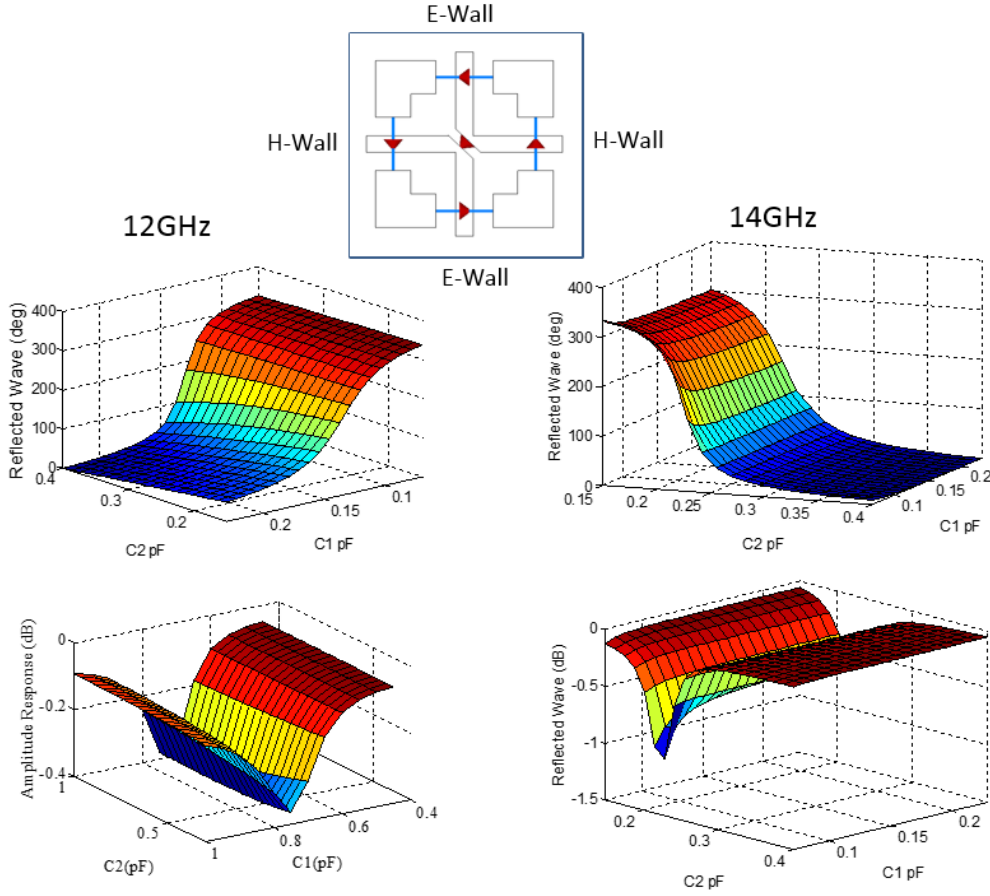
Figure 5.4: Phase response of the reconfigurable cell using E-H wall waveguide at 12 and 14 GHz. With an E-H wall waveguide, which corresponds to a chessboard arrangement, we achieve enough phase range and the cross-polarization issue is solved. Losses are only due to the varactor diode losses.

Where d_x and d_y are array element spacing along x and y axis, respectively, $sinc(x) = \frac{\sin(\pi x)}{\pi x}$ and:

$$u = \sin(\theta)\cos(\phi), \quad v = \sin(\theta)\sin(\phi), \quad u_0 = \sin(\theta_0)\cos(\phi_0), \quad v_0 = \sin(\theta_0)\sin(\phi_0) \qquad (5.3)$$

From equation 5.4 the direction of the cross-polar main lobes can be obtained by solving the following equations:

$$u = \frac{p - 1/2}{\frac{d_x}{\lambda}} + u_0, \qquad\qquad v = \frac{q - 1/2}{\frac{d_y}{\lambda}} + v_0 \qquad\qquad (5.4)$$

Where p and q are any integer number for which, the values of u and v are obtained and hence the direction of the main lobes are achieved. It is of course desired that no main lobe appear for the cross-polar array. This means that for any integer values of p and q no real

values must exist for u and v. In other words:

$$u^2 + v^2 > 1 \Rightarrow \left(\frac{p-1/2}{\frac{d_x}{\lambda}} + u_0\right)^2 + \left(\frac{q-1/2}{\frac{d_y}{\lambda}} + v_0\right)^2 > 1 \tag{5.5}$$

As a result, it can be proved that for the case where $d_x = d_y = d$, the following condition should be met in order to rule out the appearance of any cross-polarization lobes:

$$d < \frac{\lambda}{\sqrt{2}(1 + \sin\theta_0)} \tag{5.6}$$

Compared to equation 3.8, 5.6 simply means that, if we want to use a chessboard configuration, the elements spacing should be smaller than that of the case where we are using a conventional element arrangement by a factor of $\frac{1}{\sqrt{2}}$.

5.4.1 Dual-polarized performance of a chessboard arrangement

Referring to figure 5.3b, a question might arise concerning whether the depicted chessboard arrangement is dual-linearly polarized. To clarify this issue, figure 5.5 shows the chessboard arrangement illuminated by two perpendicular incident waves. The generated co and cross currents on the elements in each case show that in each case the unwanted cross currents have the direction opposing each other in the neighbouring cell. As a result we can conclude that the presented chessboard array is dual-polarized.

5.5 Full-array simulation of a reconfigurable reflectarray with a chessboard arrangement

5.5.1 Practical scenario for the unit-cell phase response simulation

In order to verify the performance of a chessboard arrangement, we take the high cross-polar unit-cell shown in figure 5.6 where a practical topology has been considered for the reconfiguration. As shown, the varactor diode which is replaced by a capacitor (light green), a resistor of 0.3Ω (black) and an inductor of 0.35nH (brown), is biased through vias from beneath through two $1k\Omega$ resistors as AC isolators. We have used here simple resistors instead of RF chokes, since the varactor diode does not consume any DC current and as a result, the applied voltage to the vias will drop directly across the varactor. In order to estimate the phase response, in practice we cannot implement an E-H wall waveguide and instead we can use a Waveguide Simulator (WGS). The WGS model is a well-known method to measure the active element performance of array elements in the array environment [1, 90, 91]. In this technique, by putting the element at the end of a single-mode waveguide one can measure the reflection response (phase and amplitude) of that element in an infinite chessboard arrangement for a specific value of incident angle and frequency at a single polarization. In a WGS, the frequency
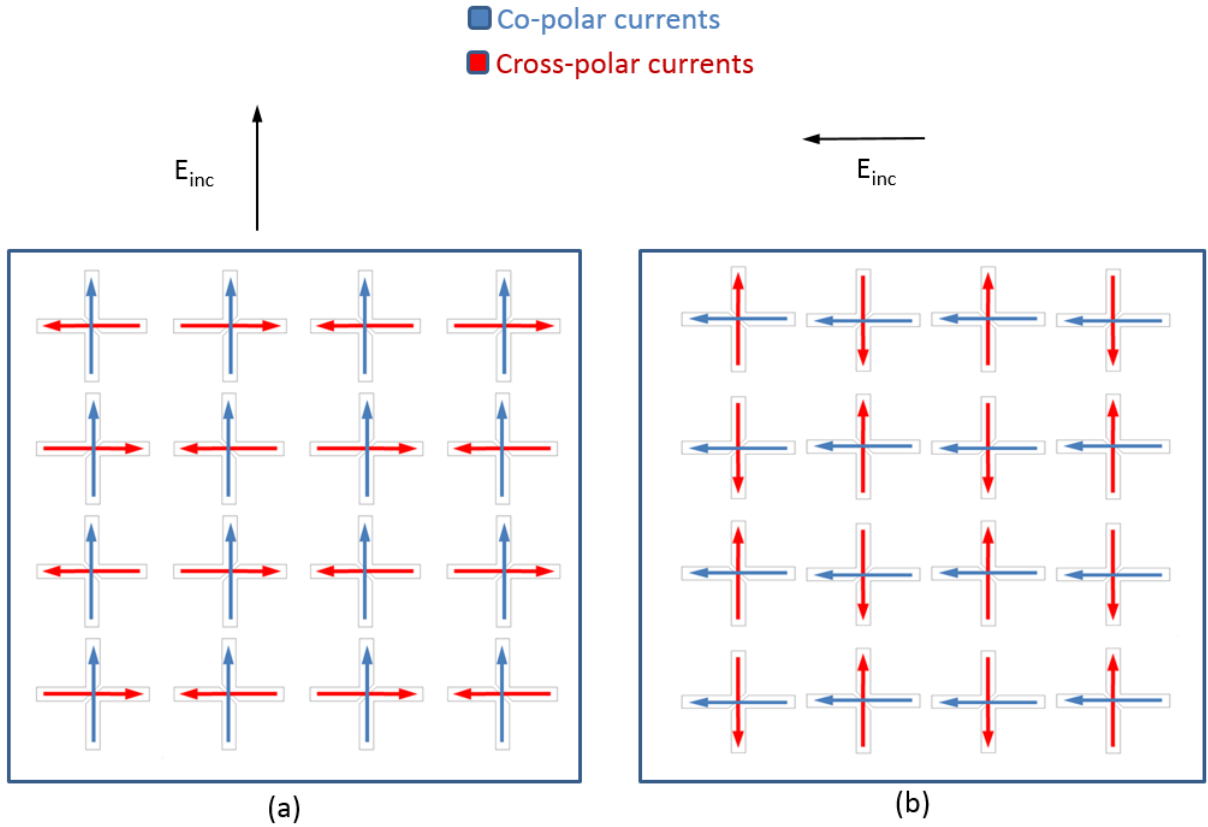
Figure 5.5: Dual-polarization performance of chessboard arrangement. a) The array is excited by a vertically polarized incident wave. b) The array is excited by a horizontally polarized incident wave.

and the angle of incidence have the following relationship:

$$\sin(\theta_{in}) = \frac{\pi}{k_0 a} \tag{5.7}$$

Where a is the H-plane or generally the long dimension of the waveguide. Figure 5.7 shows the simulation scenario of the reconfigurable unit-cell with WGS carried out in HFSS. In this scenario, two elements, each with the exact same varactor diode but flipped with respect to each other, are installed at the end of a WR75 standard waveguide with single mode (TE10) operational frequency of 10 to 15 GHz. Knowing the fact that the large and small dimensions of WR75 waveguide are $a = 19mm$ and $b = 9.5mm(= \frac{a}{2})$, respectively, the reflection coefficient of the waveguide will be the phase response of a chessboard configuration with grid spacing of $9.5mm$ and an incident angle of 40° at 12 GHz according to 5.7. In addition, the incorporation of vias will make the measurement scenario less complicated and we can easily design the biasing circuit behind the ground plane. Figure 5.7c compares the phase response obtained using an E-H wall waveguid with that of achieved using WR75 waveguide. As shown, the two phase responses have minor discrepancy with respect to each other and as a result the
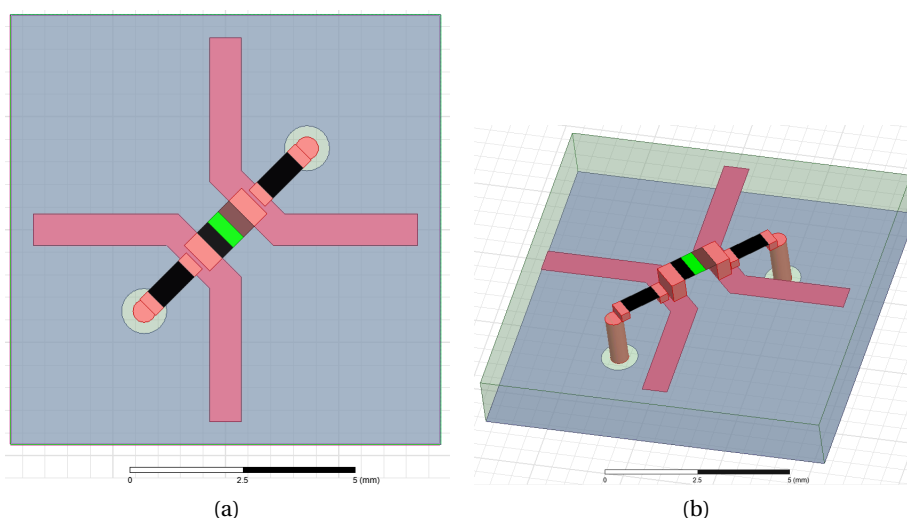
Figure 5.6: a) top view and b) 3D view of the reconfigurable high-cross polarization unit-cell with biasing scheme. The varactor diode which is replaced by a capacitor (light green), a resistor of 0.3Ω (black) and an inductor of 0.35 nH (brown) is biased through vias from beneath through two $1k\Omega$ resistors as AC isolators.

final reconfigurable reflectarray is designed based on the practical element phase response obtained with the practical WGS method (the red curve in 5.7c). The cross-dipole is printed on a RogersRT5880 ($\epsilon_r = 2.2$) having thickness of $1.5mm$.

5.5.2   Full-array simulation

In order to get the preliminary performance of a reflectarray with the element of figure 5.6, a full array has been simulated in the HFSS environment shown in figure 5.8. The array is fed in an offset configuration using an imported pattern of a horn antenna with $14dB$ of gain at 12 GHz placed $95mm$ above the edge of the antenna plate. The feed horn has an aperture size of $31 \times 41.5mm^2$ and its gain vs frequency is shown in figure 4.14. The full array is composed of 10×10 elements printed on a $124 \times 124mm^2$ RogersRT5880 grounded substrate ($\epsilon_r = 2.2$) having thickness of 1.5 mm. This number of elements is chosen so as to facilitate the simulation and to represent the proof-of-concept. Figure 5.9 and figure 5.10 show the beam scanning performance at three different planes of $\phi = 0°, 45°, 90°$ for $\theta = 0°, 20°, 40°$. It should be noted that the maximum scan angle (40°) and array spacing ($9.5mm$) satisfy the condition of 5.6 at 12 GHz. The average gain is estimated to be around 17.5 dB, corresponding to an aperture efficiency of 20% and the maximum cross-polarization level (not shown) is below -16dB for all the cases. The slight pattern degradation seen in Figure 5.10b is due to the fact that, the scanning plane ($\phi = 90°$) is also the incidence plane due to the position of the feed-horn (see figure 5.8). The 2D patterns for all the cases are simulated and compared in figures 5.11,5.12 and 5.13.

(a)

(b)

(c)

(d)
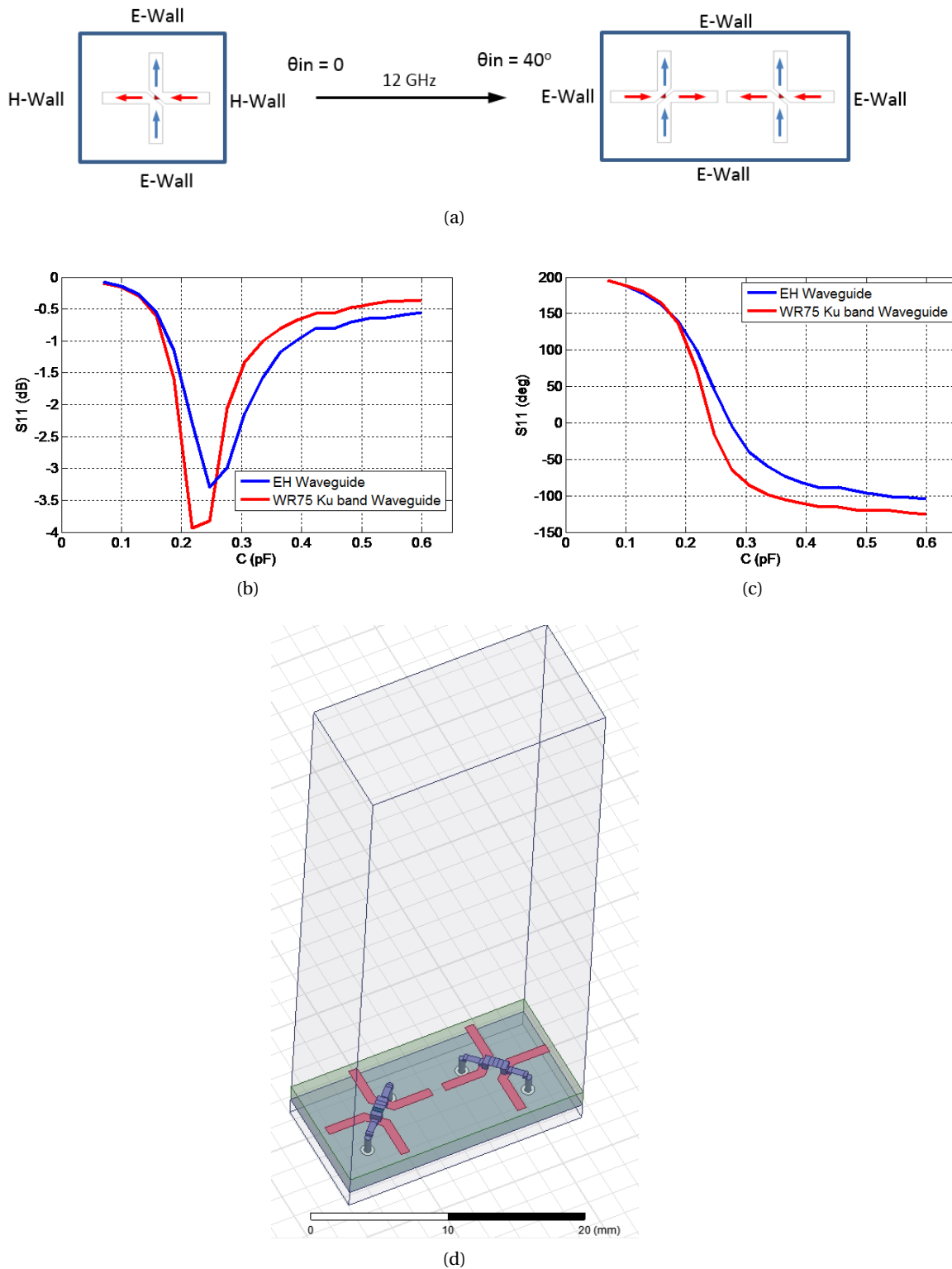
Figure 5.7: WGS simulation scenario of the high cross-polar element in a chessboard arrangement. a) The impractical simulation with an E-H wall waveguide for a normal incidence can become practical using a WR75 standard waveguide for a 40° incidence b,c) Amplitude and phase response of the unit-cell obtained with EH-wall waveguide and WR75 waveguide d) 3D view of the simulation scenario in HFSS.
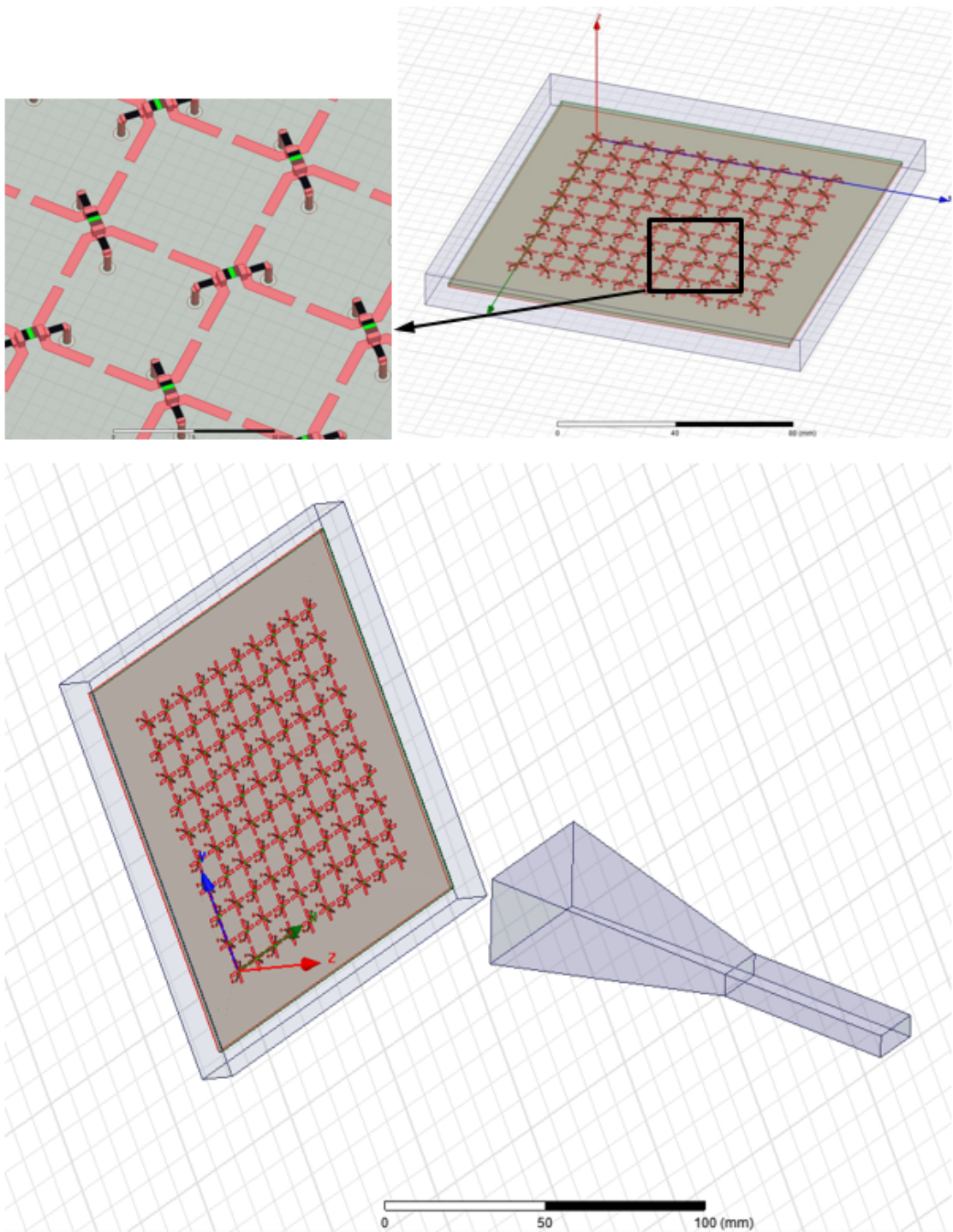
Figure 5.8: Fullarray simulated reconfigurable reflectarray with a chessboard element arrangement in HFSS environment. The array is illuminated by an imported pattern of the shown virtual horn antenna.

(a)

(b)

(c)

(d)

(e)

(f)
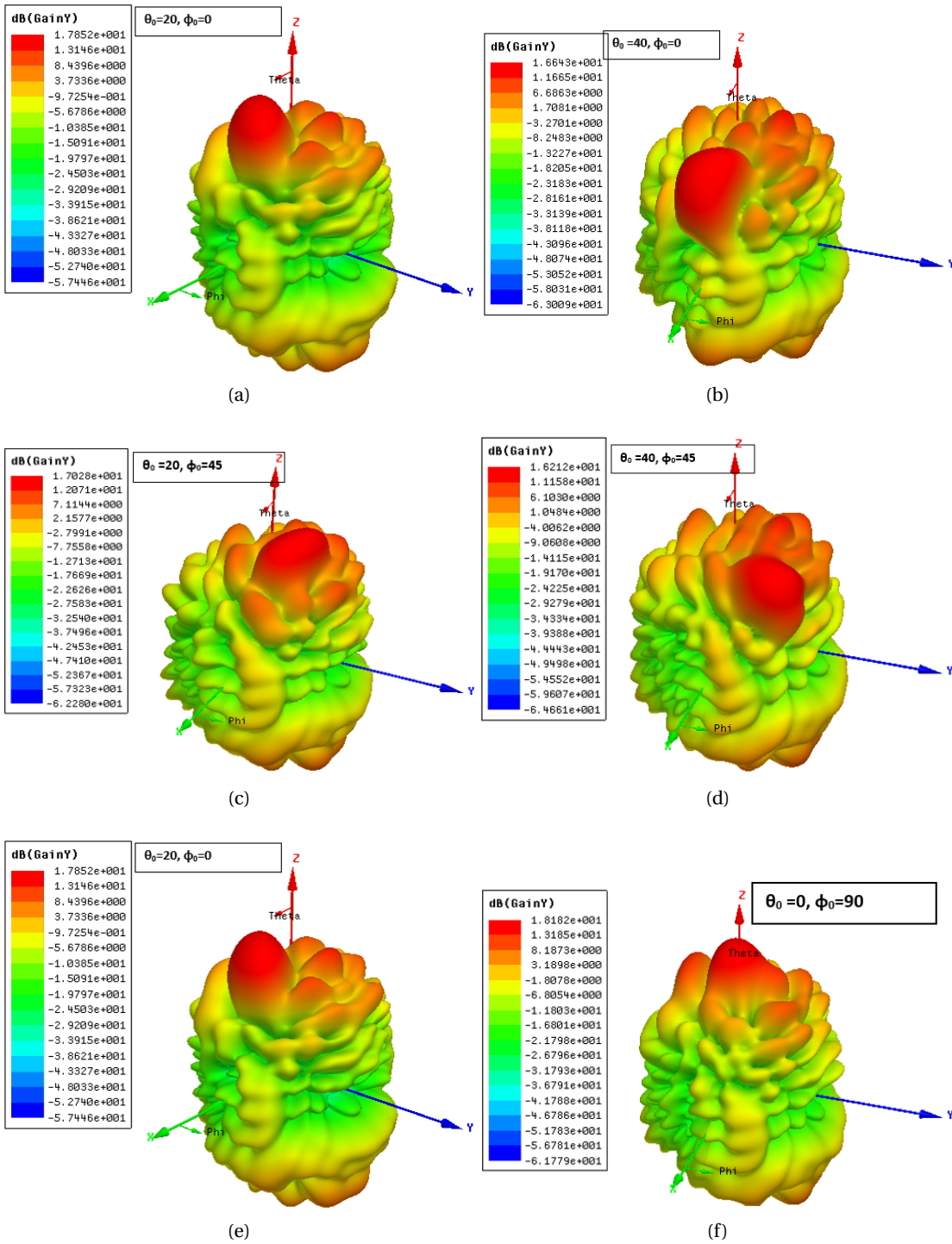
Figure 5.9: 3D co-polar radiation pattern of the reconfigurable reflectarray antenna with a chessboard configuration at different scan angles at 12 GHz. The cross-polarization level stays below -16dB for all the cases. The average gain is estimated to be around 17.5 dB, corresponding to an aperture efficiency of 20%.

(a) (b)
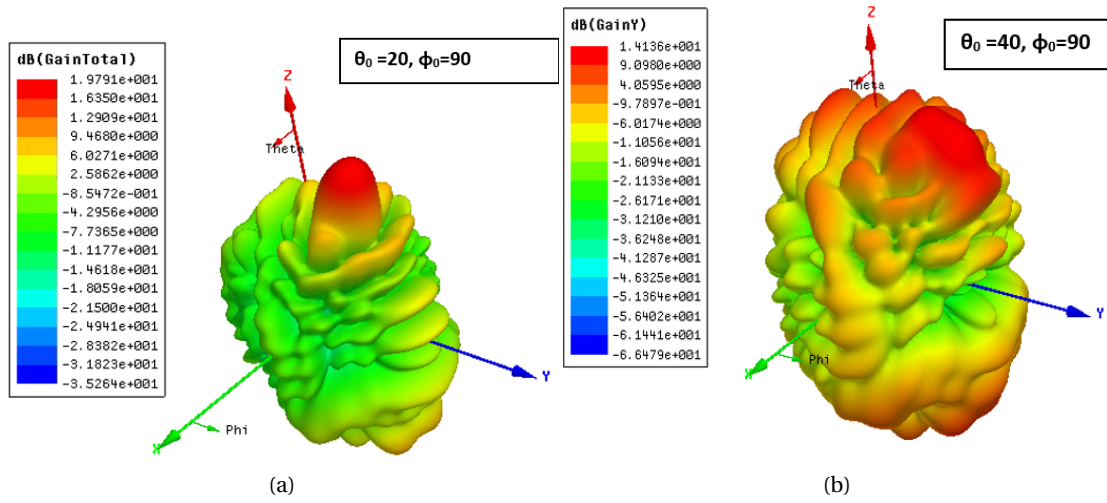
Figure 5.10: 3D co-polar radiation pattern of the reconfigurable reflectarray antenna with a chessboard configuration at at $\phi = 90°$ (specular plane) at 12 GHz. Degradation of radiation pattern is expected in this plane due to the presence of the feed horn. Small dimension of the reflectarray surface has also negative effect on the overall performance.
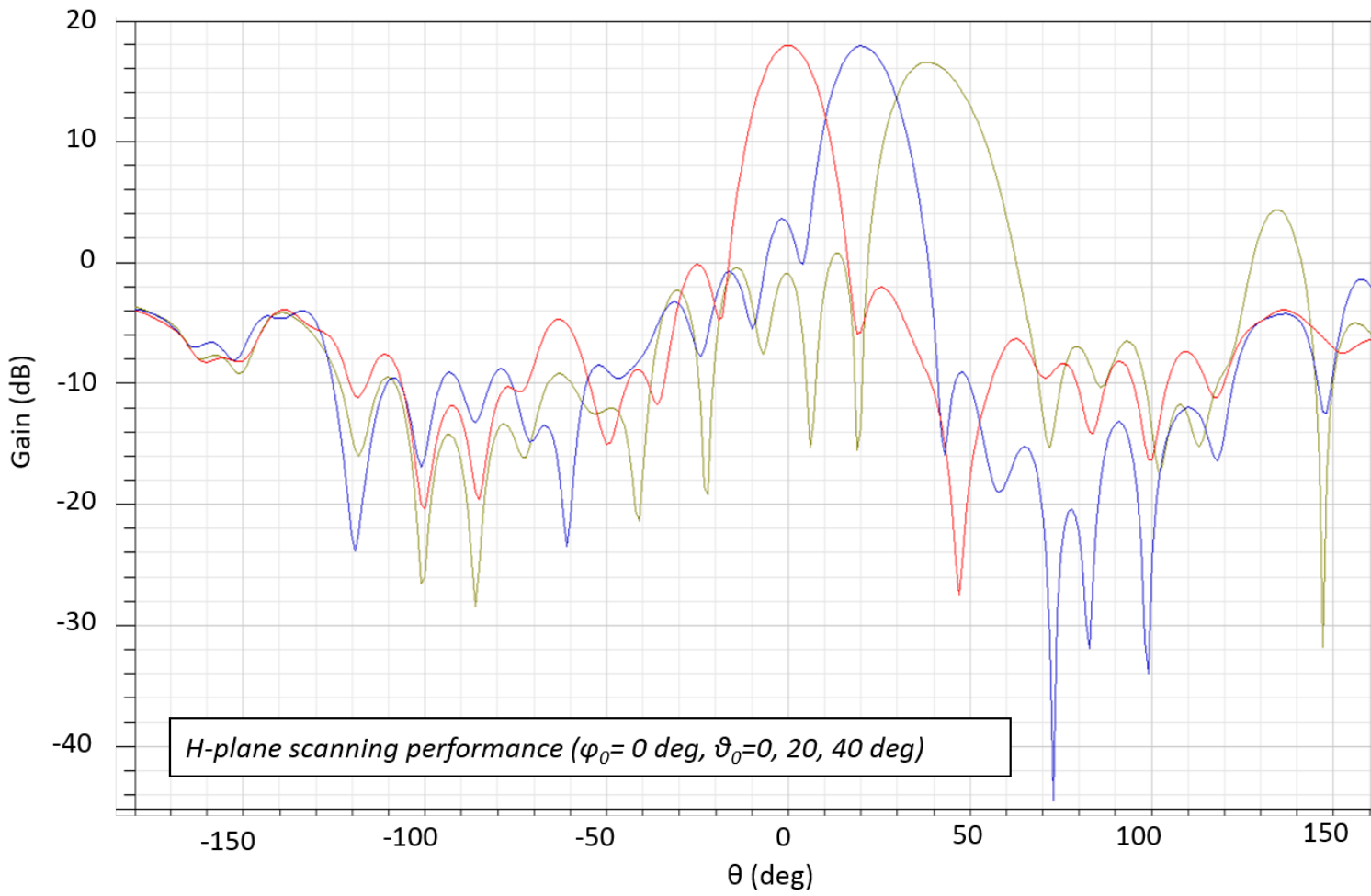
Figure 5.11: 2D co-polar radiation pattern of the reconfigurable reflectarray antenna with a chessboard configuration at $\phi_0 = 0°$ at 12 GHz.
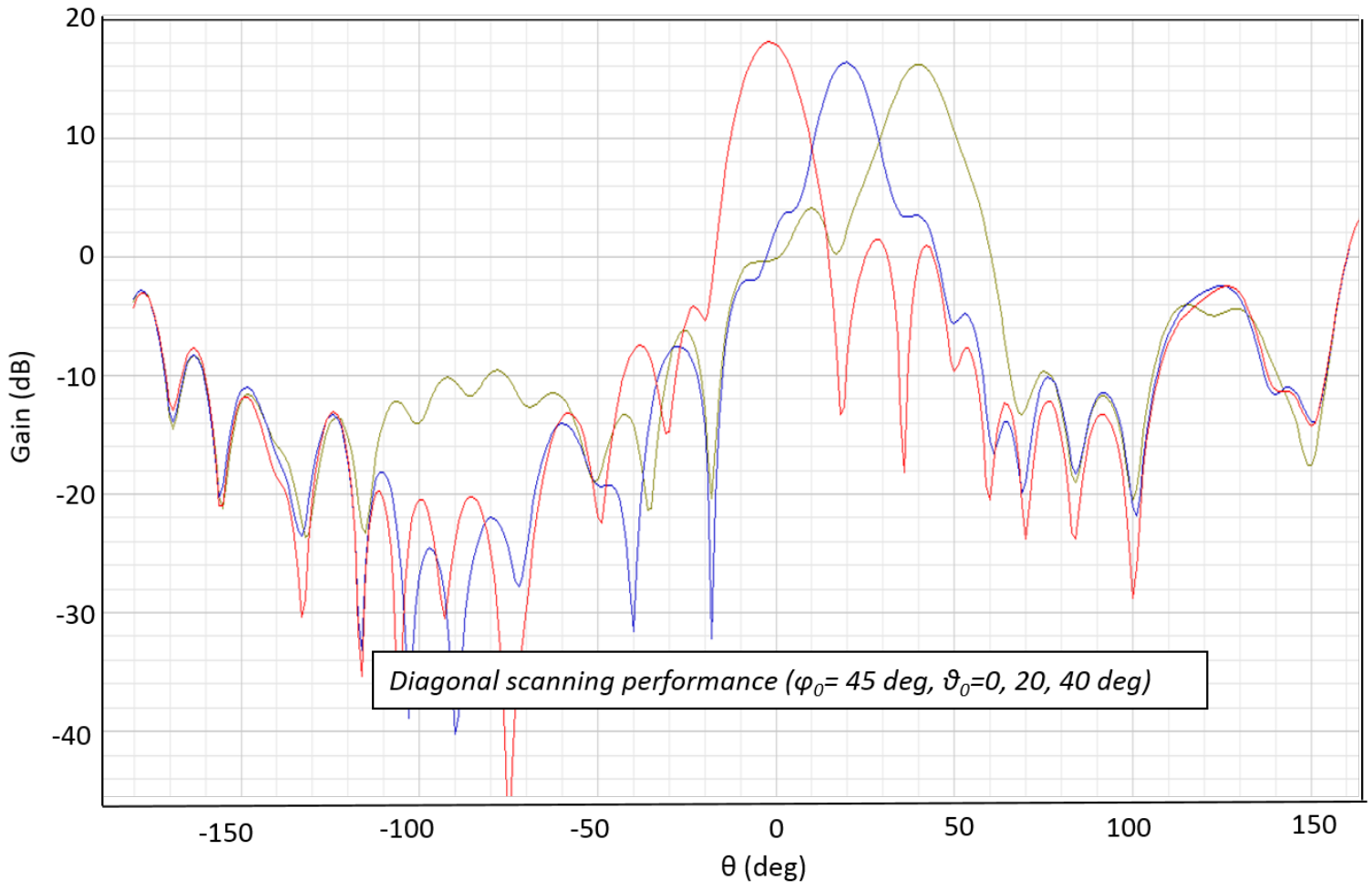
Figure 5.12: 2D co-polar radiation pattern of the reconfigurable reflectarray antenna with a chessboard configuration at $\phi_0 = 45°$ at 12 GHz.
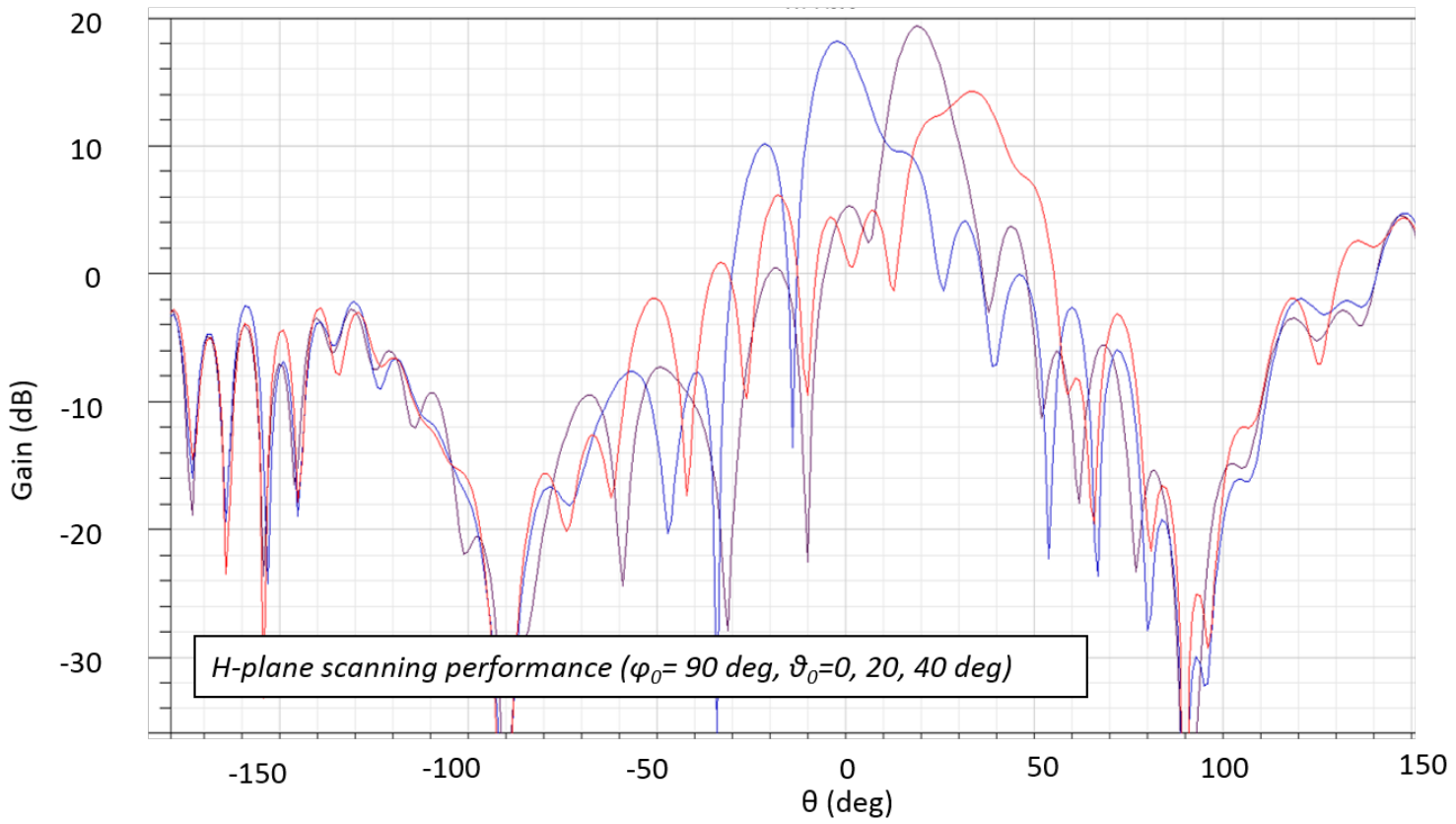
Figure 5.13: 2D co-polar radiation pattern of the reconfigurable reflectarray antenna with a chessboard configuration at $\phi_0 = 90°$ at 12 GHz.

5.6   Improvements on chessboard configuration

As discussed in the previous sections, thanks to the chessboard arrangement we could implement a low-cross polarization reconfigurable reflectarray antenna out of a high-cross polar unit-cell by satisfying the condition of 5.6. In this section we try to show that, even if 5.6 is not met, modifications can be applied to this arrangement so as to mitigate the resulting cross-polar lobe. Consider figure 5.14 where the first modification scenario is demonstrated. It shows a reflectarray surface (top left) with a regular chessboard arrangement in which white elements are flipped with respect to black ones.

Using the technique introduced in [89], the array surface can be divided into four planes and all of the cells of the two diagonal quadrants are flipped which results in the first modified arrangement shown at the bottom right side of the figure.

Figure 5.15 shows the second modification where all of the elements inside the green rectangle are flipped. Figure 5.16 compares the effect of each of these two modifications on the cross-polarization suppression. The figure shows the cross-polar radiation pattern of a chessboard array computed using 5.4 where the condition of 5.6 is violated and as a result, when the array beam is pointed to $\theta_0 = 60°$, high level radiation of cross-polarization occurs. The blue curve corresponds to the cross-polarization pattern of a regular chessboard array while the green and red curves correspond to the cross-polar patterns of the first and second modification, respectively.

As shown in Figure 5.16, these modifications have resulted in 9dB reduction in the cross-polar radiation. The effect of these modifications can be better understood by observing the 3D simulated total-field radiation pattern of such structures carried out in FEKO environment and presented in figure 5.17. In this case, the co-polar beam is directed to $(\theta_0 = 60°, \phi_0 = 135°)$ while the cross-lobe appears right behind the main lobe (at $\phi = -45°$). The patterns from left to right, correspond to regular, first and second modification. The positive effect shown in figure 5.16, can now be visualized in 3D. It should be noted that, these modifications have no effect on the main co-polar beam.

5.7   discussion on the chessboard arrangement

Although chessboard method showed its effectiveness in cross-polarization suppression, but it not without disadvantages. the first disadvantage is that it requires a cell with smaller dimensions than a conventional array antenna.

In fact the main motivation behind the design and simulation of the proposed single band reconfigurable reflectarray at 12 GHz was the utilization of a *single* varactor diode per cell for a *dual-polarization* performance. However, since the size of the cell needs to be reduced to a factor of $\frac{1}{\sqrt{2}}$, for a given reflectarray plate size, the total number of diodes would be the same if we were to use two diodes in a cell without cross-polarization. In other words, whether we use a high cross-polar cell with a single diode or a low cross-polar cell with two diodes, both give the same number of diodes on a given area.

The second disadvantage of a chessboard arrangement is that, compared to a reflectarray
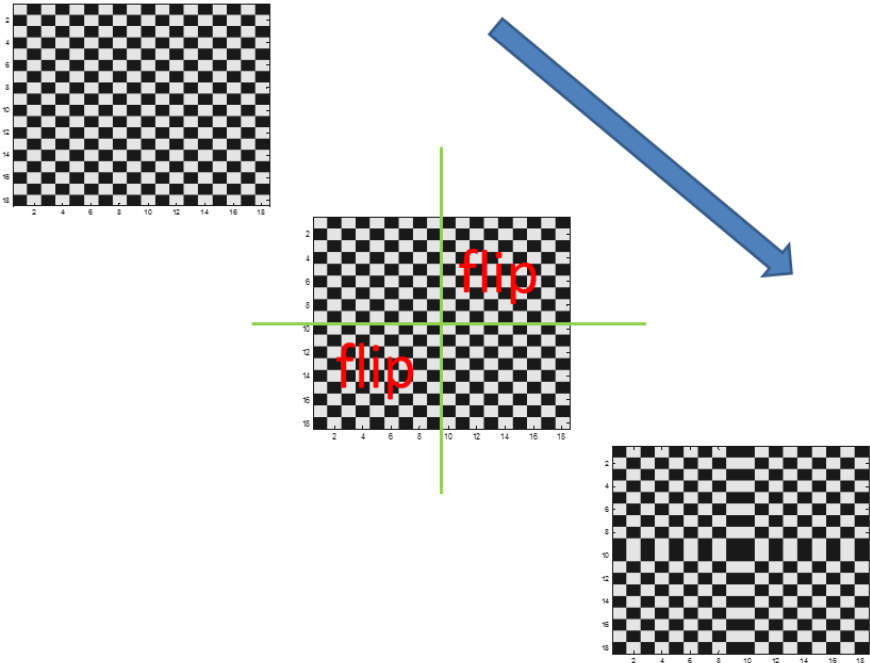
Figure 5.14: First modification of the chessboard configuration.
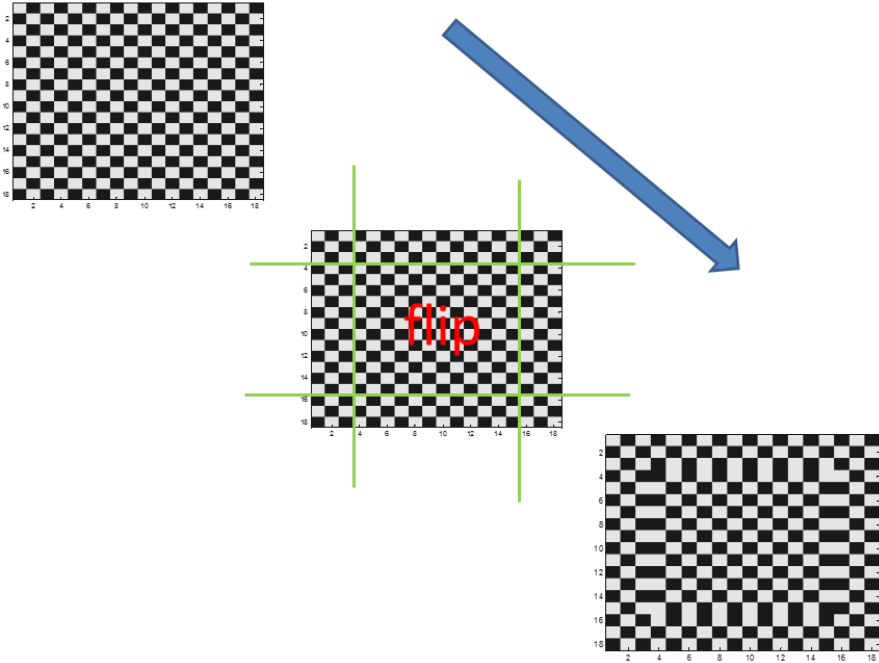
Figure 5.15: Second modification of the chessboard configuration.

Figure 5.16: Simulated effect of first and second modification of chessboard arrangement on the cross-polar level suppression.
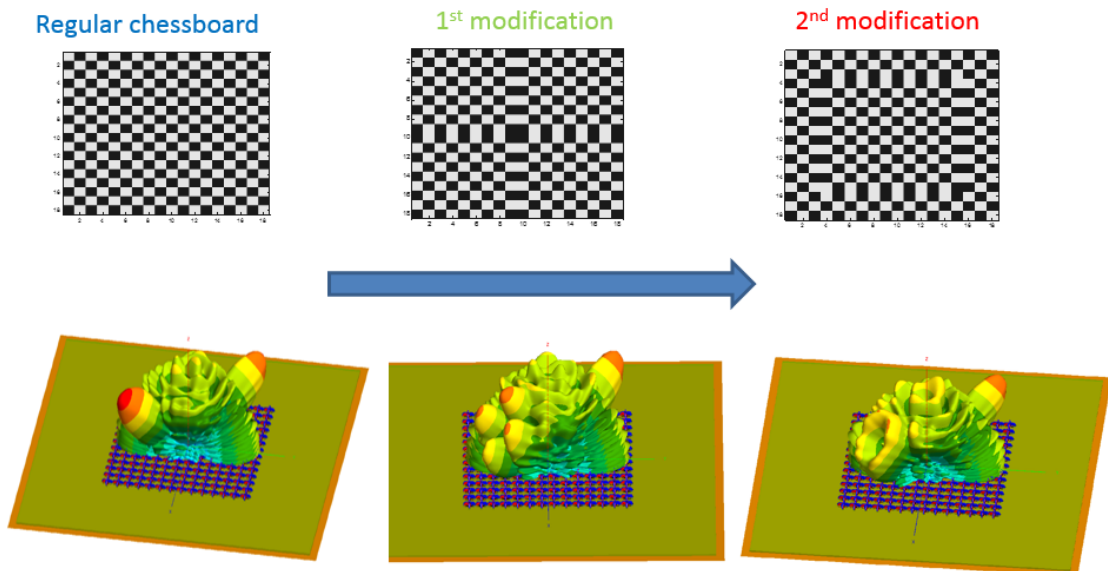
Figure 5.17: 3D visualization of the effect of first and second modification of chessboard arrangement on the cross-polar level suppression. the main co-polar lobe is directed to $(\theta_0 = 60°, \phi_0 = 135°)$ causing the appearance of the cross-polar back lobe which is suppressed as a result of modifications.

using a low-cross-polar cell, there is approximately 2 dB reduction in antenna's overall gain. This gain reduction is due to the leakage of the incident co-polar field power into the cross-polar radiation.

Despite these disadvantages, chessboard arrangement is a promising method for reflectarray antennas that, due to special constraints, have to use a cell with high cross-polarization level.

5.8   Conclusion

In this chapter we introduced a topology for a reconfigurable dual-band dual-polarized reflectarray cell at Ku band centred around 12 and 14 GHz wherein 5 varactor diodes controlled by only two voltages- one for each frequency- were employed for phase-shift regulation. The resultant single layer printed reflectarray antenna will possess independent beam scanning capability in two closely separated frequency bands. The main issue in the design was the unit-cell high cross polarization level because of its non-symmetrical geometry. In order to circumvent this issue, cells were arranged on the array surface in a particular way namely chessboard arrangement. In order to verify the effective performance of this arrangement, a single-layer, single band (12 GHz) and dual-polarized reconfigurable cell was introduced with major cross-polarization issues. By applying chessboard cell arrangement on the reflectarray using such a cell, full-wave simulation results along with the developed theory for the proposed arrangement showed the effectiveness of the chessboard arrangement i.e. the cross-polarization level was mitigated at the antenna far-field region.

6 Tri-Band Reflectarray Surface in the THz Frequency Band

This chapter presents a single layer, dual-polarized unit-cell topology that is capable of independent reflection phase-shift at three frequencies 0.7, 1.0 and 1.5 THz. These frequencies have been chosen just to demonstrate the performance of reflectarray at frequencies with relatively close proximity. Based on this new cell, Terahertz reflectarray surfaces can be designed with the prominent feature of independent deflection at three frequencies (see figure 6.1). To this aim, two reflectarray surfaces, each with a specific frequency-vs-deflection angle profile are designed, simulated, fabricated and measured. The first design deflects a plane wave with an incidence angle of 30° to broad side direction at all of the three frequencies whereas the second design deflects a plane wave with an incidence angle of 40° to deflection angles 20°, 0° and 50° at 0.7, 1.0 and 1.5 THz, respectively. The purpose of these designs is merely to demonstrate the capability of the unit-cell in complete independent performance at each frequency.

Both fabricated samples are composed of an array of 100×100 cells, each comprised of gold crosses and parasitic dipoles on thin grounded high resistivity silicon. The measurement results obtained using Terahertz time-domain spectroscopy (THz TDS) demonstrates a satisfactory performance of each design.

In addition, for the first time in the THz domain, high resistivity silicon is used as substrate. This feature paves the way for integration of reconfigurable technologies in future designs.

This chapter starts describing the cell configuration with its geometrical details in order to achieve tri-band deflection at the frequencies 0.7, 1.0, and 1.5 THz. Afterwards simulation results of the two tri-band reflectarray surfaces are presented each having a specific frequency-vs-deflection angle profile and finally the fabrication process is explained followed by the presentation of experimental results.

The design methodology and results presented in this chapter have been published in [92]. There is thus a certain overlapping between the materials of this chapter and [92].
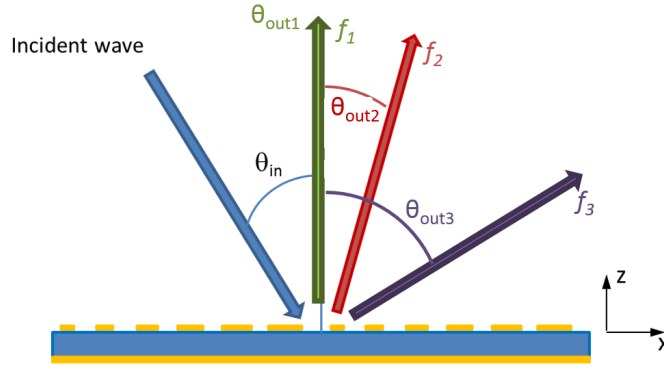
Figure 6.1: Schematic 2D view of the reflectarray deflection mechanism at three frequencies f_1, f_2, f_3 to different arbitrary angles $\theta_{out1}, \theta_{out2}, \theta_{out3}$, respectively [92].

6.1 The tri-band cell

In order to implement a reflectarray surface that is capable of simultaneous deflection at the three frequencies 0.7, 1.0, and 1.5 THz (see figure 6.1), an effective solution would be to design a cell with three geometrical parameters, each controlling the phase-shift at one of the three frequencies independently. By independence we mean that at each frequency the phase-shift is a function of only one of the parameters and thus invariant to the remaining two. This feature leads to a straightforward design by avoiding time consuming optimizations. Figure 6.2 shows the schematic view of the proposed tri-band cell along with a demonstrative segment of a 3×3 array of the proposed cell. The cell is composed of three resonant printed structures each responsible for the phase-shift at one of the three frequencies. The cell in fact combines a dual-band structure composed of interlaced cross-dipoles [85] with four equi-length parasitic tilted dipoles in order to arrive to the final tri-band cell. We should mention that, this cell topology is in fact the down scaled version of the tri-band cell shown in figure 4.10b.

The geometrical parameters used to control the phase-shifts are denoted as L_1, L_2 and L_3. Table 6.1 summarizes the variation range of each of these parameters for the phase-shift regulation required at its respective frequency. Other parameters of the cell are fixed to the values $d = 100\,\mu m$ and $w_1 = w_2 = 2w_3 = 10\,\mu m$. As for the substrate, high resistivity silicon ($> 1000\,\Omega cm$) with thickness $h = 15\,\mu m$, loss tangent 0.001 (at 1 THz) is used. The use of silicon has the advantage of allowing the integration of solid state active components for reconfigurable technologies.

Figure 6.3 presents the simulated phase-shift versus lengths of the cell at the three frequencies that are obtained in CST microwave studio environment by applying periodic boundary condition to the cell's walls. In the simulations, silver with thickness $0.2\,\mu m$ is chosen for the material of the resonant structures since it is the best metallic conductor known. As shown, at each frequency the cell provides more than 270° phase range which is adequate for the reflectarray surface's intended functioning. As for the cell losses, at each frequency it reaches its maximum value at resonance which in the worst case is $2dB$. It should be emphasized that in the present work the parameters of the cell are not fully optimized in order
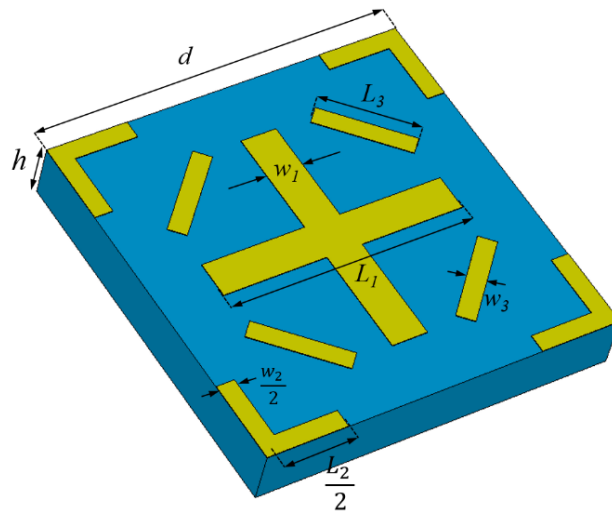
(a) The tri-band cell
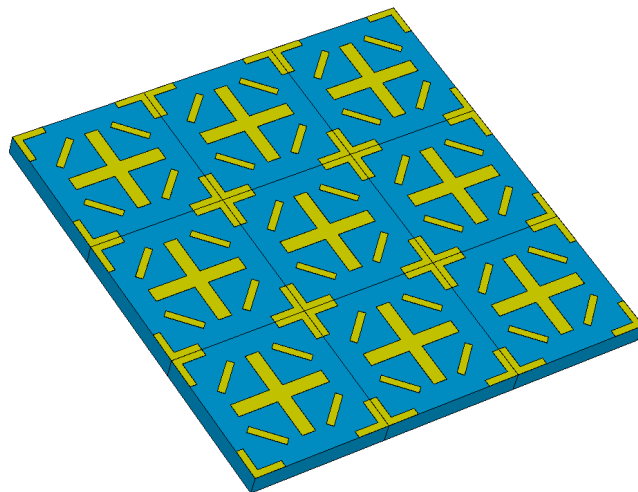
(b) 3×3 array of tri-band cell

Figure 6.2: a) Proposed tri-band cell and b) Corresponding 3×3 array sample [92].

Table 6.1: Variation range of the cell parameters for phase regulation at each frequency.

Parameter	Intended Frequency (THz)	Variation (μm)
L_1	0.7	60-75
L_2	1.0	40-50
L_3	1.5	20-30

to minimize the losses since here the main goal is to present a cell *configuration* that allows us an independent multi-band performance. One of the important characteristics of the cell is that at each frequency the phase-shift depends on only one of the varying parameters and remains invariant to the other two. For example, at 1 THz the phase-shift is only dependent on L_2, and is invariant with respect to the variations of L_1 or L_3 (as long as L_1 or L_3 vary within the limits specified in Table 6.1). This advantage will simplify the reflectarray design by eliminating the need for building a huge database by sweeping all the parameters at all the frequencies by the multi-frequency phase-matching method [36].

6.2   Simulation results

Based on the phase responses versus regulating parameters L_1, L_2 and L_3 two reflectarray surfaces have been designed and simulated. The first is designed to deflect an incident wave with 30 degrees of incidence angle to the normal direction in all of the three intended frequencies and the second one will deflect an incident wave of $40°$ to the deflection angles $20°$, $0°$ and $50°$ degrees at 0.7, 1.0 and 1.5 THz, respectively. The deflection performance of these two reflectarrays are chosen merely to demonstrate the fact that the reflectarray performance is completely independent at each frequency. In addition, the metal of the printed elements is replaced by a PEC with zero thickness, rather than silver with 200 nm thickness, in order to facilitate the simulations. As for the simulation scenario, the reflectarrays are assumed to be infinite in y direction while containing 20 cells in the x direction (xz being the deflection plane). Due to the deflection performance of the reflectarrays, the required reflection phase of the cells (and hence their sizes) are invariant with respect to y direction and as a result, we have placed 20 cells in x direction and applied periodic boundary condition along y direction.

6.2.1   First design

The first reflectarray is designed in order to deflect a plane wave with an incidence angle $30°$ to broadside direction at all of the three frequencies 0.7, 1.0, and 1.5 THz. Figure 6.4 shows the scattered instantaneous near-field of the reflectarray sample (Figure 6.4d) obtained in HFSS environment where the deflection to the broadside direction can be clearly observed at each frequency. In addition, the normalized far-field radiation pattern of the device has also been obtained at each frequency and is presented in Figure 6.5.a with an inset showing a tolerance of maximum $\pm 1°$ in the direction of maximum radiation.
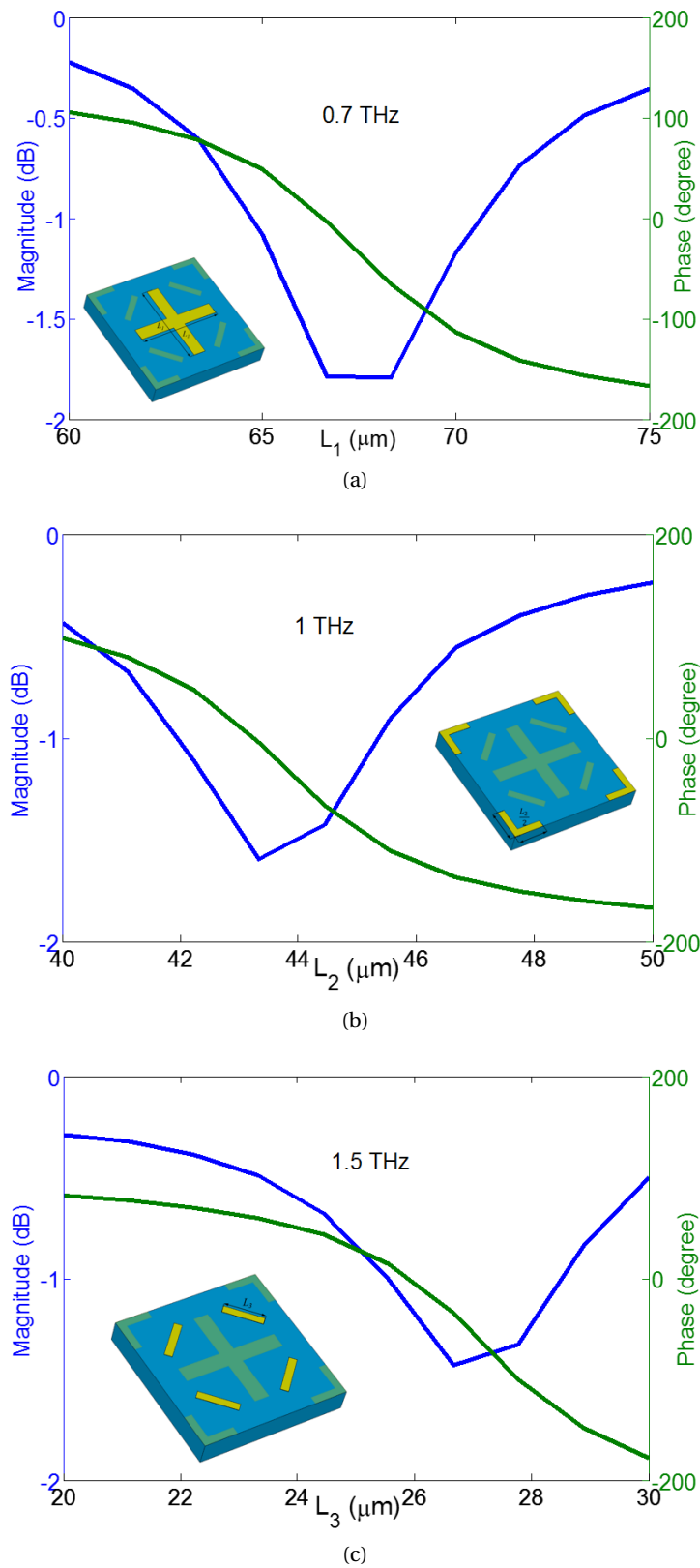
Figure 6.3: The phase and amplitude responses of the proposed cell in terms of the varying parameters at a) 0.7 THz b) 1 THz c) 1.5 THz [92].

Further more, in order to estimate the losses in the substrate and scattering performance of the reflectarray, the reflectarray is replaced by a PEC plate illuminated by a normal incident wave. In this case the periodic boundary conditions in the y direction are replaced by PEC walls. This scenario will provide us with the reflection response of a PEC plate extended to infinity in y direction while having a limited size in x direction (the size of the array sample). By comparing the deflection magnitude of the reflectarray with the reflection magnitude of a PEC plate, we can estimate the amount of losses dissipated inside the silicon substrate as well as the leakage of radiation into unwanted directions. As shown in figure 6.5.b we can observe that at 0.7, 1.0 and 1.5 THz, 80%, 77% and 90% of the incident power is deflected to broadside direction, respectively. The rest of the incident power is thus either dissipated in the substrate or leaked into unwanted directions.
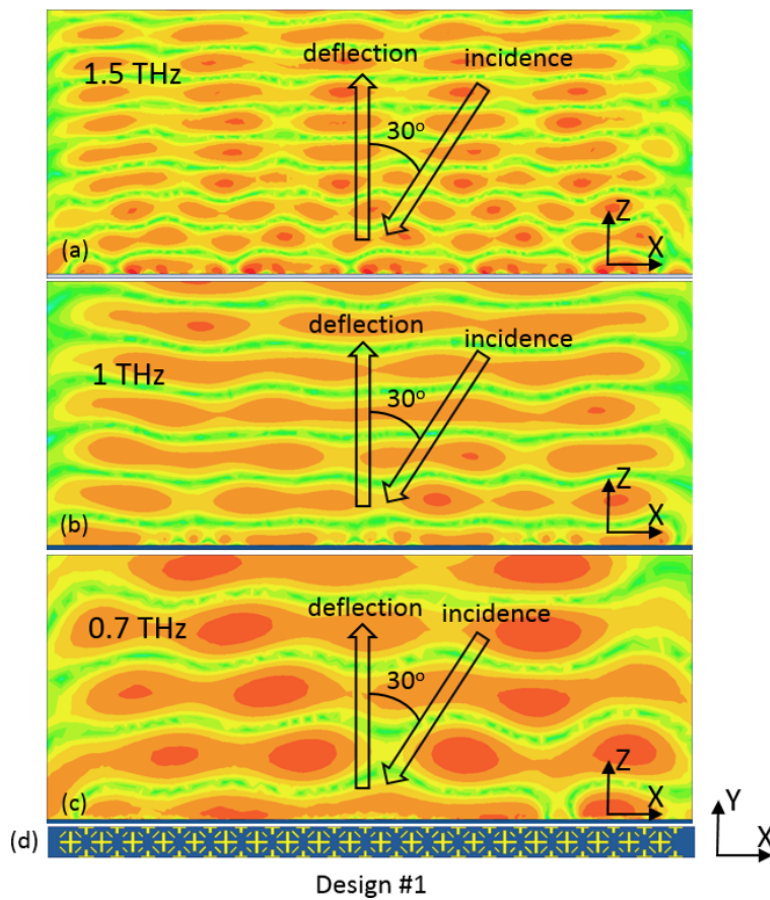
Figure 6.4: Simulated instantaneous scattered near-field of the first design [92].

6.2.2 Second design

The second reflectarray is designed in order to deflect a plane wave with an incidence angle of 40° to the angles 20°, 0° and 50° at the frequencies 0.7, 1.0, and 1.5 THz, respectively. Figure 6.6 shows the scattered instantaneous near-field of the reflectarray (Figure 6.6d) obtained in

(a)

(b)
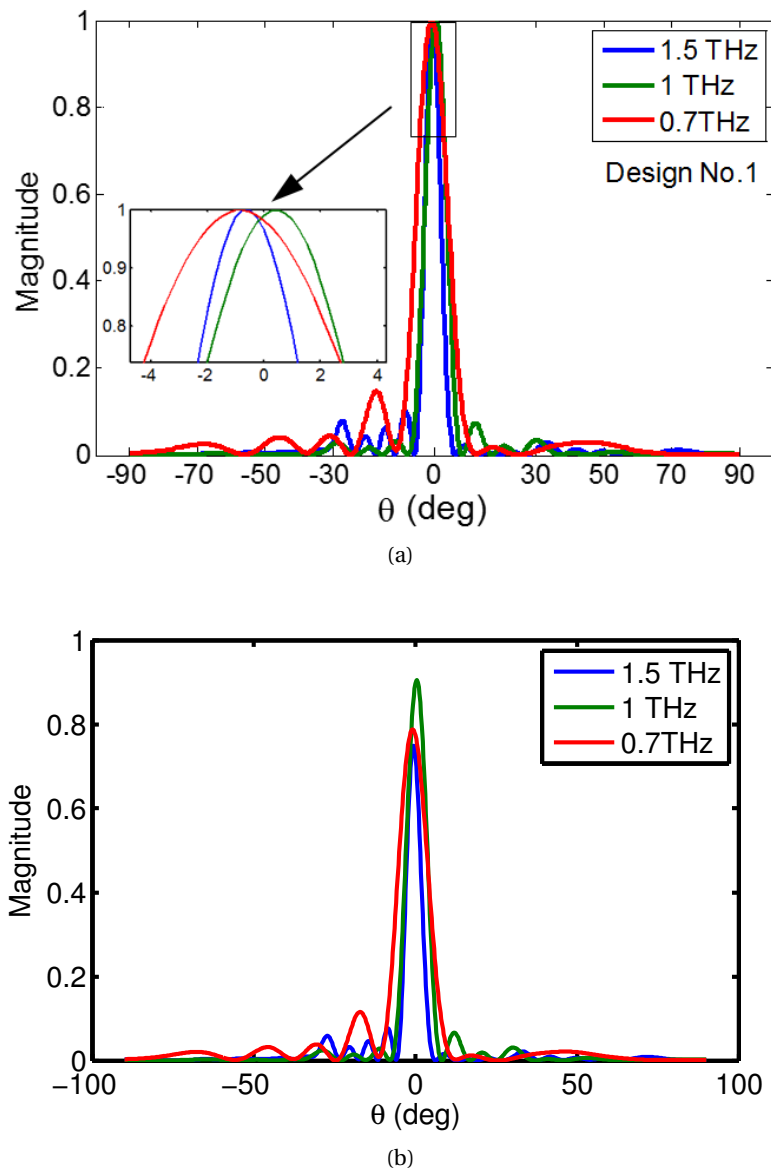
Figure 6.5: Simulated far-field radiation pattern of the first designs on the incidence plane i.e. xz a) Normalised radiation patterns each with respect to its maximum b) Normalised radiation patterns with respect to the radiation pattern of a PEC plate [92].

HFSS environment where the deflection to the intended angles can be clearly verified at each frequency. In addition, the normalized far-field radiation pattern of the device has also been obtained at each frequency and is presented in Figure 6.7.a. The maximum variation of the direction of maximum radiation in the second design is ±0.5°. Figure 6.7.b, similar to figure 6.5.b, shows the percentage of incident power deflected into the intended angles.
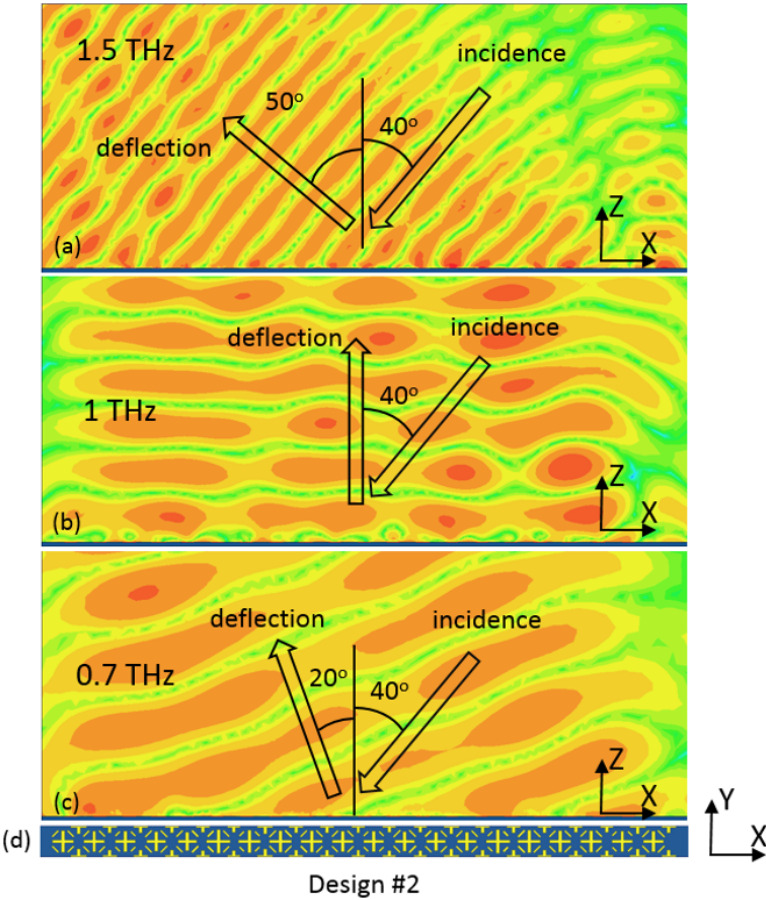
Figure 6.6: Simulated instantaneous scattered near-field of the second design [92].
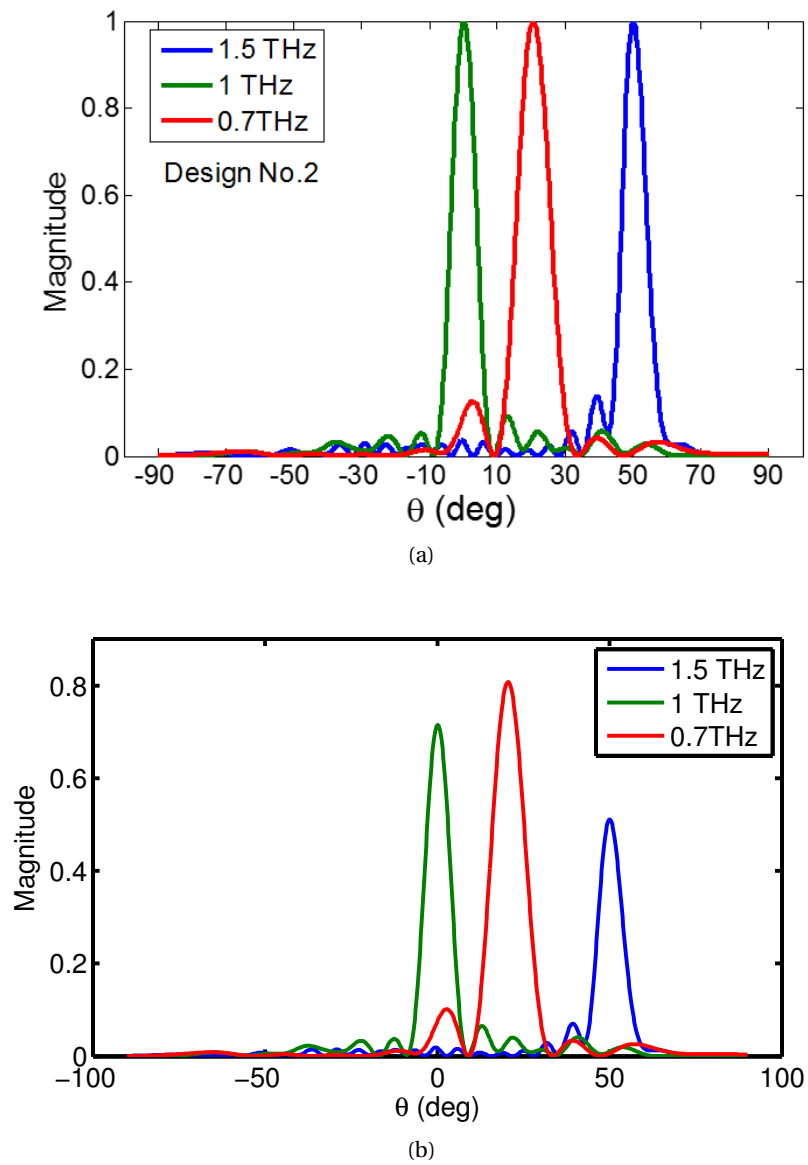
Figure 6.7: Simulated far-field radiation pattern of the second designs on the incidence plane i.e. *xz* a) Normalised radiation patterns each with respect to its maximum b) Normalised radiation patterns with respect to the radiation pattern of a PEC plate [92].

6.3   Fabrication process [1].

The proposed design, as many other printed reflectarrays, is based on a multilayer structure which terminates with a ground plane reflector. For microwave reflectarrays, the dielectric spacing layer has usually a thickness in the order of millimetres or fractions of millimetres, and it is easily realized using for instance PCB technologies. At THz frequencies, however, its realization is one of the most challenging processes of the device fabrication. Such a layer must in fact satisfy a number of requirements, such as:

1- It must have a low loss tangent at THz frequencies;

2- It must be compatible with the subsequent fabrication of metallic patterns;

3- Its thickness must be in the order of fractions of the wavelength in the material ($15\mu m$ in this design).

An interesting candidate is found in Silicon on Insulator (SOI) wafers which are characterized by a silicon handle substrate (in the order of hundreds of micrometers), a thin SiO2 box layer (from hundreds of nanometers to few microns) and a device silicon layer the thickness of which greatly varies according to the applications (from hundreds of nanometres to hundreds of micrometers). For the present design SOI wafers (manufactured by Ultrasil Corporation) having a high resistivity ($> 1000\,\Omega cm$) and a device layer with $15\,\mu m$ of thickness (the substrate thickness) were chosen for this application since the device layer satisfies the three requirements listed above. However, the reflectarray cannot be fabricated on the SOI directly because of the absence of the ground plane. This issue has been solved using the technological process flow shown in figure 6.8 that has been implemented at the Center of Micro-Nano Technology (CMi) of EPFL. First, two metallic layers are evaporated on the device layer of the SOI wafer, namely a gold layer (the high conductivity of which ensures good THz reflection) and an aluminium layer. Both layers are $100\,nm$ thick and 5 nm of Chromium is used as adhesion layer for both. The device layer is then placed in contact with a borofloat (Pyrex) wafer and anodic bond between aluminium and Pyrex is performed using a vacuum anodic bonding equipment (Süss Microtech SB6). The handle wafer is then reduced through a grinding process to a thickness of $100\,\mu m$, and the rest is etched using a dry silicon etching process selective over SiO2. The $2\,\mu m$ SiO2 layer is then etched in a 49% hydrofluoridric acid (HF) solution, which ensures very fast etching of SiO2 without attacking the Al bonding layer. The wafer is then diced and a standard electron beam lithography plus lift-off is used to define the metallic crosses on the top layer. Three metals are used for this last evaporation: 5 nm of chromium for adherence, 165 nm of silver and 30 nm of gold. The silver has been chosen because it is the best metallic conductor known, and the 30 nm of gold have the purpose of protecting the silver from oxidation. Figure 6.9 shows an optical picture of the metallic pattern, and Figure 6.10 a SEM view. AFM has also been performed to confirm the actual thickness of the metal which is

---

[1]The fabrication process was carried out by Michele Tamagnone (michele.tamagnone@epfl.ch), Clara Moldovan (clara.moldovan@epfl.ch) and Pietro Maoddi (pietro.maoddi@cern.ch) [92]

composed of gold (100 nm), Aluminium (100 nm) and Chromium (5 nm) arriving to the final metal thickness of 205 nm (see figure 6.11b).
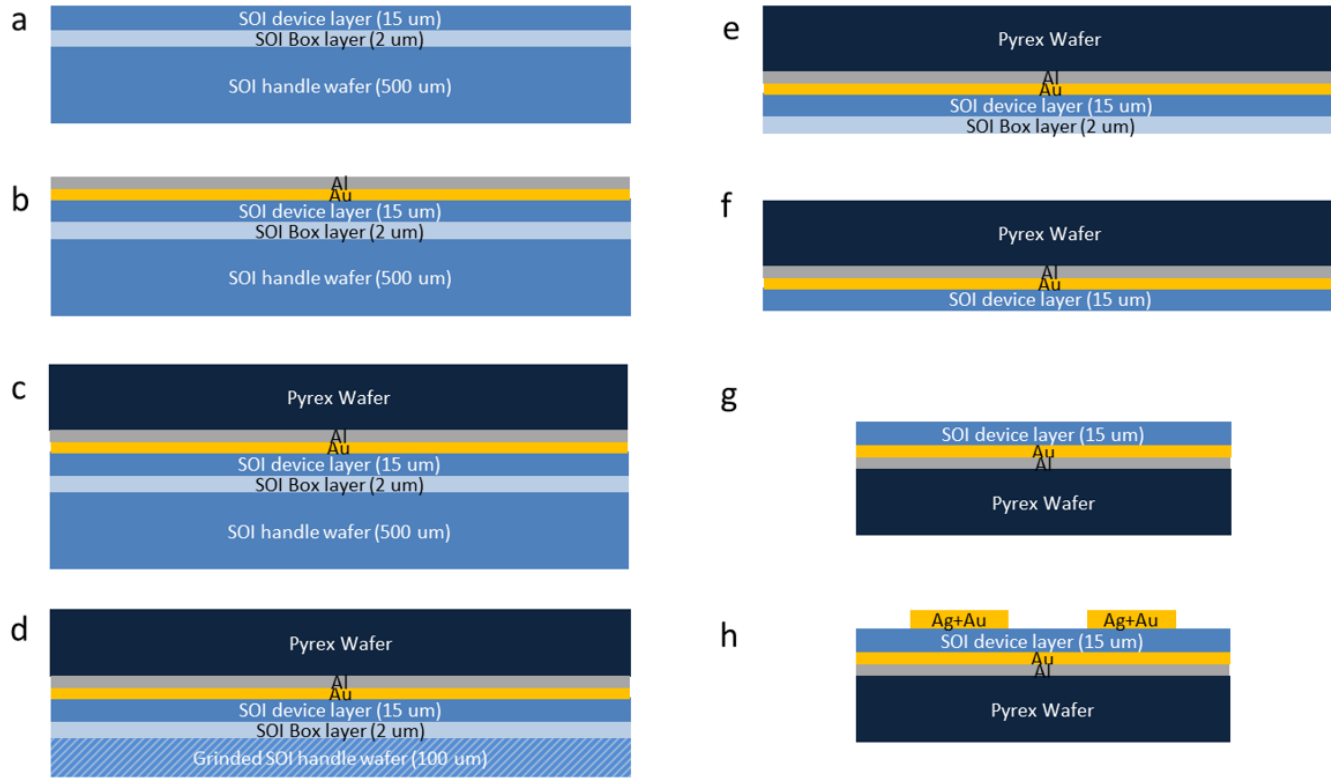
Figure 6.8: Reflectarray fabrication process. a) Initial SOI wafer. b) Evaporation of 100 nm of Au and 100 nm of Al. c) Anodic bonding of the pyrex wafer. d) Grinding 400 um of silicon. e) Dry etching of the remaining silicon. f) HF etching of the SiO2 box. g) Dicing. h) E-beam lithography, evaporation of 165 nm of Ag and 30 nm of Au and lift-off [92].
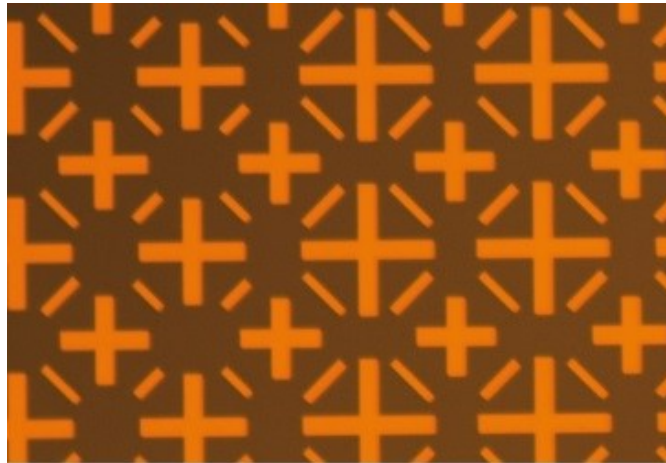
Figure 6.9: Optical image of the realized tri-band reflectarray structure [92].

6.4 Measurement[2]

6.4.1 First design

The images shown in figures 6.9 and 6.10 in the previous section, correspond to the first design described in section 6.2, and it contains a total of 100×100 cells with an area of $1.0 cm^2$. After fabrication, an experimental characterization of its deflection capabilities was carried out using the Tera K15, THz-TDS measurement system developed by Menlo System GmbH (see figure 6.13). In order to study the deflection capabilities, the receiver of the Tera K15 system was mounted at a fix angle of $30°$ from the normal incidence. The transmitter was mounted on top of a rotary arm, which allowed changing its position, and thus being able to measure at different incident angles. The reflectarray was then mounted on a vertical surface along with a fully metallized substrate, which will act as reference mirror. The size of the THz beam was adjusted to no more than 8 mm using an iris.

Figure 6.12 presents the three basic measurement setups that allow to obtain the preliminary performance of the reflectarray shown in figure 6.14. Indeed, figure 6.12a which corresponds to the blue curve in figure 6.14 presents the specular reflection of the fabricated design. In normal conditions we would expect a maximum, and this is the case for most frequencies. However, for the frequencies of interest (0.7, 1, and 1.5 GHz) we clearly observe a notch, thus the energy is prevented to proceed in the specular direction. By moving now towards figure 6.12b (and the corresponding green curve in figure 6.14), we can observe the field reflected off the normal direction. We clearly observe that at the frequencies of interest we have clear peaks of deflection. Finally figure 6.12c is a measurement of the reference mirror structure, to be able to assess the losses of the system.

With this aim, the specular and deflection power spectra were normalized to the mirror

---

[2]The measurements were carried out with the help of Dr. Santiago Capdevila Cascante (santiago.capdevila@epfl.ch)
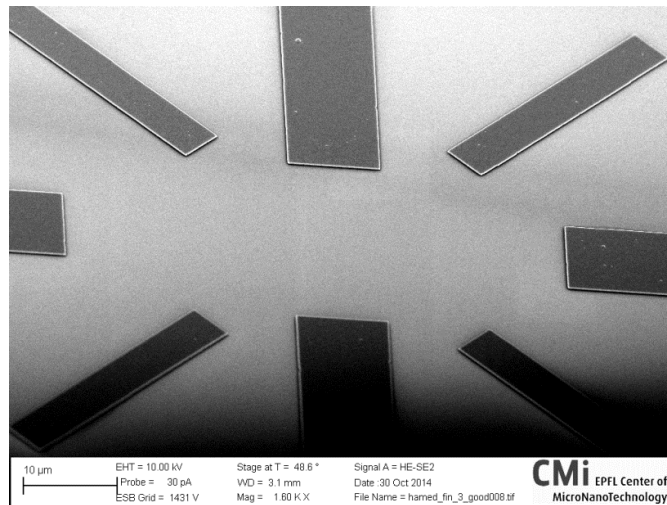
Figure 6.10: SEM view of a detail of the tri-band reflectarray [92].

reflection spectrum, arriving to the results illustrated in figure 6.15. As shown, at 0.7, 1, and 1.5 THz, about 40%, 30% and 50% of the incident wave power was deflected. The remaining power of the incident field, was either dissipated due to the metallic and dielectric losses or leaked into specular direction (or other directions), due to defects in the manufacturing process or misalignments during the measurement.

Finally, thanks to the rotational capability of the transmitters in the THz system, a radiation-like scattered pattern was measured, as shown in figure 6.16. It can be clearly observed that the reflected field is mostly concentrated on the normal direction of the beam (broadside), while still having some field reflected towards the specular direction. However, it should be noted that the range of measurement was limited from $\theta = -90°$ to $\theta = 5°$ due to mechanical constraints (Tx and Rx angular separation had to be at least 25°).

6.4.2 Second design

The fabrication process and measurement setup were the same for the second design except that the received spectrum was measured at different angles. Figure 6.17 shows the measured spectrum at the intended design angles $\theta = 0°$, $\theta = -20°$ and $\theta = -50°$ where deflection occurs at 1.0, 0.7 and 1.5 THz, respectively, as expected. In the measurement setup, the receiver was fixed to the angle of 40° and the transmitter is rotated within its limits, similarly as presented in the inset of figure 6.16. As shown in figure 6.17, at each angle the deflection at the intended frequency occurs and about 40%, 33% and 60% of power is deflected at 0.7, 1.0 and 1.5 THz, respectively. The radiation pattern of the second reflectarray is shown in figure 6.18 at the three frequencies 0.7, 1.0 and 1.5 THz. The radiation pattern at each frequency is normalized to its maximum value. As shown, the maximum power occurs at the three intended angles of $\theta = 0°$, $\theta = -20°$ and $\theta = -50°$ although, as expected, we have notable radiation in the specular direction ($\theta = -40°$).
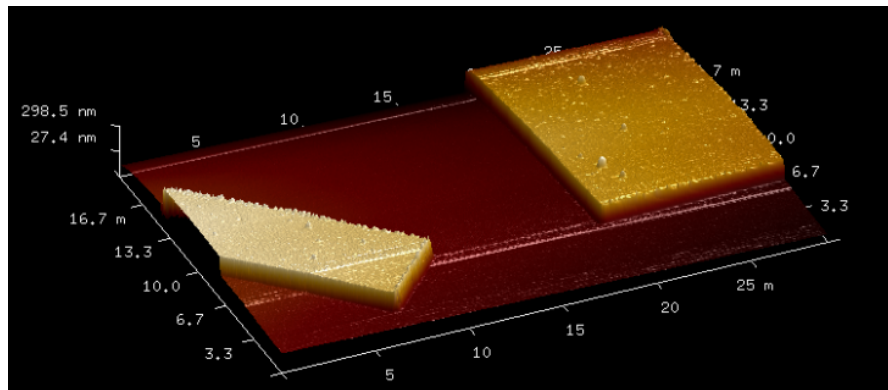
(a)
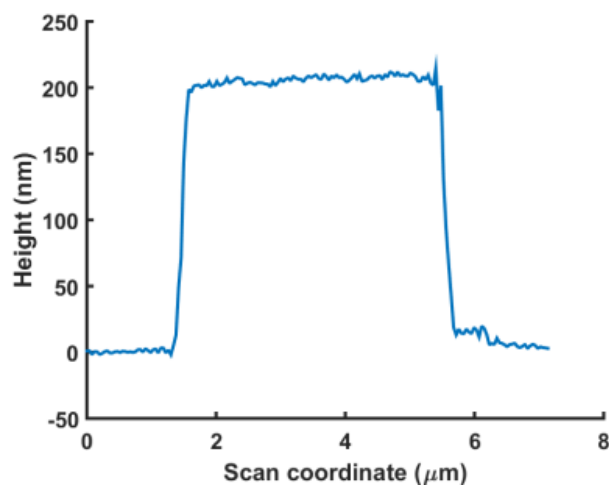
(b)

Figure 6.11: AFM imaging of a detail of the tri-band reflectarray pattern a) 3D view and profile b) Confirmation of the metal thickness of around 205 nm [92].

6.5   Conclusion

In this chapter we presented a cell configuration that allowed us to implement a reflectarray surface which possesses completely independent performance at three frequencies of the THz region (0.7, 1.0, and 1.5 THz). Two reflectarray surfaces, each with a specific frequency-vs-deflection angle profile, have been designed and fabricated demonstrating a satisfactory performance which is verified by the measurement results of the fabricated prototypes. The resulting device benefits from several advantages. The proposed cell is a simple single-layer structure that, thanks to its symmetrical geometry, is able to perform at any polarization (e.g. linear, circular, slant, etc). In addition, the phase response of the cell at each frequency is completely independent of the other two, a characteristic that gives a notable contribution to the ease of design by eliminating the need for time consuming optimizations. Furthermore, for the first time, high resistivity silicon was used as the device substrate. This feature prominently
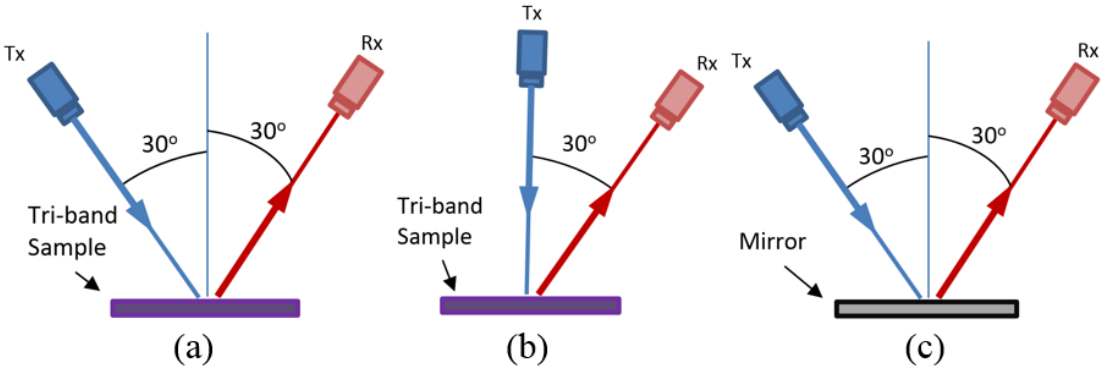
Figure 6.12: Schematic view of the measurement setup for the tri-band reflectarry surface, design No. 1 a) Specular radiation measurement b) Deflection intensity measurement c) Reference measurement in order to estimate losses [92].

facilitates the integration of solid-state devices for potential reconfiguration in future designs.
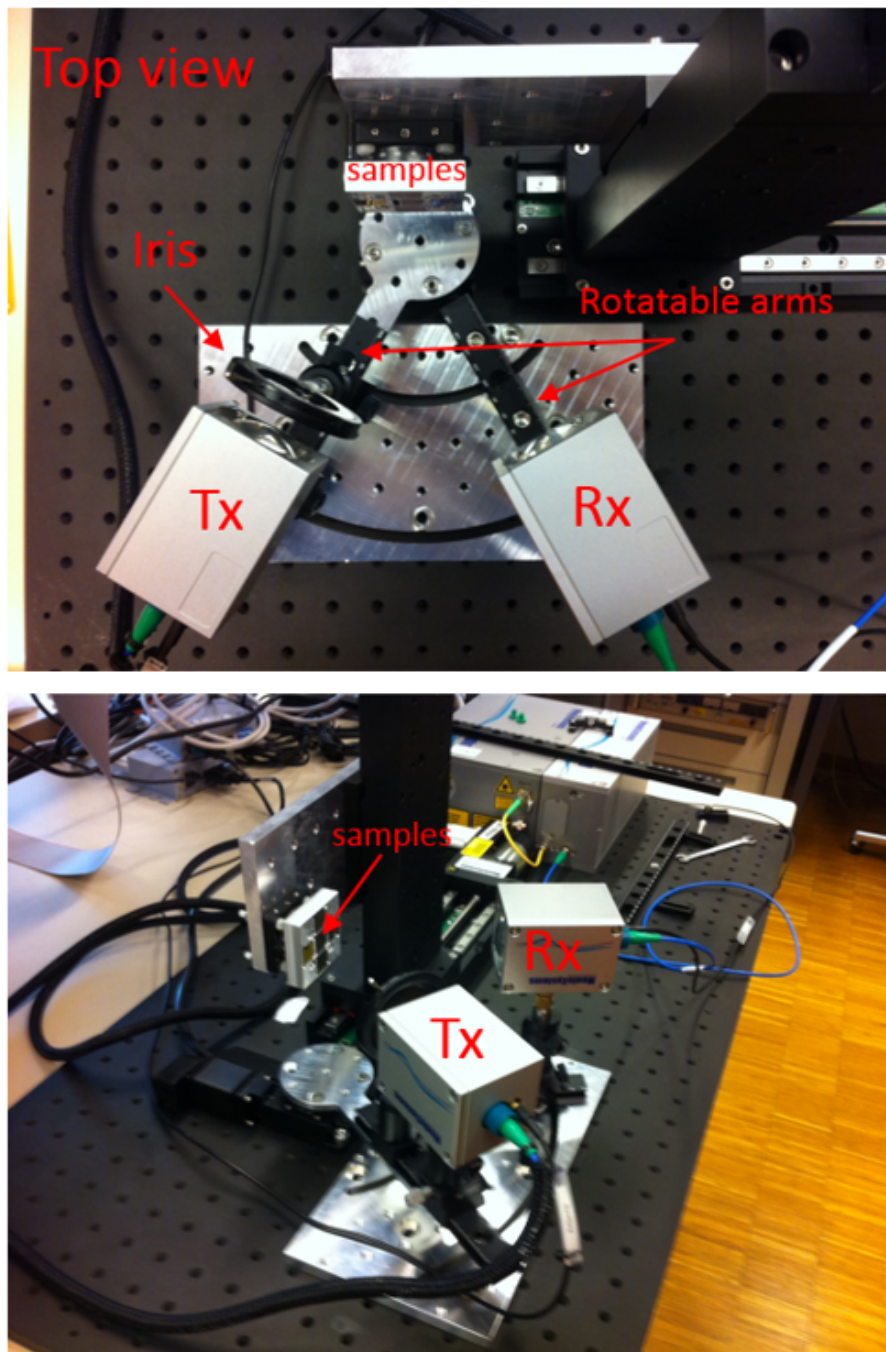
Figure 6.13: THz measurement setup [92].
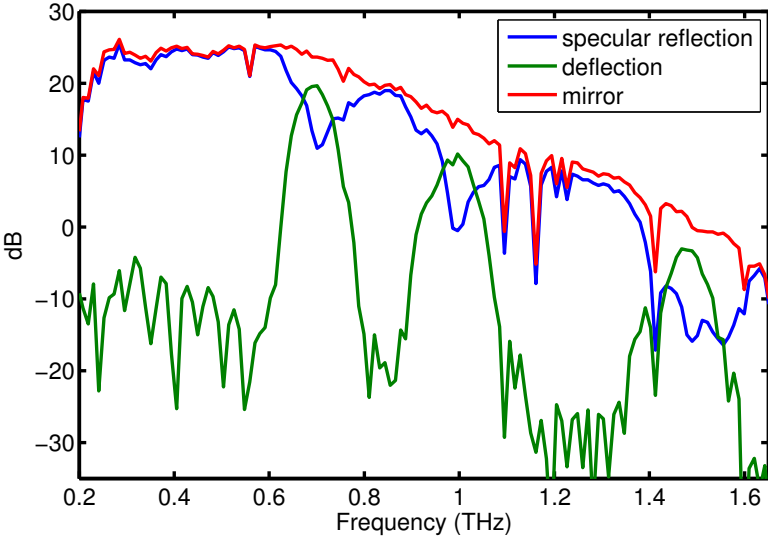
Figure 6.14: Measured spectra in the TM polarization for deflection intensity (green), specular reflection (blue) and perfect (mirror) reflection (red).
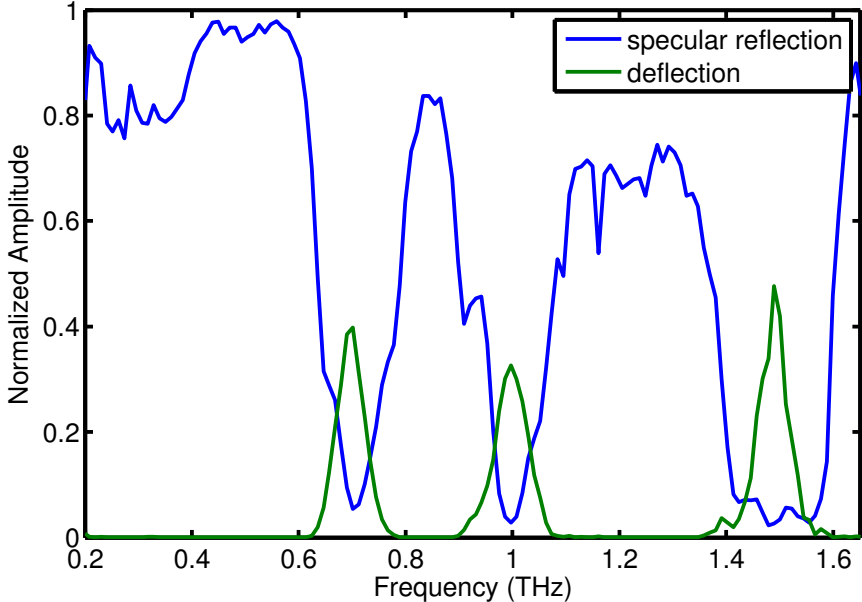
Figure 6.15: Spectra measured amplitude for specular reflection (blue) and deflection (green) normalized to the mirror reflection spectra.
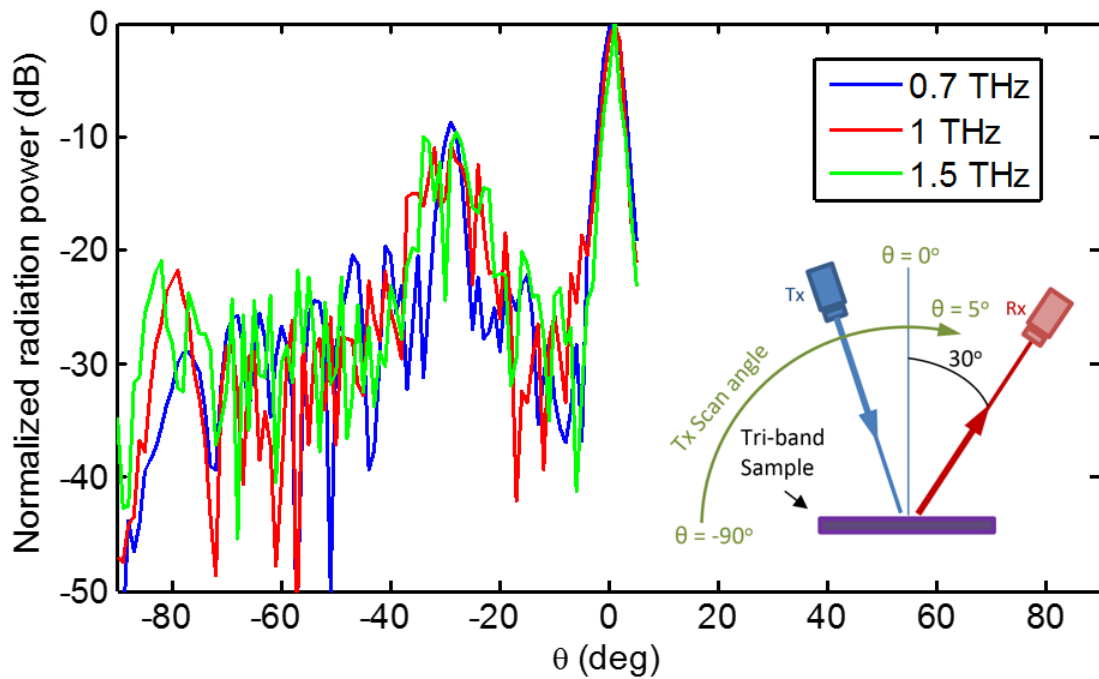
Figure 6.16: Schematic view of measurement setup for radiation pattern measurement with angle step of 1°, and measured radiation pattern at the three designed frequencies 0.7, 1, and 1.5 THz [92].
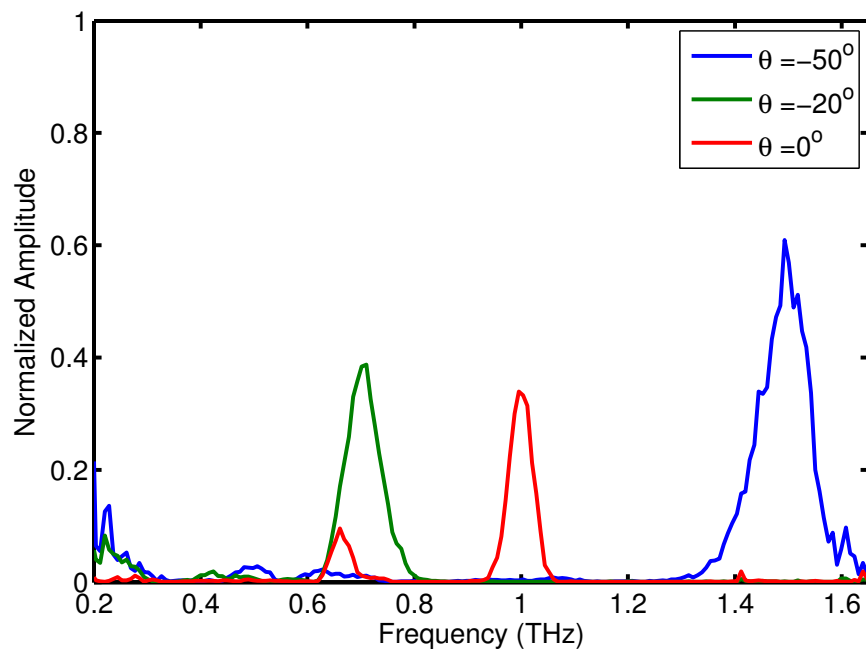
Figure 6.17: Measured spectra amplitude of the second reflectarray for deflection normalized to the mirror reflection spectra at the three intended angles $\theta = 0°$, $\theta = -20°$ and $\theta = -50°$.
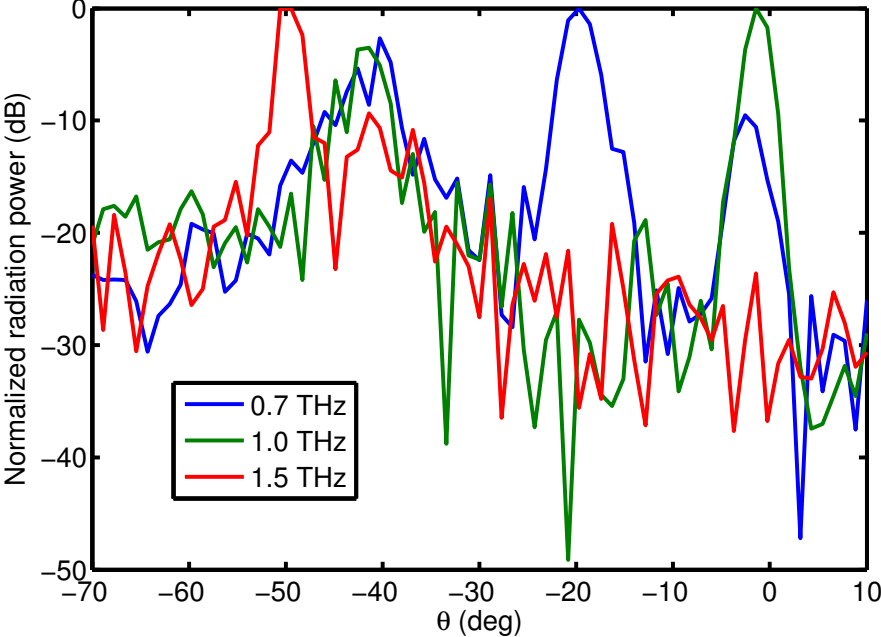
Figure 6.18: Measured radiation pattern of the second reflectarray at the three designed frequencies 0.7, 1, and 1.5 THz with a step angle of 1°.

7 Conclusions and Perspectives

Printed reflectarray antennas have emerged as a high gain, low-cost and low profile substitutes for the conventional bulky parabolic reflectors and high cost phased array antennas specially for satellite communication systems. However the advantages of printed reflectarrays are not limited to the above mentioned features.

In addition to low-cost and low-profile advantages, printed reflectarrays possess notable potentials in multi-band performance and polarization versatility. These antennas can be designed in order to demonstrate completely independent performance at several frequency bands and/or to achieve a circularly polarized pencil beam using a linearly polarized illuminating source with no additional implementation costs. Features that are unattainable with conventional parabolic reflectors.

When combined with reconfigurable devices, a printed reflectarray can demonstrate above-mentioned features in addition to reconfigurability (i.e beam steering) in a low-cost way which is considered as a distinctive advantage over costly phased-array antennas.

Recently, in THz, infra-red and optic region, the concept of reflectaray antennas has given rise to the so-called meta-surfaces which are basically devices that manipulate an incoming plane wave source. The resulting device possesses all the advantages and capabilities of a typical reflectarray antenna. The distinctive difference is that, in higher frequencies of THz, infra-red and optics the illuminating source is a plane wave rather than a point source (e.g a horn antenna). In addition, the fabrication process and the materials losses at these frequencies poses new challenges for implementation of reflectarray surfaces.

7.1 Conclusion

The aim of this theses was to exploit the potentials of printed reflectarrays by design and fabrication of low-cost and yet highly functional reflectarrays in Ku band as well as in THz region. The high-functionality stems from the fact that presented prototypes perform at several frequencies on the same aperture in addition to their capability of working at any polarization. Furthermore, the proposed designs consume the minimum cost and complexity owing to their single-layer structure and straightforward design procedure.

Chapter 7. Conclusions and Perspectives

The Ku band is the 12-18 GHz portion of the electromagnetic spectrum in the microwave range of frequencies which is primarily used for satellite communications, notably for broadcast services. THz region on the other hand consists of frequencies from 0.3 to 3 THz. Terahertz (THz) radiation has numerous applications in stand-off security scanning, biology, medical sciences and broadband short-range wireless communication systems and one of the prominent topics in this field has been to manipulate the THz incoming wave using reflectarry antenna concept.

The main research goals concerning the resultant reflectarrays in Ku band and THz region were the following:

1- Completely independent performance at several closely separated frequency band.

2- Single-layer designs in order to reduce the complexity and costs.

3- Dual-linearly polarized structures so that the reflectarray would be able to perform at *any* polarization (e.g. linear, circular, slant, etc)

These research goals has led to the design, simulation and/or fabrication of low-cost, highly functional fixed and reconfigurable reflectarrays wherein all the three goals have been achieved. The multi-band reflectarray design procedure was based on multi-band unit-cells with several resonant printed structures each with its own varying parameter regulating the phase-shift at a certain frequency. In all of the unit-cell designs we started with a single structure and hence a single band unit-cell. Later on, the second structure was added for phase-shift control for the second frequency and then the third and/or fourth structure. However, at each step where we add a structure, there are two conditions that must be taken into account:

1- Since the size of each structure is variant, structures should not have physical overlapping with one another in order to avoid disturbances in the phase-shifts. This issue becomes specially challenging with dual-polarized and single-layer structures since they occupy more space inside the cell.

2- When adding a structure for phase-shift control for a certain frequency, the size variation of the new structure should not affect the phase-shift at other targeted frequencies. For example, if we have a unit-cell performing at 12 and 13 GHz, the size variation of the first structure within its variation limits (designated for 12 GHz) should not affect the cell's phase-shift at 13 GHz. The same condition applies to the structure of 13 GHz with respect to the phase-shift at 12 GHz.

The second term avoids the optimization procedure and makes the design straight forward. Otherwise one has to create a huge data base by simulating the cell in all the possible combination of structures parameters at each design frequency.

110

the above conditions have been met and reflectarray prototypes were designed, fabricated and measured. These antenna prototypes were explained in detail in following chapters:

Chapter 3 : This chapter started with a general introduction to printed reflectarray antennas and their performance principle. However this chapter introduced the idea of a versatile flat prism which is a reflectarray antenna with a pre-designed frequency-vs-beam direction profile. Limitations of such a device were presented and solutions were provided for the possible realization though without experimental results. One prominent solution resulted in the conversion of a complex electromagnetic problem into a simple circuit synthesis problem.

Chapter 4: In this chapter we presented dual-band and quad-band unit-cells based on which, several prototypes were designed, fabricated and measured. The dual-band antenna was designed to operate independently at 12 and 14 GHz and later on the dual-band design was engineered for operation at *four* frequencies of 12, 13, 14 and 15.5 GHz. Both designs were dual-polarized and single-layer so as to satisfy the research goal. Measurement results of several prototypes showed the satisfactory performance of both dual-band and quad-band reflectarray antennas.

Chapter 5: In this chapter a topology for a reconfigurable dual-band dual-polarized reflectarray cell at Ku band centred around 12 and 14 GHz was proposed wherein 5 varactor diodes controlled by only two voltages- one for each frequency- were employed for phase-shift regulation. The resultant single layer printed reflectarray antenna would demonstrate an independent beam scanning capability in the two closely separated frequency bands.
The main issue in the design was the unit-cell high cross polarization level because of its non-symmetrical geometry. In order to circumvent this issue, cells were arranged on the array surface in a particular way called chessboard arrangement. In order to verify the effective performance of this arrangement, a single-layer, single band (12 GHz) and dual-polarized reconfigurable cell was introduced with major cross-polarization issues. By applying chessboard cell arrangement on the reflelectarray using such a cell, full-wave simulation results of the proposed arrangement showed the effectiveness of the chessboard arrangement i.e. the cross-polarization level was suppressed at the antenna far-field region. In addition, the theory of a chessboard arrangement was developed which established the maximum size of the unit-cell.

Chapter 6: This chapter presented a tri-band reflectarray surface deflecting an incoming plane wave with any polarization to arbitrary directions at three frequencies of 0.7, 1.0 and 1.5 THz. Base on the corresponding unit-cell, a reflectarry surface was designed and fabricated as a proof-of-concept whose satisfactory performance was verified by experimental results. Compared to the previously reported reflectarray surfaces in the literature (also known under the name of meta-surfaces), it was the first time that a THz reflectarray was proposed that

demonstrated a completely independent performance not at one but *three* frequencies. In addition, for the first time in this area, high resistivity silicon was used as the substrate. A feature that paves the way for future reconfigurable THz reflectarray surfaces using solid-state devices. Similar to the multi-band reflectarrays presented in chapter 4, the prototype in THz meets the three established research goals.

7.2 Future work

The concepts, topologies and methods presented in the thesis revealed the exquisite potentials of reflectarrays as a cost-effective and versatile components in wireless telecommunication systems. The most interesting topic in this theses that seems to possess a huge application in the future, is the flat versatile prism introduced at the end of chapter 3. It is believed that by perusing the solutions provided in the same chapter and by taking note of the limitations and challenges posed by the unit-cell, realization of such device will become possible and considering the vast application of a flat versatile prism, reflectarray antenna field will be revolutionized.

Concerning the multi-band reflectarrays, the research can be focused on maximizing the number of the frequency bands as well as establishing a theoretical bound on the operating frequencies proximity given the substrate permittivity and thickness. This process will be of great importance in designing broadband reflectarrays out of multi-resonance cells.

Finally, as emphasized in Chapter 6, the use of silicon facilitates the integration of solid-state devices in order to achieve reconfigurable and/or multi-band reflectarray surfaces at THz frequency bands.

Bibliography

[1] J. Huang and J. A. Encinar, *Introduction to reflectarray antennas*. Hoboken, New Jersey: John Wiley and Sons, Inc, 2008.

[2] T. Niu, W. Withayachumnankul, A. Upadhyay, P. Gutruf, D. Abbott, M. Bhaskaran, S. Sriram, and C. Fumeaux, "Terahertz reflectarray as a polarizing beam splitter," *Opt. Express*, vol. 22, no. 13, pp. 16 148–16 160, Jun 2014. [Online]. Available: http://www.opticsexpress.org/abstract.cfm?URI=oe-22-13-16148

[3] W. L. Stutzman and G. A. Thiele, *Antenna Theory and Design, 3rd Ed.* US: John Wiley & Sons, 2012.

[4] G. Maral and M. Bousquet, *Satellite Communications Systems: Systems, Techniques and Technology.* John Wiley & Sons, 2011.

[5] R. Dybdal, *Communication Satellite Antennas: System Architecture, Technology, and Evaluation.* McGraw-Hill, 2009.

[6] M. Skolnik, *Introduction to Radar Systems.* New York: McGraw-Hill, 2002.

[7] J. W. M. Baars, *The Paraboloidal Reflector Antenna in Radio Astronomy and Communication: Theory and Practice.* Springer Science & Business Media, 2007.

[8] R. J. Mailloux, *Phased Array Antenna Handbook.* 685 Canton Street, Nordwood, MA 02062: Artech House, 2005.

[9] H. Schjaer-Jacobsen and K. Madsen, "Synthesis of nonuniformly spaced arrays using a general nonlinear minimax optimisation method," *Antennas and Propagation, IEEE Transactions on*, vol. 24, no. 4, pp. 501–506, Jul 1976.

[10] R. L. Haupt, "Thinned arrays using genetic algorithms," *Antennas and Propagation, IEEE Transactions on*, vol. 42, no. 7, pp. 993–999, July 1994.

[11] S. Hum, M. Okoniewski, and R. Davies, "Modeling and design of electronically tunable reflectarrays," *Antennas and Propagation, IEEE Transactions on*, vol. 55, no. 8, pp. 2200–2210, Aug 2007.

Bibliography

[12] H. Kamoda, T. Iwasaki, J. Tsumochi, T. Kuki, and O. Hashimoto, "60-ghz electronically re-configurable large reflectarray using single-bit phase shifters," *Antennas and Propagation, IEEE Transactions on*, vol. 59, no. 7, pp. 2524–2531, July 2011.

[13] S. Bildik, S. Dieter, C. Fritzsch, W. Menzel, and R. Jakoby, "Reconfigurable folded reflec-tarray antenna based upon liquid crystal technology," *Antennas and Propagation, IEEE Transactions on*, vol. 63, no. 1, pp. 122–132, Jan 2015.

[14] H. Legay, B. Pinte, M. Charrier, A. Ziaei, E. Girard, and R. Gillard, "A steerable reflectar-ray antenna with mems controls," in *Phased Array Systems and Technology, 2003. IEEE International Symposium on*, Oct 2003, pp. 494–499.

[15] S. Hum, G. McFeetors, and M. Okoniewski, "Integrated mems reflectarray elements," in *Antennas and Propagation, 2006. EuCAP 2006. First European Conference on*, Nov 2006, pp. 1–6.

[16] J. Perruisseau-Carrier and A. Skrivervik, "Monolithic mems-based reflectarray cell digi-tally reconfigurable over a 360 degree phase range," *Antennas and Wireless Propagation Letters, IEEE*, vol. 7, pp. 138–141, 2008.

[17] J. Perruisseau-Carrier, "Dual-polarized and polarization-flexible reflective cells with dynamic phase control," *Antennas and Propagation, IEEE Transactions on*, vol. 58, no. 5, pp. 1494–1502, May 2010.

[18] C. Guclu, J. Perruisseau-Carrier, and O. Civi, "Proof of concept of a dual-band circularly-polarized rf mems beam-switching reflectarray," *Antennas and Propagation, IEEE Trans-actions on*, vol. 60, no. 11, pp. 5451–5455, Nov 2012.

[19] M. Farmahini-Farahani and H. Mosallaei, "Birefringent reflectarray metasurface for beam engineering in infrared," *Opt. Lett.*, vol. 38, no. 4, pp. 462–464, Feb 2013. [Online]. Available: http://ol.osa.org/abstract.cfm?URI=ol-38-4-462

[20] J. Ginn, B. Lail, J. Alda, and G. Boreman, "Planar infrared binary phase reflectarray," *Opt. Lett.*, vol. 33, no. 8, pp. 779–781, Apr 2008. [Online]. Available: http://ol.osa.org/abstract.cfm?URI=ol-33-8-779

[21] D. J. Shelton, K. R. Coffey, and G. D. Boreman, "Experimental demonstration of tunable phase in a thermochromic infrared-reflectarray metamaterial," *Opt. Express*, vol. 18, no. 2, pp. 1330–1335, Jan 2010. [Online]. Available: http://www.opticsexpress.org/abstract.cfm?URI=oe-18-2-1330

[22] J. C. Ginn, B. Lail, and G. D. Boreman, "Infrared patch reflectarray," in *Antennas and Propagation Society International Symposium 2006, IEEE*, July 2006, pp. 4315–4318.

[23] F. Yang, P. Nayeri, A. Elsherbeni, J. C. Ginn, D. Shelton, G. D. Boreman, and Y. Rahmat-Samii, "Reflectarray design at infrared frequencies: Effects and models of material loss," *Antennas and Propagation, IEEE Transactions on*, vol. 60, no. 9, pp. 4202–4209, Sept 2012.

[24] J. C. Ginn, B. Lail, and G. D. Boreman, "Phase characterization of reflectarray elements at infrared," *Antennas and Propagation, IEEE Transactions on*, vol. 55, no. 11, pp. 2989–2993, Nov 2007.

[25] J. C. Ginn, J. Alda, and G. D. Boreman, "Infrared focusing mirror based on multilevel reflectarray," in *Antennas and Propagation (EuCAP), 2010 Proceedings of the Fourth European Conference on*, April 2010, pp. 1–5.

[26] A. Ahmadi, S. Ghadarghadr, and H. Mosallaei, "An optical reflectarray nanoantenna: The concept and design," *Opt. Express*, vol. 18, no. 1, pp. 123–133, Jan 2010. [Online]. Available: http://www.opticsexpress.org/abstract.cfm?URI=oe-18-1-123

[27] Y. Yang, W. Wang, P. Moitra, I. I. Kravchenko, D. P. Briggs, and J. Valentine, "Dielectric meta-reflectarray for broadband linear polarization conversion and optical vortex generation," *Nano Letters*, vol. 14, no. 3, pp. 1394–1399, 2014, pMID: 24547692. [Online]. Available: http://dx.doi.org/10.1021/nl4044482

[28] L. Zou, W. Withayachumnankul, C. M. Shah, A. Mitchell, M. Bhaskaran, S. Sriram, and C. Fumeaux, "Dielectric resonator nanoantennas at visible frequencies," *Opt. Express*, vol. 21, no. 1, pp. 1344–1352, Jan 2013. [Online]. Available: http://www.opticsexpress.org/abstract.cfm?URI=oe-21-1-1344

[29] N. Yu, P. Genevet, M. A. Kats, F. Aieta, J.-P. Tetienne, F. Capasso, and Z. Gaburro, "Light propagation with phase discontinuities: Generalized laws of reflection and refraction," *Science*, vol. 334, no. 6054, pp. 333–337, 2011. [Online]. Available: http://www.sciencemag.org/content/334/6054/333.abstract

[30] F. Aieta, P. Genevet, N. Yu, M. A. Kats, Z. Gaburro, and F. Capasso, "Out-of-plane reflection and refraction of light by anisotropic optical antenna metasurfaces with phase discontinuities," *Nano Letters*, vol. 12, no. 3, pp. 1702–1706, 2012, pMID: 22335616. [Online]. Available: http://dx.doi.org/10.1021/nl300204s

[31] A. Pors, O. Albrektsen, I. P. Radko, and S. I. Bozhevolny, "Gap plasmon-based metasurfaces for total control of reflected light," *Sci. Rep.PY*, vol. 3, no. 2155, 2013.

[32] S. Sun, K.-Y. Yang, C.-M. Wang, T.-K. Juan, W. T. Chen, C. Y. Liao, Q. He, S. Xiao, W.-T. Kung, G.-Y. Guo, L. Zhou, and D. P. Tsai, "High-efficiency broadband anomalous reflection by gradient meta-surfaces," *Nano Letters*, vol. 12, no. 12, pp. 6223–6229, 2012, pMID: 23189928. [Online]. Available: http://dx.doi.org/10.1021/nl3032668

[33] M. Kang, T. Feng, H.-T. Wang, and J. Li, "Wave front engineering from an array of thin aperture antennas," *Opt. Express*, vol. 20, no. 14, pp. 15 882–15 890, Jul 2012. [Online]. Available: http://www.opticsexpress.org/abstract.cfm?URI=oe-20-14-15882

[34] T. Niu, W. Withayachumnankul, B. S.-Y. Ung, H. Menekse, M. Bhaskaran, S. Sriram, and C. Fumeaux, "Experimental demonstration of reflectarray antennas at terahertz

frequencies," *Opt. Express*, vol. 21, no. 3, pp. 2875–2889, Feb 2013. [Online]. Available: http://www.opticsexpress.org/abstract.cfm?URI=oe-21-3-2875

[35] T. Niu, A. Upadhyay, W. Withayachumnankul, D. Headland, D. Abbott, M. Bhaskaran, S. Sriram, and C. Fumeaux, "Polarization-dependent thin-film wire-grid reflectarray for terahertz waves," *Applied Physics Letters*, vol. 107, no. 3, pp. –, 2015. [Online]. Available: http://scitation.aip.org/content/aip/journal/apl/107/3/10.1063/1.4927386

[36] S.-W. Qu, W.-W. Wu, B.-J. Chen, H. Yi, X. Bai, K. B. Ng, and C. H. Chan, "Controlling dispersion characteristics of terahertz metasurface," *Sci. Rep. PY*, vol. 5, 2015.

[37] "www.br-labs.com." [Online]. Available: www.br-labs.com

[38] P. Siegel, "Terahertz technology," *Microwave Theory and Techniques, IEEE Transactions on*, vol. 50, no. 3, pp. 910–928, Mar 2002.

[39] D. Berry, R. Malech, and W. Kennedy, "The reflectarray antenna," *Antennas and Propagation, IEEE Transactions on*, vol. 11, no. 6, pp. 645–651, Nov 1963.

[40] C. S. Malagisi, "Microstrip disc element reflect array," in *Electronics and Aerospace Systems Convention*, Sept 1978, pp. 186–192.

[41] J. P. Montgomery, "A microstrip reflectarray antenna element," in *Antenna Applications Symposium, University of Illinois*, Sept 1978.

[42] D. Pozar and T. Metzler, "Analysis of a reflectarray antenna using microstrip patches of variable size," *Electronics Letters*, vol. 29, no. 8, pp. 657–658, April 1993.

[43] A. Kelkar, "Flaps: conformal phased reflecting surfaces," in *Proc. IEEE National Radar Conf., Los Angeles, California*, March 1991, pp. 58–62.

[44] N. Misran, R. Cahill, and V. Fusco, "Reflection phase response of microstrip stacked ring elements," *Electronics Letters*, vol. 38, no. 8, pp. 356–357, Apr 2002.

[45] R. E. Munson and H. Haddad, "Microstrip reflectarray for satellite communication and rcs enhancement and reduction," Patent US 4 684 952, US Patent 4684952, August, 1987.

[46] J. Huang, "Bandwidth study of microstrip reflectarray and a novel phased reflectarray concept," in *Antennas and Propagation Society International Symposium, 1995. AP-S. Digest*, vol. 1, June 1995, pp. 582–585 vol.1.

[47] J. Huang and R. Pogorzelski, "A ka-band microstrip reflectarray with elements having variable rotation angles," *Antennas and Propagation, IEEE Transactions on*, vol. 46, no. 5, pp. 650–656, May 1998.

[48] H. Hasani, M. Kamyab, and A. Mirkamali, "Broadband reflectarray antenna incorporating disk elements with attached phase-delay lines," *Antennas and Wireless Propagation Letters, IEEE*, vol. 9, pp. 156–158, 2010.

[49] E. Carrasco, M. Barba, and J. Encinar, "Reflectarray element based on aperture-coupled patches with slots and lines of variable length," *Antennas and Propagation, IEEE Transactions on*, vol. 55, no. 3, pp. 820–825, March 2007.

[50] J. Encinar, "Design of two-layer printed reflectarrays using patches of variable size," *Antennas and Propagation, IEEE Transactions on*, vol. 49, no. 10, pp. 1403–1410, Oct 2001.

[51] J. Encinar and J. Zornoza, "Three-layer printed reflectarrays for contoured beam space applications," *Antennas and Propagation, IEEE Transactions on*, vol. 52, no. 5, pp. 1138–1148, May 2004.

[52] M. Chaharmir and J. Shaker, "Broadband reflectarray with combination of cross and rectangle loop elements," *Electronics Letters*, vol. 44, no. 11, pp. 658–659, May 2008.

[53] Q.-Y. Chen, S.-W. Qu, X.-Q. Zhang, and M.-Y. Xia, "Low-profile wideband reflectarray by novel elements with linear phase response," *Antennas and Wireless Propagation Letters, IEEE*, vol. 11, pp. 1545–1547, 2012.

[54] R. Florencio, R. Boix, V. Losada, J. Encinar, E. Carrasco, and M. Arrebola, "Comparative study of reflectarrays based on cells with three coplanar dipoles and reflectarrays based on cells with three stacked patches," in *Antennas and Propagation (EUCAP), 2012 6th European Conference on*, March 2012, pp. 3707–3710.

[55] J. Yoon, Y. Yoon, W.-S. Lee, and J.-h. So, "Broadband microstrip reflectarray with five parallel dipole elements," *Antennas and Wireless Propagation Letters, IEEE*, vol. PP, no. 99, pp. 1–1, 2015.

[56] Y. Mao, S. Xu, F. Yang, and A. Elsherbeni, "A novel phase synthesis approach for wideband reflectarray design," *Antennas and Propagation, IEEE Transactions on*, vol. PP, no. 99, pp. 1–1, 2015.

[57] Q. Wang, z. Shao, Y. Chen, and P. Li, "Broadband low-cost reflectarray using modified double square loop loaded by spiral stubs," *Antennas and Propagation, IEEE Transactions on*, vol. PP, no. 99, pp. 1–1, 2015.

[58] D. Wu, R. Hall, and J. Huang, "Dual-frequency microstrip reflectarray," in *Antennas and Propagation Society International Symposium, 1995. AP-S. Digest*, vol. 4, June 1995, pp. 2128–2131 vol.4.

[59] C. Han, J. Huang, and K. Chang, "A high efficiency offset-fed x/ka-dual-band reflectarray using thin membranes," *Antennas and Propagation, IEEE Transactions on*, vol. 53, no. 9, pp. 2792–2798, Sept 2005.

[60] A. Yu, F. Yang, A. Elsherbeni, and J. Huang, "Experimental demonstration of a single layer tri-band circularly polarized reflectarray," in *Antennas and Propagation Society International Symposium (APSURSI), 2010 IEEE*, July 2010, pp. 1–4.

[61] S.-W. Oh, J.-K. Lee, J. Huang, and K. Chang, "A six-band reflectarray antenna," in *Antennas and Propagation Society International Symposium, 2009. APSURSI '09. IEEE*, June 2009, pp. 1–4.

[62] C. Han, S. Hsu, K. Chang, and J. Huang, "A ku/ka-dual band reflectarray to emulate a cylindrical reflector for titan cloud precipitation radar and altimeter," in *Antennas and Propagation Society International Symposium, 2007 IEEE*, June 2007, pp. 1445–1448.

[63] M. Chaharmir and J. Shaker, "Design of a multilayer x-/ka-band frequency-selective surface-backed reflectarray for satellite applications," *Antennas and Propagation, IEEE Transactions on*, vol. 63, no. 4, pp. 1255–1262, April 2015.

[64] C. Han, C. Rodenbeck, J. Huang, and K. Chang, "A c/ka dual frequency dual layer circularly polarized reflectarray antenna with microstrip ring elements," *Antennas and Propagation, IEEE Transactions on*, vol. 52, no. 11, pp. 2871–2876, Nov 2004.

[65] N. Misran, R. Cahill, and V. Fusco, "Concentric split ring element for dual frequency," *Electronics Letters*, vol. 39, no. 25, pp. 1776–1777, Dec 2003.

[66] M. Chaharmir, J. Shaker, N. Gagnon, and D. Lee, "Design of broadband, single layer dual-band large reflectarray using multi open loop elements," *Antennas and Propagation, IEEE Transactions on*, vol. 58, no. 9, pp. 2875–2883, Sept 2010.

[67] J. Encinar, M. Arrebola, L. de la Fuente, and G. Toso, "A transmit-receive reflectarray antenna for direct broadcast satellite applications," *Antennas and Propagation, IEEE Transactions on*, vol. 59, no. 9, pp. 3255–3264, Sept 2011.

[68] G. Floquet, "Sur les équations différentielles linéaires à coefficients périodiques," *Annales de l'École Normale Supérieure*, vol. 12, pp. 47–88, 1883.

[69] G. Trentini, "Partially reflecting sheet arrays," *Antennas and Propagation, IRE Transactions on*, vol. 4, no. 4, pp. 666–671, October 1956.

[70] B. Munk, *Frequency Selective Surfaces: Theory and Design*. John Wiley, 2000.

[71] I. Bardi, R. Remski, D. Perry, and Z. Cendes, "Plane wave scattering from frequency-selective surfaces by the finite-element method," *Magnetics, IEEE Transactions on*, vol. 38, no. 2, pp. 641–644, Mar 2002.

[72] "https://www.cst.com/." [Online]. Available: https://www.cst.com/

[73] F. Costa and A. Monorchio, "Closed-form analysis of reflection losses in microstrip reflectarray antennas," *Antennas and Propagation, IEEE Transactions on*, vol. 60, no. 10, pp. 4650–4660, Oct 2012.

[74] S. Targonski and D. Pozar, "Minimization of beam squint in microstrip reflectarrays using an offset feed," in *Antennas and Propagation Society International Symposium, 1996. AP-S. Digest*, vol. 2, July 1996, pp. 1326–1329.

[75] M. Born, E. Wolf, and A. B. Bhatia, *Principles of Optics: Electromagnetic Theory of Propagation, Interference and Diffraction of Light*. Cambridge University Press, 1999.

[76] H. Kosaka, T. Kawashima, A. Tomita, M. Notomi, T. Tamamura, T. Sato, and S. Kawakami, "Photonic crystals for micro lightwave circuits using wavelength dependent angular beam steering," *Applied Physics Letter*, vol. 74, no. 10, pp. 1370–1372, March 1999.

[77] K. Hammond, S. Massidda, W. Capecchi, and F. Volpe, "Metamaterial lens of specifiable frequency-dependent focus and adjustable aperture for electron cyclotron emission in the diii-d tokamak," *Journal of Infrared, Millimeter, and Terahertz Waves*, vol. 34, no. 7-8, pp. 437–455, 2013. [Online]. Available: http://dx.doi.org/10.1007/s10762-013-9987-1

[78] M. G. Silveirinha, "Anomalous refraction of light colors by a metamaterial prism," *Phys. Rev. Lett.*, vol. 102, p. 193903, May 2009. [Online]. Available: http://link.aps.org/doi/10.1103/PhysRevLett.102.193903

[79] J. Ethier, D. McNamara, M. Chaharmir, and J. Shaker, "Reflectarray design with similarity-shaped fragmented sub-wavelength elements," *Antennas and Propagation, IEEE Transactions on*, vol. 62, no. 9, pp. 4498–4509, Sept 2014.

[80] W.-C. Weng, W.-H. Ho, and M.-C. Chang, "Optimal design of a planar antenna using binary particle swarm optimization," in *Electromagnetics (iWEM), 2014 IEEE International Workshop on*, Aug 2014, pp. 68–69.

[81] Y. Rahmat-Samii and E. Michielssen, *Electromagnetic Optimization by Genetic Algorithms*. New York, NY: John Wiley and Sons, Inc, 1999.

[82] H. Hasani, C. Peixeiro, A. K. Skrivervik, and J. Perruisseau-Carrier, "Single-layer quad-band microstrip reflectarray antenna with dual linear polarization," *Submitted to Antennas and Propagation, IEEE Transactions on*, 2015.

[83] H. Hasani and C. Peixeiro, "Dual-band, dual-polarized microstrip reflectarray antenna in ku band," in *Antennas and Propagation Conference (LAPC), 2012 Loughborough*, Nov 2012, pp. 1–3.

[84] "http://www.feko.com." [Online]. Available: http://www.feko.com

[85] R. Chaharmir, J. Shaker, and M. Cuhaci, "Development of dual-band circularly polarised reflectarray," *Microwaves, Antennas and Propagation, IEE Proceedings*, vol. 153, no. 1, pp. 49–54, Feb 2006.

[86] R. El hani and J.-J. Laurin, "Specular reflection analysis for off-specular reflectarray antennas," *Antennas and Propagation, IEEE Transactions on*, vol. 61, no. 7, pp. 3575–3581, July 2013.

[87] "http://www.aeroflex.com/." [Online]. Available: http://www.aeroflex.com/

[88] H. Hasani, M. Kamyab, and A. Mirkamali, "Low cross-polarization reflectarray antenna," *Antennas and Propagation, IEEE Transactions on*, vol. 59, no. 5, pp. 1752–1756, May 2011.

[89] D.-C. Chang and M.-C. Huang, "Multiple-polarization microstrip reflectarray antenna with high efficiency and low cross-polarization," *Antennas and Propagation, IEEE Transactions on*, vol. 43, no. 8, pp. 829–834, Aug 1995.

[90] J. Perruisseau-Carrier, "Microwave periodic structures based on microelectromechanical systems (mems) and micromachining technique," Ph.D. dissertation, Ecole Polytechnique Fédérale de Lausanne (EPFL), Lausanne, Switzerland, November 2007.

[91] P. Hannan and M. Balfour, "Simulation of a phased-array antenna in waveguide," *Antennas and Propagation, IEEE Transactions on*, vol. 13, no. 3, pp. 342–353, May 1965.

[92] H. Hasani, M. Tamagnone, S. Capdevila, C. Moldovan, P. Maoddi, A. M. Ionescu, C. Peixeiro, J. R. Mosig, A. K. Skrivervik, and J. Perruisseau-Carrier, "Multi-band, polarization-independent reflectarray surface at terahertz frequencies: design and fabrication," *Submitted to Terahertz Science and Technology, IEEE Transactions on*, 2015.

HAMED HASANI

Chemin de la cocarde 13
1024 Ecublens VD,
Switzerland
Tel: +41 78 6196664
E-mail: h.hassani1985@gmail.com
      hamed.hasani@epfl.ch

20.09.1985
Iranian

EDUCATION

10.2011-Present   Joint PhD student in Electrical Engineering at EPFL (Switzerland) and Universidade de Lisboa (Portugal)

09.2007-09.2010   Master in Electrical Engineering at K.N.Toosi University of Technology, Tehran, Iran
>> Major in Wave Telecommunications

09.2003-09.2007   Bachelor in Electrical Engineering at Zanjan University, Zanjan, Iran
>> Major in Telecommunications

PROFESSIONAL EXPERIENCE

10.2011-Present   Doctoral Assistant - EPFL
>> Antenna System Design Engineer
>> Design and measurement of multiband reflectarray antennas in Ku and THz frequency bands.
>> Teacher assistant of Electromagnetism I,II

03.2009-07.2011   Faraz sanat sharif company, Tehran, Iran
>> Antenna/Propagation Engineer,
>> Design and development of HF antennas for very long-range radars through ionosphere
>> Mutual coupling compensation for Direction of Arrival (DOA) estimation in antenna arrays
>> Design and optimization of a large aperture size parabolic reflector antenna in X band

09.2003-09.2007   Zanjan University
>> Teacher assistant of Electromagnetism
>> Teacher assistant of Digital Communications

09.2000-09.2003   High school
>> Implementation of a short-wave (SW) radio transmitter incorporating a Vacuum Tube and a Quartz-Crystal.

KEY SKILLS

Electromagnetics: Antenna Theory and Design, RF and Microwave Circuit and System Design, Numerical Methods in EM, Wave Propagation.

Software Packages: MATLAB, Ansys HFSS, CST Microwave Studio, FEKO.

PUBLICATIONS

+ **H. Hasani**, Peixeiro, C., "Dual-band, Dual-polarized Reflectarray antenna in Ku Band", Proc Loughborough Antennas and Propagation Conf. LAPC, Loughborough, United Kingdom, Vol. 1, pp. 1 - 4, November, 2012.

+ **H. Hasani**, Peixeiro, C., "Dual-band Dual-Polarized Reflectarray Antenna with close Frequencies in Ku Band", Proc IEEE AP-S/URSI International Symp., Chicago, United States, July, 2012

+ **H. Hasani**, C. Peixeiro, A. K. Skrivervik, J. Perruisseau-Carrier,"Single-Layer Quad-Band Microstrip Reflectarray Antenna with Dual Linear Polarization," *Antennas and Propagation, IEEE Transactions on*. (Accepted with major revision)

+ **H. Hasani**; Perruisseau-Carrier, J.; Peixeiro, C.; Mosig, J.R., "Dual-band dual-polarized reconfigurable unit-cell for reflectarray antenna in Ku-Band," Antennas and Propagation (EuCAP), 2013 7th European Conference on, vol., no., pp.861, 862, 8-12 April 2013.

+ **H. Hasani**, M. Tamagnone, S. Capdevila, C. Moldovan, P. Maoddi, A. M. Ionescu, C. Peixeiro, J. R. Mosig, A. K. Skrivervik and J. Perruisseau-Carrier "Multi-band, polarization-independent reflectarray surface at terahertz frequencies: design and fabrication," *Submitted to Transactions on Terahertz Science and Technology.*

+ **H. Hasani**, M. kamyab, A. mirkamali, "Broadband reflectarray antenna incorporating disk elements with attached phase-delay lines" *IEEE Antennas and Wireless Propagation Letters, Vol. 9, pp. 156 – 158, 2010.08.29*

+ **H. Hasani**, M. kamyab, A. mirkamali, "Low cross-polarization reflectarray antennas" *IEEE Transactions on Antenna and Propagation.* Vol. 59, pp. 1752 – 1756, 2011.

+ **H. Hasani**, M. kamyab, A. mirkamali, "Reflectarray antenna consisting of circular disk elements: Design and Measurement" Asia-Pacific Microwave Conference, Japan, Yokohama, 2010.

LANGUAGES

Persian: Native
Azerbaijani: Native
English: Full professional proficiency
French: Full professional proficiency
German: Very good knowledge (B2)
Italian: Elementary knowledge (A1)

HOBBIES

Traveling, Reading, Playing piano, Theatre (Member of the EPFL theatre group: Les Polyssons).